TECHNISCHE UNIVERSITÄT MÜNCHEN

Fakultät für Medizin

Functional relevance of rare genetic variants in the *PDE5A* gene for coronary artery disease

Tan An Dang

Vollständiger Abdruck der von der Fakultät für Medizin der Technischen Universität München zur Erlangung des akademischen Grades einer

Doktorin der Naturwissenschaften (Dr. rer. nat.)

genehmigten Dissertation.

Vorsitz: Prof. Dr. Dr. Stefan Engelhardt

Prüfer*innen der Dissertation:

1. Prof. Dr. Heribert Schunkert
2. Prof. Dr. Johannes Beckers

Die Dissertation wurde am 17.02.2022 bei der Technischen Universität München eingereicht und durch die Fakultät für Medizin am 12.07.2022 angenommen.

To my family.

Table of Contents

List of Abbreviations

a.u.	arbitrary unit
ADP	adenosin diphosphate
ANP	atrial natriuretic peptide
APOB	apolipoprotein B
BMI	body mass index
CAD	coronary artery disease
cAMP	cyclic adenosine monophosphate
cDNA	complementary DNA
CDS	coding sequence
cGMP	cyclic guanosine monophosphate
CI	confidence interval
CVD	cardiovascular disease
DBB	desoxyribonucleic acid binding buffer
ddH_2O	double distilled water
ddPCR	droplet digital PCR
DNA	desoxyribonucleic acid
E.coli	*Escherichia coli*
EDN1	endothelin 1
eNOS	endothelial nitric oxide synthase
FACS	fluorescence-activated cell sorter
FH	familial hypercholesterolemia
fs	frameshift
GAF	phosphodiesterases, adenylyl cyclases and FhIA
GSNO	S-nitrosoglutathione
GUCY1A1 formerly GUCY1A3	guanylate cyclase soluble subunit alpha 1
GWAS	genome-wide association study
H&E	hematoxylin and eosin staining
HCASMC	human coronary artery smooth muscle cell
HCl	hydrochloric acid
IgG	immunoglobulin G
IHD	ischemic heart disease
iNOS	inducible nitric oxide synthase
KO	knock-out
LDL	low-density lipoprotein
LDLR	low-density lipoprotein receptor
LDLRAP1	low-density lipoprotein receptor adapter protein 1
LOD	logarithm of the odds
MAF	minor allele frequency
MI	myocardial infarction
mRNA	messenger ribonucleic acid
MRVI1	murine retrovirus integration site 1 homolog

MUT	mutant
nNOS	neuronal nitric oxide synthase
NO	nitric oxide
NOS	nitric oxide synthase
NOS3	nitric oxide synthase 3
OR	odds ratio
PAM	protospacer adjacent motif
PBB	protein binding buffer
PBS	phosphate buffered saline
PC	principal component
PCA	principal component analysis
PCR	polymerase chain reaction
PCSK9	proprotein convertase subtilisin/kexin type 9
PDE	phosphodiesterase
PDE1	phosphodiesterase 1
PDE2	phosphodiesterase 2
PDE3/PDE3A	phosphodiesterase 3/3A
PDE5/PDE5A	phosphodiesterase 5/5A
pGC	particulate guanylate cyclase
PKG	protein kinase G
PLB	passive lysis buffer
qPCR	qualitative real-time PCR
REST	RE1-silencing transcription factor
RIPA	radioimmunoprecipitation assay
RNA	ribonucleic acid
RPLP0	ribosomal protein lateral stalk subunit P0
SD	standard deviation
SEM	standard error mean
sGC	soluble guanylate cyclase
siRNA	small interfering ribonucleic acid
SMC	smooth muscle cell
SNP	single nucleotide polymorphism
TBE	TRIS-borate-EDTA
VASP	vasodilator-stimulated phosphoprotein
VSMC	vascular smooth muscle cell
WB	wash buffer
WES	whole exome sequencing
WT	wild-type
ZFX	zinc finger X-chromosomal protein

List of Figures

List of Tables

Summary

Despite all efforts to detect and understand cardiovascular risk factors, cardiovascular diseases remain the leading cause of death worldwide. Therefore, genome-wide association studies have added vital contributions to uncover novel coronary artery disease risk genes. So far, more than 300 risk variants could be identified, including the common variant rs7678555 at the chromosomal locus 4q27. This signal was mapped to the vicinity of the *PDE5A* gene. However, the role of PDE5 in coronary artery disease is unclear and functional investigation of common variants is complex. For that reason, we aimed to gain first mechanistic insights on how PDE5 might modulate coronary artery disease risk by studying rare *PDE5A* variants.

This study demonstrates that PDE5 overexpression contributes to increased coronary artery disease risk. On the one hand, by performing an association analysis, we could show that carriers of inactivating *PDE5A* variants may be at lower risk for coronary artery disease. On the other hand, we mechanistically investigated another rare *PDE5A* variant (dbSNP: rs201005905; ClinGen Allele Registry: NM_033430.3:c.19A>T, NP_236914.2:p.Lys7Ter; gnomAD: 4-120548312-T-A, MAF $2.1*10^{-4}$), which had been identified in an extended family with a high prevalence of premature coronary artery disease and myocardial infarction (LOD score = 3.16). Here, we demonstrated that the variant leads to the expression of a truncated yet active PDE5A2 isoform. In addition, the variant affected the function of an alternative *PDE5A* promoter encompassing the variant due to differential binding of the transcription factor ZFX to the mutation site. We demonstrated that the transcription factor ZFX preferentially binds to the non-risk allele of the variant. Most notably, lack of ZFX led to increased *PDE5A* expression in vascular smooth muscle cells, suggesting vascular smooth muscle cell dysfunction as the mechanism in the presented family. The analysis of rare variant genetic burden and the mechanism underlying the disease phenotype in the presented family vigorously promote PDE5 inhibition as a promising strategy to encounter coronary artery disease. However, this remains to be studied.

We anticipate our study to serve as a starting point to identify further gain-of-function *PDE5A* variants, which may present suitable genetic markers for determining individuals with increased risk for coronary artery disease. Genetic risk profiles may contribute to developing personalized treatment strategies for improved prevention or mitigation of coronary artery disease.

Zusammenfassung

Trotz der großen Fortschritte, die zum heutigen Verständnis von kardiovaskulären Erkrankungen und deren Risikofaktoren geführt haben, bleiben koronare Herzerkrankungen weltweit die häufigste Todesursache. Genomweite Assoziationsstudien haben beträchtlich zur Entdeckung neuer Risikovarianten beigetragen. So wurden bereits über 300 Risikovarianten, meist mit unbekannter Funktion, identifiziert. Eine davon ist die häufige Variante rs7678555 am Genlocus 4q27, welche dem *PDE5A* Gen zugeordnet wurde. Jedoch ist der Zusammenhang zwischen PDE5 und koronarer Herzerkrankung nicht hinreichend geklärt und die funktionelle Untersuchung häufiger Varianten mitunter sehr komplex. Im Rahmen dieser Studie sollte daher mithilfe der Charakterisierung seltener *PDE5A* Varianten erstmalig geklärt werden, auf welche Weise PDE5 das Risiko für koronare Herzerkrankungen beeinflusst.

Unsere Studie zeigt, dass eine Überexpression von PDE5 zu einer Erhöhung des Risikos für koronare Herzerkrankungen beiträgt. Zum einen konnten wir mithilfe einer Assoziationsanalyse zeigen, dass das Risiko für koronare Herzerkrankungen bei Trägern inaktivierender Varianten geringer ausfällt. Zum anderen charakterisierten wir eine weitere seltene *PDE5A* Variante (dbSNP: rs201005905; ClinGen Allele Registry: NM_033430.3:c.19A>T, NP_236914.2:p.Lys7Ter; gnomAD: 4-120548312-T-A, MAF $2.1*10^{-4}$), die bei einer Familie mit einer ungewöhnlich hohen Prävalenz koronarer Herzerkrankungen entdeckt wurde (LOD score = 3.16). Hier konnten wir zum einen zeigen, dass es durch die Variante zur Expression einer verkürzten jedoch aktiven PDE5A2 Variante kommt. Zum anderen konnten wir nachweisen, dass sich die Variante in einem alternativen *PDE5A* Promotor befindet und dessen Funktion aufgrund von differentieller Bindung des Transkriptionsfaktors ZFX an die Mutationsstelle beeinflusst. Tatsächlich konnten wir zeigen, dass ZFX bevorzugt an das Wildtypallel anstelle des Risikoallels der Variante bindet. Dies scheint besonders bei glatten Gefäßmuskelzellen eine wichtige Rolle zu spielen, denn dort führte die Reduktion von ZFX zu einer erhöhten *PDE5A* Expression. Somit könnte eine Dysfunktion von glatten Gefäßmuskelzellen der zugrundeliegende pathogene Mechanismus in der hier vorgestellten Familie darstellen. Diese Erkenntnisse erwecken den Eindruck, dass die Anwendung eines PDE5-Hemmers bei koronaren Herzerkrankungen von großem Nutzen sein könnte, was jedoch weiterer Untersuchungen bedarf.

Ausgehend von unserer Studie, könnte die weitere Identifizierung sogenannter gain-of-function *PDE5A* Varianten dazu führen, geeignete genetische Marker zu finden, um Individuen mit erhöhtem Risiko für koronare Herzerkrankungen zu identifizieren. Dies ist besonders interessant im Hinblick auf die Entwicklung von personalisierten Therapiestrategien, die die individuellen Bedürfnisse des Patienten berücksichtigen und somit zur verbesserten Prävention oder Abmilderung von koronaren Herzerkrankungen beitragen könnten.

1 Introduction

1.1 Coronary artery disease

1.1.1 Epidemiology

Cardiovascular diseases (CVDs) describe a class of diseases comprising all diseases of the heart and the blood vessels, for example, coronary artery disease (CAD) (for a comprehensive overview, see the review of Nabel (2003)). To this day, CVDs remain the leading cause of morbidity and mortality on a global scale, adding to approximately one-third of all deaths (Roth *et al.*, 2020). Between 1990 to 2019, CVD incidences have doubled from 271 million to 523 million. In parallel, the number of deaths has increased from 12.1 million to 18.6 million (Roth *et al.*, 2020). Most CVD deaths are caused by atherosclerotic CVDs, commonly due to stroke or CAD, also known as ischemic heart disease (IHD) (Benjamin *et al.*, 2019, Libby *et al.*, 2019, Roth *et al.*, 2020). In 2019 alone, stroke and CAD had a share of 17.7% and 49.2%, respectively, of total cardiovascular deaths (Roth *et al.*, 2020). Access to preventive measures and healthcare have led to improvements, especially in high-income countries, but remain a challenge for medium- to low-income countries (Libby *et al.*, 2019, Roth *et al.*, 2020).

1.1.2 Atherosclerosis

Atherosclerosis is a particular form of arteriosclerosis characterized by the development of seemingly fatty lesions in artery walls (Libby *et al.*, 2019). It is the underlying cause for most CVDs, such as CAD. To current knowledge, atherosclerosis is understood as a complex chronic disorder with an interplay of lipid- and inflammation-driven alterations at the intima of arterial walls that progresses with age and eventually leads to the occlusion of arterial vessels (Libby *et al.*, 2019). Although first noticeable symptoms, for example, angina, rarely occur before the age of 40 (Mozaffarian *et al.*, 2015), aortic fatty streaks can already be detected in children, while first atherosclerotic lesions seem to form during adolescence and early adulthood (Strong *et al.*, 1992). In the early stages of atherosclerosis, low-density lipoprotein (LDL) particles, transporting cholesterol through the bloodstream, accumulate in the intima of arterial walls (Tabas *et al.*, 2007). Within the intima, processes may occur that lead to the oxidation of LDL particles (Matsuura *et al.*, 2008), which harbor proinflammatory properties attracting circulating monocytes to the intima (Bekkering *et al.*, 2014). Recruited monocytes differentiate into macrophages, taking up resident LDL particles and becoming foam cells (Li and Glass, 2002). Additional immune response, e.g., the infiltration of the intima with T lymphocytes, affects endothelial and vascular smooth muscle cell (VSMC) function. On the one hand, inflammation promotes endothelial dysfunction (Bautista, 2003). On the other hand, VSMCs can respond to inflammation by secretion of extracellular matrix molecules

(Bennett *et al.*, 2016) and increased migration, protruding from the tunica media layer of the arterial wall into the intima (Gerthoffer, 2007, Bennett *et al.*, 2016), where they eventually differentiate into foam cells (Pryma *et al.*, 2019). Due to the unique properties of the extracellular matrix within atherosclerotic plaques, accumulated lipid particles and foam cells become trapped within the lesion site (Nakashima *et al.*, 2008, Chistiakov *et al.*, 2013). Throughout progressing atherosclerosis, macrophages and smooth muscle cells eventually undergo apoptosis, leaving lipid-filled necrotic cores in advanced atherosclerotic plaques (Clarke and Bennett, 2006, Gautier *et al.*, 2009). Moreover, calcification may lead to plaque destabilization, increasing the likelihood of plaque rupture and thrombosis (Ruiz *et al.*, 2015, Libby *et al.*, 2019) (Figure 1).

Though many essential aspects of atherogenesis and atherosclerosis progression have been uncovered, the mechanism that initiates atherosclerosis remains controversial (Libby *et al.*, 2019). The causal role of LDL cholesterol in atherogenesis is well established (Goldstein and Brown, 2015, Libby *et al.*, 2019, Boren *et al.*, 2020). However, LDL particles can leave the arterial wall (Schwenke and St Clair, 1993) and cannot be accounted for initiation of atherosclerosis alone (Goldstein and Brown, 2015). Thus, interaction with risk factors (chapters 1.1.3 and 1.1.4), impaired response to LDL (Williams and Tabas, 1995) or inflammation (Fernandez-Friera *et al.*, 2019), alterations in LDL processing (Bartels *et al.*, 2015), or endothelial dysfunction (Davignon and Ganz, 2004) may be necessary prerequisites. Unraveling these mechanisms might propose meaningful strategies to prevent CAD.

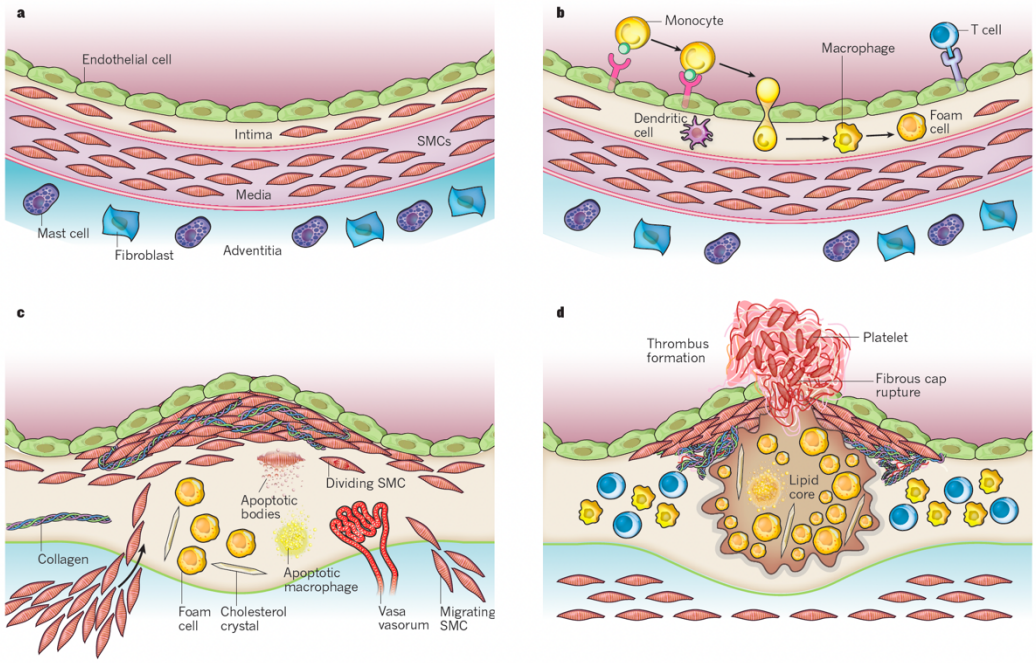

Figure 1 Atherosclerosis initiation and progression

1.1.3 Modifiable risk factors

Numerous factors were shown to increase CAD risk and accelerate CAD progression, including metabolic factors such as high blood pressure, high LDL cholesterol, high body mass index (BMI), high glucose levels, and kidney dysfunction (Roth *et al.*, 2020). Furthermore, behavioral habits, e.g., diet, cigarette smoking, and alcohol use, are associated with increased CAD risk (Yusuf *et al.*, 2004, Roth *et al.*, 2020). Apart from metabolic and behavioral risk, awareness about the role of the environment on cardiovascular health is rising. In particular, air pollution appears to be a key driver (Roth *et al.*, 2020). The risk factors mentioned above share a high treatability; hence they are called modifiable risk factors. While usually being addressed in patients showing first symptoms of CAD as a means of secondary prevention, a study by Pahkala *et al.* demonstrated that life quality could be improved tremendously if modifiable risk factors are focused on long before symptoms occur (Pahkala *et al.*, 2013). Recommended lifestyle changes include preventing or reducing obesity, increased physical activity, quitting smoking, blood pressure control, and diabetes management. Many of these factors are modulated by poor educational attainment, which is a genetically driven risk factor by itself (Schunkert *et al.*, 2020). Additional treatment with, for example, statins or other lipid-lowering agents, antiplatelet drugs, and anti-inflammatory medication might further reduce CAD risk (Pahkala *et al.*, 2013, Libby *et al.*, 2019).

1.1.4 Genetic risk factors

Aside from modifiable risk factors, genetic burden plays a decisive role in the outcome of CAD, which has a heritability of approximately 40-60 % (Vinkhuyzen *et al.*, 2013, McPherson and Tybjaerg-Hansen, 2016). Furthermore, genetic effects on CAD seem to impact early-onset forms of CAD in particular (Zdravkovic *et al.*, 2002, Schunkert *et al.*, 2011, McPherson and Tybjaerg-Hansen, 2016).

One of the most extreme examples of the genetic influence on CAD is familial hypercholesterolemia (FH). FH presents a genetic disorder that leads to disturbed lipid metabolism, particularly LDL cholesterol. Several mutations have been discovered so far (Soutar and Naoumova, 2007). Most of them are located in the LDL receptor (*LDLR*) gene (Goldstein and Brown, 2015, Braenne *et al.*, 2016). Other mutations were found in *APOB* (Alves *et al.*, 2014), *PCSK9* (Abifadel *et al.*, 2003, Braenne *et al.*, 2016), *LDLRAP1* (Garcia *et al.*, 2001). Being involved in LDL cholesterol uptake into the liver, alterations of those genes lead to impaired LDL cholesterol uptake, thus increasing circulating LDL cholesterol levels in the body (Soutar and Naoumova, 2007). Heightened LDL cholesterol levels are associated with an increased risk for atherosclerosis (Boren *et al.*, 2020). Indeed, FH mutation carriers feature higher CAD risk than non-mutation carriers and even non-mutation carriers with high LDL cholesterol levels (Khera *et al.*, 2016). Moreover, the average age of CAD onset is

noticeably decreased in FH patients, while mortality is increased accordingly. Homozygous FH mutation carriers may even die from myocardial infarction (MI) during early childhood (Raal *et al.*, 2011).

Studies of familial forms of CAD, such as FH, have provided essential insights into the impact of single-gene mutations on CAD. However, monogenic forms of CAD are rare, hence, fail to explain CAD risk in those unaffected by these mutations (Khera *et al.*, 2018). Data from genome-wide association studies (GWAS) have revealed that common CAD risk does not derive from one gene. In contrast, complex interactions of several genetic variants with small effect sizes, each individually favoring atherogenic traits, eventually result in disease manifestation (Khera *et al.*, 2018, Schunkert *et al.*, 2018). To date, GWAS analyses led to the identification of more than 300 risk loci associated with CAD (Erdmann *et al.*, 2018, Chen and Schunkert, 2021, Kessler and Schunkert, 2021) (Figure 2). Some identified risk variants are involved in pathways that coincide with previously mentioned modifiable risk factors, such as lipid metabolism, blood pressure, insulin resistance, and adiposity. Other variants have been mapped to genes involved in platelet function, inflammation, angiogenesis, and vascular remodeling (Chen and Schunkert, 2021). However, most variants are non-coding or are associated with genes of unknown function concerning CAD (Chen and Schunkert, 2021, Kessler and Schunkert, 2021). Above all, the enrichment of risk genes within the nitric oxide (NO)-cyclic guanosine monophosphate (cGMP) pathway has attracted attention, instigating a reevaluation of NO and participating molecules within the NO-cGMP pathway for their potential in the prevention of CAD. Identified risk genes within the NO-cGMP pathway comprise *NOS3 (Nikpay et al., 2015)*, *GUCY1A1* (formerly known as *GUCY1A3*) (International Consortium for Blood Pressure Genome-Wide Association Studies *et al.*, 2011, CARDIoGRAMplusC4D Consortium *et al.*, 2013, Erdmann *et al.*, 2013), *MRVI1 (Webb et al., 2017)*, and *PDE5A* (Nelson *et al.*, 2017) (further explained in chapter 1.3). In addition, other genes, being remotely connected to the NO-cGMP pathway, have been identified, namely *PDE3A* (Nelson *et al.*, 2017) and *EDN1* (Myocardial Infarction Genetics Consortium *et al.*, 2009, Schunkert *et al.*, 2011, Gupta *et al.*, 2017, Dang *et al.*, 2020).

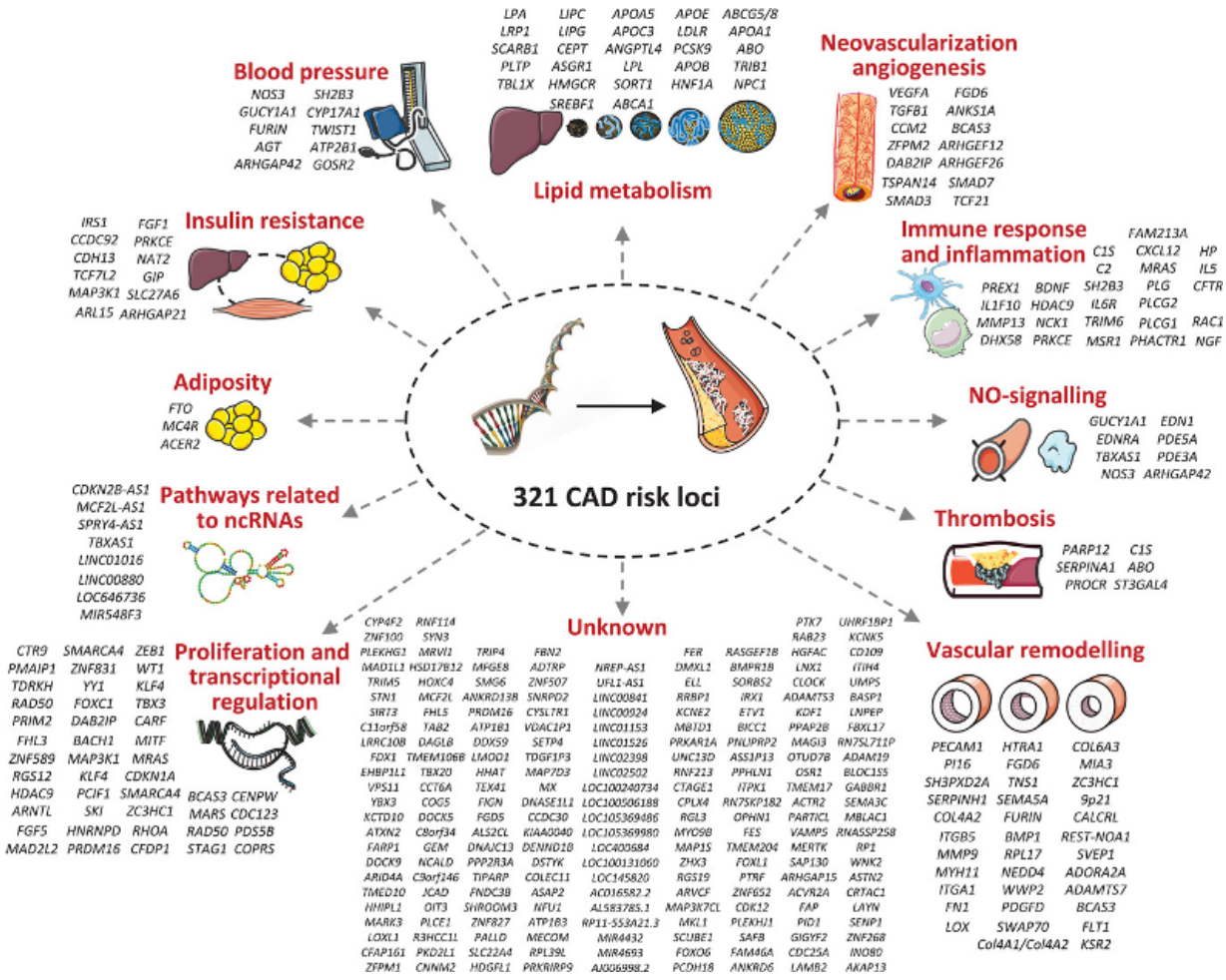

Figure 2 Identified CAD risk genes

List of genes that have been mapped to coronary artery disease (CAD) risk loci. NO: nitric oxide. Reprinted with permission: Figure 2 from "Genetics of coronary artery disease in the post-GWAS era" by Chen and Schunkert, *J Intern Med* 2021. 290 (5): 980-992. Copyright © 2021 by John Wiley & Sons Ltd.

1.2 The NO-cGMP pathway in vascular cells

1.2.1 Molecules involved in cGMP synthesis

NO is a soluble gas produced by nitric oxide synthases (NOS). NOS has three isoforms, i.e., neuronal NOS (nNOS, NOS1), inducible NOS (iNOS, NOS2), and endothelial NOS (eNOS, NOS3). The latter is primarily expressed in endothelial cells (Forstermann and Sessa, 2012) and is, to current knowledge, the main contributor of NO in the vasculature (Ursell and Mayes, 1993, Forstermann and Munzel, 2006). However, growing evidence suggests additional involvement of nNOS-derived NO in cardiovascular function (Xu *et al.*, 2000, Shabeeh *et al.*, 2017). NO acts mainly through an enzyme called soluble guanylate cyclase (sGC), synthesizing the secondary messenger cGMP (Stasch *et al.*, 2002). sGC consists of two subunits, an α and a β subunit. Several heterodimer combinations of different α and β subunits are expressed in humans, however, only the $\alpha_1\beta_1$ and $\alpha_2\beta_1$ sGC isoforms are relevant for NO-dependent cGMP formation. Since the $\alpha_2\beta_1$ sGC isoform is exclusively located in the

brain, the $\alpha_1\beta_1$ heterodimer seems to be the most relevant for vascular function (Mergia *et al.*, 2003). Besides sGC, the membrane-bound particulate guanylate cyclase (pGC) also produces cGMP, however, in a NO-independent manner (Schmidt *et al.*, 1993). cGMP mediates signaling pathways with great importance for vascular function (Moro *et al.*, 1995), e.g., regulation of smooth muscle cell tone (Ignarro and Kadowitz, 1985, Carvajal *et al.*, 2000) and inhibition of platelet aggregation (Walter and Gambaryan, 2009, Zhang *et al.*, 2011) (for an overview, see Dang *et al.* (2020)).

1.2.2 cGMP effectors

One group of cGMP effectors are cGMP-gated ion channels (Schmidt *et al.*, 1993), which are less involved in vascular function. However, they hold importance for signal transduction in photoreceptors, olfactory sensory neurons, and spermatozoa (Kaupp and Seifert, 2002). Most of the cGMP signaling, however, is conveyed by the cGMP-dependent protein kinases (PKG), which target, among others, vasodilator-stimulated phosphoprotein (VASP) (Benz *et al.*, 2009), and murine retrovirus integration site 1 homolog (MRVI1; also known as IRAG) (Ammendola *et al.*, 2001). Although VASP is ubiquitously expressed, it may play a more critical role in regulating platelet aggregation (Aszodi *et al.*, 1999, Pula *et al.*, 2006), while IRAG is somewhat involved in smooth muscle cell relaxation (Geiselhoringer *et al.*, 2004). Moreover, it is also involved in the regulation of platelet aggregation and thrombus formation (Antl *et al.*, 2007). Another PKG interaction partner is phosphodiesterase 5 (PDE5) (Francis *et al.*, 2010), which also interacts with cGMP directly (Yanaka *et al.*, 1998). PDE5 belongs to the family of phosphodiesterases (PDEs) comprising 11 isoenzymes. These enzymes regulate intracellular concentrations of cAMP, cGMP, or both. Besides PDE5, PDE1, PDE2, and PDE3 are the most relevant PDEs for regulating intracellular cGMP levels, thereby modulating cGMP effects (see chapter 1.2.3) (Francis *et al.*, 2010) (for an overview, see Dang *et al.* (2020)).

1.2.3 cGMP degradation

PDE1 degrades cAMP and cGMP in a calcium-/calmodulin-dependent manner (Francis *et al.*, 2010). Interestingly, PDE1 preferentially degrades cGMP (Wallis *et al.*, 1999). Similar to PDE1, PDE3 is a dual-specific PDE. In contrast to PDE1, PDE3 catalyzes cAMP rather than cGMP. Notably, cGMP can competitively inhibit cAMP catalyzation by PDE3. Hence PDE3 is also known as the cGMP-inhibited PDE (Degerman *et al.*, 1997). Increasing evidence suggests that PDE3 controls cGMP levels at low cGMP concentrations and is somewhat involved in intracellular cGMP compartmentation than degradation (Tsai and Kass, 2009). Spatial segregation of secondary messengers is an essential cellular mechanism, enabling the cell to facilitate multiple responses using one single kind of molecule (McCormick

and Baillie, 2014). PDE2 and PDE5 belong to the group of cGMP-activated PDEs. Activation of both enzymes requires phosphorylation and cGMP-binding to an allosteric cGMP binding site (Jager *et al.*, 2010). PDE2 has a dual-specific catalyzation site, regulating natriuretic cGMP levels and cardiomyocyte contractility (Francis *et al.*, 2011). PDE5 degrades cGMP only (Francis *et al.*, 2010) and is necessary for smooth muscle tone and platelet inhibition signaling (Rybalkin *et al.*, 2002, Gresele *et al.*, 2011) (for an overview, see Dang *et al.* (2020)).

1.2.4 PDE5 function

PDE5 is encoded by the *PDE5A* gene at the chromosomal locus 4q26. This locus codes for three *PDE5A* isoforms, termed *PDE5A1*, *PDE5A2*, and *PDE5A3*, with three distinct first exons (Lin *et al.*, 2000a) (Figure 3). While *PDE5A1* and *PDE5A2* are expressed in various tissues, *PDE5A3* expression is more specific to tissues with smooth muscle or cardiac muscle content (Lin *et al.*, 2000b, Lin, 2004). PDE5 acts as a homodimer (Thomas *et al.*, 1990b, Corbin, 2004). Each monomer contains several N-terminal phosphorylation sites, two “cGMP-specific phosphodiesterases, adenylyl cyclases and FhIA” (GAF) domains (GAF A and GAF B), and a C-terminal catalytic domain (Figure 3). The regulation of PDE5 function follows a negative cGMP feedback loop (Mullershausen *et al.*, 2004). Increasing cGMP levels lead to the enhanced binding affinity of cGMP to the GAF A domain (Rybalkin *et al.*, 2003, Corbin *et al.*, 2009) and catalytic domain, resulting in four interchangeable forms of PDE5 conformations with different properties regarding phosphorylation, cGMP binding, and catalytic activity (Corbin *et al.*, 2009). Phosphorylation of PDE5 by PKG further enhances cGMP binding affinity to the GAF A domain (Thomas *et al.*, 1990a, Mullershausen *et al.*, 2001, Francis *et al.*, 2002). It has been suggested that the GAF B domain facilitates the conformational changes of PDE5 secondary to cGMP binding to the GAF A domain (Wang *et al.*, 2010). Subsequent conformational alterations lead to the revelation of the catalytic site of the enzyme (Wang *et al.*, 2006, Wang *et al.*, 2010), where PDE5 degrades cGMP to 5’-GMP. Eventually, decreasing cGMP levels and a lack of cGMP binding to the allosteric and catalytic domain of PDE5 lead to the deactivation of the enzyme.

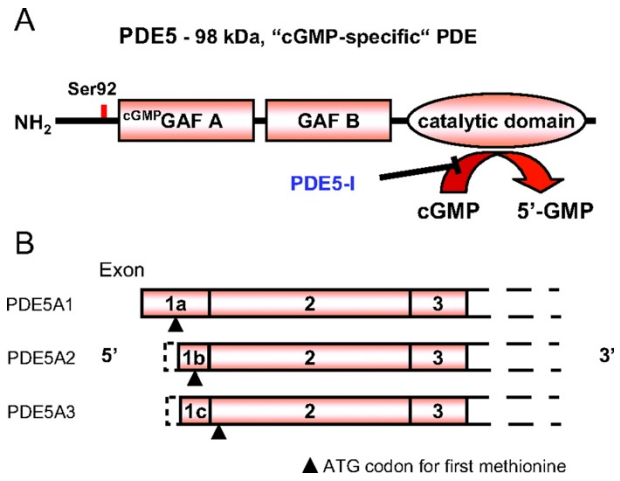

Figure 3 PDE5 structure and isoforms

A. Structure of a PDE5 monomer. Each monomer contains several N-terminal phosphorylation sites, two "cGMP-specific phosphodiesterases, adenylyl cyclases and FhlA" (GAF) domains (GAF A and GAF B), and a C-terminal catalytic domain, which is the target of PDE5 inhibitors (PDE5-I). **B.** Different first exons of the three protein-coding PDE5 isoforms. Reprinted with permission: Figure 1 from "Phosphodiesterase Type 5: Expanding roles in cardiovascular regulation" by Kass *et al.*, *Circ Res* 2007. 101: 1084-1095. Copyright © 2007 by Wolters Kluwer Health, Inc.

1.2.5 cGMP-mediated functions in the vasculature

The NO-cGMP pathway plays an essential role in regulating smooth muscle cell (SMC) relaxation. Therefore, NO, originating from endothelial cells, activates sGC in SMCs, synthesizing cGMP. cGMP, in turn, initiates a phosphorylation cascade through PKG, which results in a decrease of intracellular calcium levels, eventually culminating in smooth muscle relaxation (Ignarro and Kadowitz, 1985, Carvajal *et al.*, 2000). Furthermore, cGMP signaling mediates SMC plasticity, i.e., switches between the contractile and synthetic phenotype (Lincoln *et al.*, 2006, Lehners *et al.*, 2018). This process plays a crucial role in atherogenesis. However, the exact role of cGMP therein remains elusive (Lehners *et al.*, 2018). Besides the effects on SMCs, NO also regulates platelet function. Similar to SMC relaxation, endothelial-derived NO can stimulate sGC in platelets. Therefore, cGMP inhibits platelet aggregation in a calcium-dependent manner (Walter and Gambaryan, 2009, Zhang *et al.*, 2011). Platelets play a key role in thrombus formation (Schulz and Massberg, 2012). Hence, impaired platelet inhibition may aggravate CAD outcomes. Interestingly, NO has also been shown to feature gene regulatory properties, such as modulation of gene expression, translation, and post-translational modifications (Bogdan, 2001). Moreover, NO seems to interact with transcription factors (Pantopoulos and Hentze, 1995, Bogdan, 2001) and is suspected to influence epigenetic effects and environment-gene-interactions (Kaun *et al.*, 2007, Deschatrettes *et al.*, 2012) (for an overview, see Dang *et al.* (2020)).

1.3 Current genetic evidence linking the NO-cGMP pathway with CAD risk

cGMP is involved in many functions relevant to the cardiovascular system. Hence dysregulation thereof is likely to play a role in cardiovascular diseases. Possible modes of action have been delineated before (Tsai and Kass, 2009, Schlossmann and Schinner, 2012) but remain controversial (Lukowski *et al.*, 2014). Regardless, recent GWAS analyses revealed several association signals for different members of the NO-cGMP pathway (chapter 1.1.4), proposing a strong association of this particular pathway with CAD. Notably, besides LDL cholesterol metabolism, no other pathway is better represented in GWAS regarding CAD. The following section will focus on those GWAS findings, dissecting current knowledge on their presumable role in CAD (partially reviewed in Dang *et al.* (2020)).

1.3.1 *NOS3*

A study by Nikpay *et al.* identified the single nucleotide polymorphism (SNP) rs3918226 to be significantly associated with CAD (Nikpay *et al.*, 2015). This variant is located in the *NOS3* promoter, suggesting a regulatory effect of the SNP on *NOS3* expression. Indeed, reporter gene assays confirmed diminished *NOS3* promoter function with the risk allele of the SNP. Notably, homozygote risk allele carriers displayed increased systolic and diastolic blood pressure, indicating a role of *NOS3* in blood pressure regulation (Salvi *et al.*, 2013). Emdin *et al.*, analyzing individual-level data from over 300000 individuals of European ancestry from UK Biobank, confirmed an association of this particular SNP with blood pressure. Moreover, their analysis proposed that rs3918226 may also affect CAD through additional pathways other than blood pressure (Emdin *et al.*, 2018).

These observations coincide with data from *Nos3* knockout (KO) animal models. Similarly, *Nos3* KO mice featured increased basal blood pressure (Stauss *et al.*, 1999) and pulmonary hypertension (Fagan *et al.*, 1999). Moreover, mice lacking *Nos3* showed dysfunction in endothelial-dependent vasorelaxation (Fukumura *et al.*, 2001). Another study observed impaired neovascularization (Aicher *et al.*, 2003). Interestingly, male *Nos3* KO mice seemed to additionally develop cardiac dilation and dysfunction, resulting in increased mortality compared to female *Nos3* KO animals (Li *et al.*, 2004).

Apart from blood pressure, decreased NOS expression or activity has been associated with pulmonary hypertension (Tonelli *et al.*, 2013) or heart failure (Mungrue *et al.*, 2002). Furthermore, NOS inhibition studies provided further evidence that lack of NO causes enhanced blood pressure in animal models and humans (Sakuma *et al.*, 1992, Clarkson *et al.*, 1995, Tsai and Kass, 2009). Thus, pharmacological targeting of NOS became of interest. So far, direct stimulation of NOS function is not possible. Nevertheless, enhancing NO synthesis using folate, which mimics a crucial co-factor for NO production, showed beneficial effects in patients suffering from FH (Verhaar *et al.*, 1998, Verhaar *et al.*, 1999), diabetes (van Etten *et*

al., 2002), and CAD (Doshi *et al.*, 2001, Doshi *et al.*, 2002, Tsai and Kass, 2009). Although the underlying mechanisms remain to be solved, increasing evidence suggests that observed effects may be cGMP-independent (Tsai and Kass, 2009).

Furthermore, NOS uncoupling may contribute to CAD progression. When NOS homodimers dissociate, superoxide radicals (O_2^-) form instead of NO. This phenomenon eventually leads to oxidative stress, inflammation, and endothelial dysfunction (Forstermann and Munzel, 2006). Moreover, observations in patients with early atherosclerosis suggested that NO uncoupling may facilitate hypertension and progression of atherosclerosis (Lavi *et al.*, 2007) (for an overview, see Dang *et al.* (2020)).

1.3.2 *GUCY1A1*

The variant rs13139571 is located within an intronic region of the *GUCY1A1* gene, formerly known as *GUCY1A3*, encoding the α_1 subunit of the sGC. So far, this variant has been associated with blood pressure. However, the mechanism of this particular variant has not been studied yet (International Consortium for Blood Pressure Genome-Wide Association Studies *et al.*, 2011).

Meanwhile, further genetic studies provided valuable insights about the presumable link between genetic alterations in *GUCY1A1* and CAD. Studying a family suffering from premature CAD/MI, Erdmann *et al.* discovered a frameshift (fs) mutation in *GUCY1A1* (p.Leu163Phefs*24) (Erdmann *et al.*, 2013). Intriguingly, all family members carrying this mutation together with another missense mutation in the *CCT7* gene (p.Ser525Leu) were affected by CAD. CCT7 has been shown to interact with sGC, probably leading to inhibition of the enzyme (Hanafy *et al.*, 2004). Indeed, platelets of digenic mutation carriers featured decreased sGC activity, proposing that sGC is involved in atherogenesis and atherothrombosis (Erdmann *et al.*, 2013). Furthermore, another *GUCY1A1* variant (rs7692387) was identified (CARDIoGRAMplusC4D Consortium *et al.*, 2013) to be associated with differential sGC expression, blood pressure, and CAD (Kessler *et al.*, 2017, Emdin *et al.*, 2018). In addition, Kessler *et al.* revealed disturbed transcription factor binding to the SNP site in the presence of the risk allele G, eventually leading to reduced sGC expression, hence dysregulation of downstream cGMP functions (Kessler *et al.*, 2017). Overall, coding variants of *GUCY1A1* are overrepresented in young MI patients (Erdmann *et al.*, 2013), and most of the disease-causing variants result in decreased sGC expression or activity (Wobst *et al.*, 2016).

In line with these findings, decreased sGC expression and sGC inhibition were linked to hypertension (Brune *et al.*, 1990, Weber *et al.*, 2001, Mollnau *et al.*, 2002), which could be replicated in mice lacking *Gucy1a1* (Friebe *et al.*, 2007, Segura-Puimedon *et al.*, 2016). Controversially, a complete loss of *Gucy1a1* seemed protective against atherosclerosis in mice (Segura-Puimedon *et al.*, 2016), while partial loss of *Gucy1a1* in mice was associated with

increased plaque sizes (Kessler *et al.*, 2017). Aside from classical hypertension, Vermeersch *et al.* demonstrated that *Gucy1a1* KO might inhibit pulmonary vascular remodeling under hypoxic conditions, suggesting a further influence of sGC on pulmonary hypertension (Vermeersch *et al.*, 2007). Furthermore, platelet-specific sGC deficient mice displayed diminished bleeding times, presumably due to increased formation of platelet aggregates (Dangel *et al.*, 2010).

On a different note, oxidative stress promotes the expression of an inactive oxidized/heme-free sGC. In this state, sGC is unable to respond to NO, interrupting NO-mediated signaling. This phenomenon had been observed in patients suffering from heart failure (Greene *et al.*, 2013, Lukowski *et al.*, 2014).

Together, alterations in sGC leading to decreased bioavailability of cGMP may have detrimental effects on atherosclerosis and CAD progression (for an overview, see Dang *et al.* (2020)).

1.3.3 *MRVI1*

The SNP rs7940646 is associated with adenosine diphosphate (ADP)-induced platelet aggregation in Europeans (Johnson *et al.*, 2010). This variant is located in an intronic region of the *MRVI1* gene encoding IRAG. Another SNP (rs11042937) has also been mapped to the *MRVI1* gene (Myocardial Infarction Genetics Consortium *et al.*, 2009). Of note, both SNPs are not in linkage disequilibrium, hence seem to act independently on CAD risk.

IRAG is a vital effector molecule of cGMP signal transduction in smooth muscle cells and platelets (Geiselhoringer *et al.*, 2004, Antl *et al.*, 2007). However, not much has been reported about IRAG dysfunction and CAD. *Irag* KO mice displayed impaired atrial natriuretic peptide (ANP)-mediated smooth muscle relaxation and enhanced platelet aggregation (Desch *et al.*, 2010, Schlossmann and Desch, 2011). ANP mediates NO-independent cGMP synthesis by pGC. Thus, observed effects in this mouse model may be NO-independent (for an overview, see Dang *et al.* (2020)).

1.3.4 *PDE3A*

Another variant (rs10841443), located close to *PDE3A*, was genome-wide significantly associated with CAD (Klarin *et al.*, 2017). However, to date, the relationship between this SNP, *PDE3A*, and CAD is unclear.

PDE3 is essential for different vascular functions, e.g., cardiac myocyte regulation, VSMC cell contractility, and VSMC phenotype switching (Tsai and Kass, 2009). In a study investigating several families suffering from brachydactyly and hypertension, Maass *et al.* identified several mutations in *PDE3A* (Maass *et al.*, 2015). This study suggested that enhanced PDE3 activity, diminished cAMP levels, and reduced VASP phosphorylation may

increase peripheral vascular resistance, eventually resulting in the disease phenotype seen in these families (Maass *et al.*, 2015). In contrast, chronic PDE3 inhibition was shown to increase mortality in heart failure patients (Ding *et al.*, 2005). Therefore, the role of PDE3 in CAD remains elusive (for an overview, see Dang *et al.* (2020)).

1.3.5 *PDE5A*

Just recently, *PDE5A* had been identified to be associated with CAD at the 4q27 locus (rs7678555). Interestingly, the risk allele of this variant is linked to increased *PDE5A* mRNA levels in the human aorta (Nelson *et al.*, 2017). Furthermore, preliminary data indicate that rs7678555 influences the expression of nearby encoded long non-coding RNA *LINC02502*, which interferes with the binding of the transcription factor REST to the *PDE5A* promoter thereby increasing *PDE5A* expression and CAD risk (Hegge *et al.*, 2020, Hoehne *et al.*, 2020).

In the vasculature, PDE5 function is well-described for VSMCs and platelets (Rybalkin *et al.*, 2002, Gresele *et al.*, 2011). Besides, PDE5 may also play a role in cardiac myocytes. However, this remains somewhat controversial (Wallis *et al.*, 1999, Lukowski *et al.*, 2014).

Up to now, PDE5 could not be studied in a KO mouse model, limiting the means to study PDE5 function. Nevertheless, currently available data from animal studies vigorously promote a crucial role of PDE5 in heart failure. For example, investigating a mouse model of cardiomyocyte-specific PDE5 overexpression revealed adverse left ventricular remodeling after MI (Pokreisz *et al.*, 2009). Similar effects were observed after subjecting the hearts of the same transgenic mouse model to pressure overload instead of MI (Vandenwijngaert *et al.*, 2013). Complementary to these findings, suppression of PDE5 expression in either a transgenic mouse line with doxycycline-controllable myocyte-specific PDE5 expression (Zhang *et al.*, 2010) or using the PDE5 inhibitor sildenafil (Takimoto *et al.*, 2005) resulted in a rescue of the previously observed maladapted responses to pressure overload. On a different note, preconditioning mice with sildenafil also led to cardioprotective effects (Salloum *et al.*, 2003, Vandeput *et al.*, 2009).

Increased PDE5 expression was also reported in patients with heart failure (Pokreisz *et al.*, 2009, Shan *et al.*, 2012), severe aortic stenosis (Vandenwijngaert *et al.*, 2013), and pulmonary hypertension (Corbin *et al.*, 2005), suggesting beneficial effects from using PDE5 inhibitors to treat cardiovascular diseases (for an overview, see Dang *et al.* (2020)).

1.4 Treatment of cardiovascular diseases with PDE5 inhibitors

The first attempts to pharmacologically target the NO-cGMP pathway consisted of using NO donors, e.g., for the treatment of angina pectoris (Horowitz *et al.*, 1988). However, long-term administration led to the emergence of tolerance against NO donors, prompting the search for other ways to modulate cGMP (Ghofrani *et al.*, 2006). The first successful PDE5

inhibitor was sildenafil. While initial studies failed to show a benefit of PDE5 inhibition for the treatment of angina pectoris (Ghofrani *et al.*, 2006), sildenafil, also known as Viagra, became more famous for its effect to improving erectile dysfunction (Rajfer *et al.*, 1992, Goldstein *et al.*, 1998). Over time, other studies hinted towards promising beneficial effects of sildenafil on vasodilation and platelet aggregation (Wallis *et al.*, 1999, Ghofrani *et al.*, 2006). Since then, many more PDE5 inhibitors have been developed and approved, including vardenafil, tadalafil, and avanafil.

So far, approved applications of PDE5 inhibitors include erectile dysfunction (Goldstein *et al.*, 1998, Ghofrani *et al.*, 2006), and pulmonary hypertension (Corbin *et al.*, 2005, Ghofrani *et al.*, 2006). Furthermore, since mouse studies suggest promising cardioprotective properties of PDE5 inhibitors (Salloum *et al.*, 2003, Salloum *et al.*, 2009, Vandeput *et al.*, 2009, Das *et al.*, 2015), many more diseases may be exciting fields of application for PDE5 inhibitor use, for example, heart failure (Guazzi *et al.*, 2011, Cooper *et al.*, 2013). However, results from clinical trials are somewhat mixed to disappointing (Lukowski *et al.*, 2014, Das *et al.*, 2015, Corinaldesi *et al.*, 2016), which might partially be attributed to cross-reactions of PDE5 inhibitors with other PDEs (Bischoff, 2004). In contrast, the pharmacological elevation of cGMP has proven to be promising in context of cardiovascular disease treatment, stressing that the potential of PDE5 inhibitors to treat cardiac indications requires further study.

1.5 Aim of the study

Although PDE5 has long been suspected of playing a role in cardiovascular diseases, the scientific focus shifted away from studying its role in CAD due to the disappointing results of PDE5 inhibitors in clinical trials. Regardless, recent GWAS findings strongly suggest a role of *PDE5A* in CAD. Hence, we aimed to gain mechanistic insights on how PDE5 might modulate coronary artery disease risk by studying rare *PDE5A* variants. Therefore, rare *PDE5A* variants identified in a discovery study were functionally validated, followed by an estimation of the cumulative genetic burden of rare loss-of-function *PDE5A* variants. Furthermore, we characterized a rare variant in *PDE5A* (rs201005905) that had been identified in a family with a high prevalence of CAD and MI. Finally, we investigated the effect of chronic PDE5 inhibition in an atherosclerotic mouse model.

Acquired findings may be helpful to refine or develop new strategies for the prevention and treatment of CAD targeting PDE5.

2 Materials

2.1 Chemicals

Table 1 List of chemicals, reagents, and media

Manufacturer	Headquarters	Chemical/Reagent/Medium	Catalog #
AppliChem	Darmstadt, Germany	Ampicillin sodium salt *BioChemica*	A0839
		Dimethyl sulfoxide (DMSO), cell culture grade	A3672
		DTT *BioChemica*	A1101
		EDTA	A5097
		Kanamycin sulfate *BioChemica*	A1493
		Methanol (MeOH)	131091
		Nonfat dry milk powder *BioChemica*	A0830
		TE buffer (1x) pH 8.0 low EDTA for molecular biology BC	A8569
		Tween® 20 *BioChemica*	A1389
Becton Dickinson	Franklin Lakes, NJ, USA	BD Difco™ agar, granulated	214530
		BD Bacto™ tryptone	211705
		BD Bacto™ yeast extract	212750
Bio-Rad	Hercules, CA, USA	2x Laemmli	1610737
		10x TRIS/glycine/SDS	161-0772
		Droplet Generation Oil for Probes	1863005
		Droplet Reader Oil	1863004
Carl Roth	Karlsruhe, Germany	2-propanol ROTIPURAN® ≥99.8 %	6752
		Eosin Y solution 0.5 % in water	X883.1
		Ethanol, denatured, ≥99,8 %	K928.1
		Hemalum solution acid acc. to Mayer	T865.2
		Hydrochloric acid (HCl), 6N	281
		Glycine PUFFERAN® ≥99 %	3908
		TRIS hydrochloride (TRIS-HCl) PUFFERAN® ≥99 %	9090
		Xylol	9713.3
Envigo	Indianapolis, IN, USA	High fat diet	TD88137
Enzo Life Sciences	Farmingdale, NY, USA	S-nitrosoglutathione (GSNO)	420-002
In-house pharmacy/ Fagron GmbH & Co. KG	Glinde, Germany	Sildenafil Citrate	247216-0005
Ipracell		HeLa nuclear lysates	CC-01-20-005
Lonza	Basel, Switzerland	HEPES Buffered Saline Solution, 30 mM	CC-5024
Merck Millipore	Burlington, MA, USA	β-mercaptoethanol	M3148
		Chloroform	C2432
		EMPURA® ethanol absolute	1070172511
		FBS Superior	S0615
		HEPES	H4034
		NaCl	7647-14-5
		Penicillin-Streptomycin	P4333
		Nonidet™ P 40 Substitute solution	98379
		Sodium pyruvate (100 mM)	L0473
		Tetraethylammonium bromide (TEAB)	86608
New England BioLabs	Ipswich, MA, USA	Gel Loading Dye Purple	B7024S
		Color Prestained Protein Standard, Broad Range (10-250 kDa)	P7719S
		Quick-Load® 2-Log DNA Ladder (0.1-10.0 kb)	N4695
		RIPA (10x)	9806
Promega	Fitchburg, WI, USA	FuGENE® HD transfection reagent	E2312
PromoCell	Heidelberg, Germany	Freezing Medium Cryo-SFM	C-29910
		DetachKit (including HEPES, trypsin, and TNS)	C-41200
		Smooth Muscle Cell Growth Medium 2 (including supplement)	C-22162

Manufacturer	Headquarters	Chemical/Reagent/Medium	Catalog #
		TNT® Quick Coupled Transcription/ Translation System	L1170
Roche	Basel, Switzerland	Poly(A)	10108626001
Thermo Fisher Scientific	Waltham, MA, USA	Gibco™ DMEM, high glucose	11965084
		Gibco™ PBS (10X), pH 7.4	70011044
		Gibco™ PBS, pH 7.4	10010023
		Gibco™ Opti-MEM® I reduced serum medium	31985062
		Gibco™ RPMI 1640 Medium	11530586
		Gibco™ trypsin-EDTA (0.25 %), phenol red	25200056
		Invitrogen™ Dynabeads™ MyOne™ Straptavidin T1	65601
		Invitrogen™ GlycoBlue™ coprecipitant	AM9515
		Invitrogen™ Lipofectamine RNAiMAX™ transfection reagent	13778150
		Invitrogen™ Ultrapure™ DNase-/RNase-free distilled water	10977035
		Invitrogen™ Ultrapure™ TBE Buffer, 10x	15581028
		Invitrogen™ TRIzol	15596026
		Novex™ MagicMark™ XP Western protein standard	LC5602
		SuperSignal™ West Dura Extended Duration Substrate	34075
		Taqman™ Universal Master Mix II, no UNG	4440040
		Thermo Scientific™ EDTA-free HALT™ protease inhibitor (100x)	78425
VWR	Erlangen, Germany	PegGREEN	732-3196
		Universal agarose, peqGOLD	732-2789

2.2 Formulations

2.2.1 General buffers/dilutions

1x phosphate buffered saline (PBS):

100 ml 10x Gibco™ PBS (Thermo Fisher Scientific)

Up to 1000 ml Miilipore® water

Storage at room temperature; for all purposes except cell culture

70% v/v ethanol:

35 ml EMPURA® ethanol absolute (Merck Millipore)

Up to 50 ml DNase-/RNase-free water (Thermo Fisher Scientific)

Storage at room temperature

2.2.2 Buffer for agarose gel electrophoresis

1x TRIS-borate-EDTA (TBE) buffer:

100 ml 10x Invitrogen™ Ultrapure™ TBE Buffer (Thermo Fisher Scientific)

Up to 1000 ml Millipore® water
Storage at room temperature

2.2.3 Cell culture media

HEK293, GC-HEK, HeLa, COS-7:
445 ml Gibco™ DMEM, high glucose (Thermo Fisher Scientific)
50 ml FBS Superior (Merck Millipore)
5 ml Penicillin-Streptomycin (10000 u penicillin and 10 mg/ml streptomycin) (Merck Millipore)
Storage at 4°C

MEG-01:
443 ml Gibco™ RPMI 1640 Medium (Thermo Fisher Scientific)
50 ml FBS Superior (Merck Millipore)
5 ml Penicillin-Streptomycin (10000 u penicillin and 10 mg/ml streptomycin) (Merck Millipore)
2 ml sodium pyruvate (Merck Millipore)
Storage at 4°C

HCASMC:
Combined all components of the Smooth Muscle Cell Growth Medium 2 kit (PromoCell)
Storage at 4°C for 1 month

2.2.4 Buffer and media for bacteria

Ampicillin (100 mg/ml) and kanamycin (50 mg/ml) stock solutions:
100 mg ampicillin sodium salt or 50 mg kanamycin sulfate (both AppliChem)
Up to 1 ml Millipore® water
Sterile filtering using Stericup® filters (Merck Millipore)
Storage at -20°C

Lysogeny broth (LB) medium:
8g BD Bacto™ tryptone (Becton Dickinson)
4g BD Bacto™ yeast extract (Becton Dickinson)
8g sodium chloride (AppliChem)
Up to 800 ml Millipore® water
Autoclaved at 121°C for 20 min
Storage at 4°C

LB agar plates:

8 g BD Bacto™ tryptone (Becton Dickinson)

4 g BD Bacto™ yeast extract (Becton Dickinson)

8 g sodium chloride (AppliChem)

12 g BD Difco™ agar, granulated (Becton Dickinson)

Up to 800 ml Millipore® water

Autoclaved at 121°C for 20 min

Added 800 µl ampicillin or kanamycin stock solution when solution had cooled down to 50°C

Poured into 10 cm petri dishes

Storage at 4°C

2.2.5 Oligonucleotide pull-down buffers

Desoxyribonucleic acid (DNA) binding buffer (DBB):

With a final concentration of 10 mM HEPES, pH 8.0, 1 mM NaCl, 0.05% v/v Nonidet P-40, and 10 mM EDTA

0.12 g HEPES, pH 8.0 (Merck Millipore)

0.0029 g NaCl (Merck Millipore)

0.15 g EDTA (AppliChem)

25 µl Nonidet P-40 (Merck Millipore)

45 ml Millipore® water

Adjusted pH to 8.0

Up to 50 ml Millipore® water

Storage at 4°C

Protein binding buffer PBB:

With a final concentration of 50 mM HEPES, pH 8.0, 150 mM NaCl, 0.1% Nonidet P-40, and 1 mM DTT

0.60 g HEPES, pH 8.0 (Merck Millipore)

0.44 g NaCl (Merck Millipore)

50 µl Nonidet P-40 (Merck Millipore)

45 ml Millipore® water

Adjusted pH to 8.0

Up to 50 ml Millipore® water

Added DTT (0.1 M stock, see below) 1:100 to required amount of buffer prior each use

Storage at 4°C

Wash buffer (WB):

With a final concentration of 100 mM TEAB and 150 mM NaCl

0.21 g TEAB (Merck Millipore)

0.09 g NaCl (Merck Millipore)

Up to 10 ml Millipore® water

Storage at 4°C

0.1 M DTT:

0.02 g DTT (AppliChem)

1 ml Millipore® water

Storage at -20°C

2.2.6 Western blotting buffer and solutions

1x radioimmunoprecipitation assay (RIPA) buffer:

10 ml 10x RIPA (New England BioLabs)

Up to 100 ml Millipore® water

Storage at -20°C

2x Laemmli buffer with β-mercaptoethanol:

With a final concentration of 355 mM β-mercaptoethanol

950 µl 2x Laemmli buffer (Bio-Rad)

50 µl β-mercaptoethanol (Merck Millipore)

Storage at -20°C

1x Running buffer:

100 ml 10x Tris/Glycine/SDS (Bio-Rad)

2 ml Tween® 20 (AppliChem)

Up to 1000 ml Millipore® water

Storage at room temperature

1x Transfer buffer:
3.03 g TRIS PUFFERAN® (Carl Roth)
14.4 g glycine PUFFERAN® (Carl Roth)
200 ml methanol (AppliChem)
Up to 1000 ml Millipore® water
Storage at room temperature

1x PBS-T:
With a final concentration of 0.2% v/v Tween® 20, pH 7.4 at room temperature
100 ml 10x Gibco™ PBS (Thermo Fisher Scientific)
2.0 ml Tween® 20 (AppliChem)
Up to 1000 ml Millipore® water
Storage at room temperature

5% w/v milk in PBS:
2.5 g nonfat dry milk powder (AppliChem)
10 ml 10x Gibco™ PBS (Thermo Fisher Scientific)
Up to 100 ml Millipore® water
Storage at 4°C for up to three days

2.5% w/v milk in PBS-T:
2.5 g nonfat dry milk powder (AppliChem)
100 ml 1x PBS-T (see above)
Storage at 4°C for up to three days

2.2.7 Radioimmunoassay solutions

1 mM S-nitrosoglutathione (GSNO):
0.001 g GSNO (Enzo Life Sciences)
Up to 2.97 ml 30 mM HEPES (Lonza)
Prepared new 1 mM GNSO solution for every experiment

60 mM HCl:
500 µl HCl (6N) (Carl Roth)
Up to 50 ml Millipore® water
Storage at 4°C

2.2.8 Staining solutions

Ethanol dilution series 96% (or 70%):

96 ml (or 70 ml) Ethanol, denatured, ≥99,8 % (Carl Roth)

Up to 100 ml Millipore® water

Storage at room temperature

0.1% HCl:

5 ml HCl (6N) (Carl Roth)

Up to 1000 ml Millipore® water

Storage at room temperature

2.3 Primer

2.3.1 Gateway™ cloning primers

Table 2 Gateway™ cloning primers

Name	Purpose	Direction	Sequence (from 5' to 3')	Amplicon size (bp)
ZFX-V5 CDS	*ZFX* CDS into pDONR™221	forward	GGGGACAAGTTTGTACAAAAAA GCAGGCTTCGAAGGAGATAGA ACCATGGATGAAGATGGGCTT GAATTACAACAAGAGCCA	2535
		reverse	GGGGACCACTTTGTACAAGAA AGCTGGGTCGGGCAGGCCAAC TTCTTTATGATGTCGCATTAT	

2.3.2 Mutagenesis primers

Table 3 Mutagenesis primers

Name	Purpose	Direction	Sequence (from 5' to 3')
PDE5A2-V5 mut 1	RefSeq	forward	CGTGCAGATAACAGTGCCCCTGGAACACCAACC
		reverse	GGTTGGTGTTCCAGGGGCACTGTTATCTGCACG
PDE5A2-V5 mut 2	RefSeq	forward	GTTCCTTCTTTTCTGAGTCAGAGAGGAAGCTCACA
		reverse	TGTGAGCTTCCTCTCTGACTCAGAAAAGAAGGAAC
PDE5A2-V5 mut 3	RefSeq	forward	GTTCTATGTTGAGTTCTTTTCTCTCTCTGTCTCCTTGA TCAAAAAAT
		reverse	ATTTTTTGATCAAGGAGACAGAGAGAGAAAAGAACTC AACATAGAAC
PDE5A2-V5 mut 4	RefSeq	forward	CATGTTGCCCTTTGGAGACTAAACAAGAGAAATGGT CAA
		reverse	TTGACCATTTCTCTTGTTTAGTCTCCAAAGGGCAACA TG
PDE5A2-V5-ΔMet2	Methionine deletion	forward	CCCTTTGGAGACTAAACAAGAGAAAAGGTCAATGCA TGG
		reverse	CCATGCATTGACCTTTTCTCTTGTTTAGTCTCCAAAG GG
PDE5A2-V5-ΔMet3	Methionine deletion	forward	GGGGTTAGAGGCTTCTGTTCCTTCTTTTCTGAGTCA
		reverse	TGACTCAGAAAAGAAGGAACAGAAGCCTCTAACCCC
PDE5A2-stop	V5 removal	forward	GCTGGGTCAAGCTTTCAGTTCCGCTTGGCCT

Name	Purpose	Direction	Sequence (from 5' to 3')
		reverse	AGGCCAAGCGGAACTGAAAGCTTGACCCAGC
PDE5A2-M1	Rare variant	forward	ATCAGCATCTTCTCCTACTGTTCTGCAAGGGCC
		reverse	GGCCCTTGCAGAACAGTAGGAGAAGATGCTGAT
PDE5A2-M13	Rare variant	forward	ACAAGTTCTGCTGTCCGTTGTTGAATAGGCCAGGGT
		reverse	ACCCTGGCCTATTCAACAACGGACAGCAGAACTTGT
PDE5A2-M38	Rare variant	forward	CCGCTTGGCCTGGCTGCTTTCCCCATTAA
		reverse	TTAATGGGGAAAGCAGCCAGGCCAAGCGG
PDE5A2-M45	Rare variant	forward	GGATCTTCCAAATTGAATTGATTTTTTTTTATAAGTTC AAAAAATTCTCCTCGCC
		reverse	GGCGAGGAGAATTTTTTGAACTTATAAAAAAAAATCA ATTCAATTTGGAAGATCC
PDE5A2-M50	Rare variant	forward	GTTGAAAGGCTTAACCTGGCCAGTATTCTCCTCCA
		reverse	TGGAGGAGAATACTGGCCAGGTTAAGCCTTTCAAC
PDE5A2-M61	Rare variant	forward	GGAAGCTCACAGTTCCCACAGAATCCTTGACAACA
		reverse	TGTTGTCAAGGATTCTGTGGGAACTGTGAGCTTCC
ZFX-V5 mut	RefSeq	forward	CTGCAGCATCCTCCTCTCCTACGATCACTTCCATA
		reverse	TATGGAAGTGATCGTAGGAGAGGAGGATGCTGCAG

2.3.3 Sequencing primers

Table 4 Sequencing primers

Name	Direction	Sequence (from 5' to 3')
PDE5A2 seq	forward	GAATCATAGGGAAGAGGTTG
	forward	CAAACAAAATCAATTACATG
	forward	ATCTAATGAACAGGGAGAAG
pGL4.10 seq	forward	CTAGCAAAATAGGCTGTCCC
	reverse	GACGATAGTCATGCCCCGCG
ZFX-V5 seq	forward	GAAGTTTCTTTAGCACATTG
	forward	ACTCTCAGCCAGAAGATGAA
	forward	ACTCACAAAATGGTGCATAA
	forward	TAAGTCGCCATATTCTCTCA

2.3.4 Polymerase chain reaction (PCR) primers

Table 5 PCR primers

Target gene	Application	Direction	Sequence (from 5' to 3')	Amplicon size (bp)
Gucy1a1 mouse	qPCR	forward	CAACCGTGCCCATCTGTCAAG	147
		reverse	CATTCAGCCGTTCAAACTCTGG	
Irag mouse	qPCR	forward	ACAAGAGGCTTTCTCACCGA	118
		reverse	TCTGAGATGCTGATGTCTGGC	
Nos3 mouse	qPCR	forward	AGTGGCTGGTACATGAGCAC	189
		reverse	GGTGACTTTGGCTAGCTGGT	
PDE5A	qPCR	forward	TGGTGAGCCCTTGAACATCA	140
		reverse	GGGCTACACCAACAACCTCT	
PDE5A alt. prom.	qPCR (ChIP)	forward	AAAAGTGGGAAGGGACGTAG	75
		reverse	ACGTTTGCTATGTTGCCCTT	
Pde5a mouse	qPCR	forward	GGCAAGCACCATGGAACGA	148
		reverse	TGCGTTGACCATGTCTCTGG	
RPLP0	qPCR	forward	GGCACCATTGAAATCCTGAGTG	120
		reverse	GATGACCAGCCCAAAGGAGAAG	
Rplp0 mouse	qPCR	forward	TCACTGTGCCAGCTCAGAAC	120
		reverse	ATCAGCTGCACATCACTCAGA	
ZFX	qPCR	forward	CGAGACAGCTGAACAAGGGT	115
		reverse	TTTGAGCTCTGACGGGTGAC	
ZFX	Endpoint PCR	forward	TCTCTCATGCAGGGGCTTTG	427
		reverse	TCGCAATGCAAACACTGGTG	

2.3.5 Commercial PCR primers

Following primers were provided as 2.5 µM stocks. In contrast to other qPCR primers, no working solution was prepared from these stocks. Instead, 4 µl of the 2.5 µM primers were used per reaction.

Table 6 Commercially purchased qPCR primers

Manufacturer	Headquarter	Name	Description	Catalog #
Active Motif	Carlsbad, CA, USA	Human Negative Control Primer Set 1	Primers targeting a gene desert	71001
		Human Positive Control Primer Set GAPDH-1	Primers targeting the *GAPDH* promoter	71004

2.3.6 Probes

Probes were synthesized by Integrated DNA Technologies (Coralville, IA, USA) in HPLC grade purity and provided as a 20x stock. Stocks were stored at -20°C.

Table 7 List of probes

Target gene	Application	Direction	Sequence (from 5' to 3')
PDE5A alt. prom.	ddPCR	forward	GTAATGCCGCCTCGCTAG
		reverse	CATAGCAAACGTGGGAAGTT
		probe	FAM-TTGTCACGT-ZEN-TAAGCTGGCCC

2.3.7 Commercial probes

For the allelic imbalance assay, a probe (assay ID dMDS155472717) targeting rs201005905 was designed using the custom probe design service of Bio-Rad (Hercules, CA, USA). The probe was provided in HPLC grade purity as a 20x stock. Stocks were stored at -20°C.

For genotyping, a probe targeting rs201005905 was designed using the custom probe (assay ID AHGJ63D) design service of Thermo Fisher Scientific (Waltham, MA, USA). The probe was provided as an 80x stock, diluted to 20x using DNase-/RNase-free water, and stored as aliquots at -20°C.

2.4 Nucleic acids

2.4.1 Commercial ribonucleic acids (RNAs)

Table 8 Commercially purchased RNAs

Manufacturer	Headquarter	Name	Catalog #
BioCat GmbH	Heidelberg, Germany	Human Adult Normal Heart, total RNA	ATR1234122-50-BC

2.4.2 Small interfering ribonucleic acid (siRNA)

Table 9 Commercially purchased siRNAs

Manufacturer	Headquarter	Target gene	Assay ID	Catalog #
Thermo Fisher Scientific	Waltham, MA, USA	*ZFX*	s14990	4392420
		Scrambled control siRNA	-	4390843

2.4.3 gBlocks™

gBlocks™ were synthesized by Integrated DNA Technologies (Coralville, IA, USA). Lyophilized gBlocks™ were stored at -20°C until use.

Table 10 List of designed gBlocks™

Name	Application	Sequence (from 5' to 3')
PDE5A alt. prom. WT	ddPCR	CCCATGAGACATACAAAAAGGTAATGCCGCCTCGCTAGGTGAG CTACAGCTCGATTGTCACGTTAAGCTGGCCCCTCCTGGAGTCC AGGATCGGCGGAGTTCGAAAACGAACTTCCCACGTTTGCTATG TTGCCCTTTGGAGACAAAACAAGAGAAATGGTCAATGCATGGT TTGCTGAGAGAGTTCACACCATCCCTGTGTGCAAGGAAGGTAT CAGGTCTCGACTATACGCCCGTTTTCGGATC
PDE5A alt. prom. MUT	ddPCR	CCCATGAGACATACAAAAAGGTAATGCCGCCTCGCTAGGTGAG CTACAGCTCGATTGTCACGTTAAGCTGGCCCCTCCTGGAGTCC AGGATCGGCGGAGTTCGAAAACGAACTTCCCACGTTTGCTATG TTGCCCTTTGGAGACTAAACAAGAGAAATGGTCAATGCATGGT TTGCTGAGAGAGTTCACACCATCCCTGTGTGCAAGGAAGGTAT CAGGTCTCGACTATACGCCCGTTTTCGGATC

2.4.4 Oligo nucleotides for protein pull-down

All sequences were kindly provided by Martin Dichgans (Institute for Stroke and Dementia, LMU Munich, Munich, Germany). Oligonucleotides were synthesized by Integrated DNA Technologies (Coralville, IA, USA). Lyophilized oligonucleotides were adjusted to 100 µM stocks using DNase-/RNase-free water and stored at -20°C.

Table 11 List of oligonucleotides designed for protein pull-down

Target gene	Direction	Sequence (from 5' to 3')
PDE5A alt. prom. WT	forward	TTCTGAAGGAAGTACCTTGTTTTGTCTCCAAAGGGCAACATAG
	reverse	AACTATGTTGCCCTTTGGAGACAAAACAAGGTACTTCCTTCAG
PDE5A alt. prom. MUT	forward	TTCTGAAGGAAGTACCTTGTTTAGTCTCCAAAGGGCAACATAG
	reverse	AACTATGTTGCCCTTTGGAGACTAAACAAGGTACTTCCTTCAG
Desthiobiotin-adapter	forward	Desthiobiotin-CAGGCTCCGAATTCGCCCTT
	reverse	TTAAGGGCGAATTCGGAGCCTG

2.5 Plasmids

2.5.1 Commercially available plasmids

Table 12 Commercially purchased plasmids

Manufacturer	Headquarter	Catalog #	Name	Description	Selection
Promega	Fitchburg, WI, USA	E6651	pGL4.10[*luc2*]	Promoterless firefly luciferase reporter vector	Ampicillin
		E2241	pRL-TK	*Renilla* luciferase under control of a minimal promoter	Ampicillin
Thermo Fisher Scientific	Waltham, MA, USA	12536017	Invitrogen™ Gateway™ pDONR™221	Entry vector	Kanamycin
		12274015	Invitrogen™ Gateway™ pcDNA™-DEST40	Expression vector with V5 tag	Ampicillin

2.5.2 Cloned constructs

The pGL4.10 constructs containing the *PDE5A* alternative promoter sequence flanking rs201005905 with either the non-effect/wild-type (WT) or risk/mutant allele (MUT), named pGL4.10-*PDE5A2* alternative promoter-WT/MUT, were kindly provided by Jeanette Erdmann (Cardiogenetics, University of Lübeck, Lübeck, Germany). Another plasmid containing the full-length *PDE5A2* coding sequence (CDS) in an Invitrogen™ Gateway™ pDONR™221 vector was purchased from PlasmID (HsCD00081701; service is no longer available; the website was formerly accessed through https://plasmid.med.harvard.edu/PLASMID/Home.xhtml). All other constructs that had been cloned for this study are listed below.

Table 13 List of all cloned plasmid constructs

Backbone	Insert description	Selection	Control digest	Sizes (bp)
Invitrogen™ Gateway™ pDONR™221	*ZFX* isoform 1 CDS without stop	Kanamycin	BseYI	3417 1568
Invitrogen™ Gateway™ pcDNA™-DEST40	*PDE5A2* CDS without stop WT	Ampicillin	PstI	1534 6473
	PDE5A2 CDS without stop MUT	Ampicillin	PstI	1534 6473
	PDE5A2 CDS with stop WT	Ampicillin	PstI	1537 6473
	PDE5A2 CDS with stop MUT	Ampicillin	PstI	1537 6473
	PDE5A2 CDS-M1 with stop	Ampicillin	PstI	1537 6473
	PDE5A2 CDS-M13 with stop	Ampicillin	PstI	1537 6473
	PDE5A2 CDS-M38 with stop	Ampicillin	PstI	1537 6473
	PDE5A2 CDS-M45 with stop	Ampicillin	PstI	1537 6473
	PDE5A2 CDS-M50 with stop	Ampicillin	PstI	1537 6473
	PDE5A2 CDS-M61 with stop	Ampicillin	PstI	1537

Backbone	Insert description	Selection	Control digest	Sizes (bp)
	ZFX isoform 1 CDS without stop	Ampicillin	SacI	6473 6103 1826

2.6 Enzymes

2.6.1 Cloning enzymes

Table 14 Enzymes for cloning reactions

Manufacturer	Headquarter	Catalog #	Name
Thermo Fisher Scientific	Waltham, MA, USA	11789020	Invitrogen™ Gateway™ BP Clonase™ II enzyme mix (including Proteinase K)
		11791100	Invitrogen™ Gateway® LR Clonase® II enzyme mix (including Proteinase K)

2.6.2 Digestion enzymes

Table 15 Plasmid digestion enzymes

Manufacturer	Headquarter	Catalog #	Name	Buffer	Temperature (°C)
New England BioLabs	Ipswich, MA, USA	R0635	BseYI	NEBuffer r3.1	37°C
		R0108S	HaeIII	ddPCR master mix	ddPCR settings
		R3140S	PstI	CutSmart	37°C
		R3156	SacI	CutSmart	37°C

2.6.3 Concatemerization enzymes

Table 16 Enzymes used for concatemerization of bait oligonucleotides

Manufacturer	Headquarter	Catalog #	Name
Thermo Fisher Scientific	Waltham, MA, USA	15224041	Invitrogen™ T4 DNA Ligase (5 u/µl) (including buffers for concatemerization
		EK0031	Thermo Scientific™ T4 Polynucleotide Kinase (10 U/µL) (including buffers for concatemerization)

2.7 Antibodies

2.7.1 Western blot primary antibodies

Table 17 Western blot primary antibodies

Manufacturer	Headquarter	Catalog #	Name
Cell Signaling Technology	Danvers, MA, USA	#2118	GAPDH (14C10) Rabbit mAb
		#13202	V5-Tag (D3H8Q) Rabbit mAb
		#5419	ZFX (L28B6) Mouse mAb

2.7.2 Western blot HRP-conjugated secondary antibodies

Table 18 HRP-conjugated secondary antibodies for western blot

Manufacturer	Headquarter	Catalog #	Name
Cell Signaling Technology	Danvers, MA, USA	#7074	Anti-rabbit IgG, HRP-linked Antibody
		#7076	Anti-mouse IgG, HRP-linked Antibody

2.7.3 Chromatin immunoprecipitation (ChiP) antibodies

Table 19 ChIP antibodies

Manufacturer	Headquarter	Catalog #	Name
abcam	Cambridge, UK	ab15828	Anti-V5 tag antibody (anti-rabbit)
Merck Millipore	Burlington, MA, USA	PP64	Sigma-Aldrich IgG, Rabbit

2.8 Cell lines

2.8.1 Immortalized cell lines

HEK293 were a kind gift from Steffen Massberg (Medizinische Klinik und Poliklinik I, LMU Munich, Munich, Germany). GC-HEK (HEK293 stably overexpressing sGC) (Mullershausen *et al.*, 2004) were kindly gifted by Andreas Friebe (Department of Physiology I, University of Würzburg, Würzburg, Germany). All other immortalized cell lines used in this study are listed below.

Table 20 Immortalized cell lines

Manufacturer	Headquarter	Catalog #	Name
ATCC	Manassas, VA, USA	CRL-1651	COS-7
		CCL-2	HeLa
		CRL-2021	MEG-01

2.8.2 Primary cells

Table 21 Primary cells

Manufacturer	Headquarter	Catalog #	Name
PromoCell	Heidelberg,Germany	C-12511	HCASMC

2.9 Competent bacteria

Table 22 Competent bacteria

Manufacturer	Headquarter	Catalog #	Name
Agilent Technologies	Santa Clara, CA, USA	200317	XL10-Gold Ultracompetent Cells

Manufacturer	Headquarter	Catalog #	Name
New England BioLabs	Ipswich, MA, USA	#C2987	NEB® 5-alpha Electrocompetent *E.Coli*

2.10 Animals

B6.129P2-Apoetm1Unc/J, in the following called *Apoe* KO mice, that were used in this study were purchased either from Jackson Laboratories (Bar Harbor, ME, USA) or bred in our own animal facility.

2.11 Commercial kits

2.11.1 Kits and assays

Table 23 Kits and assays

Manufacturer	Headquarters	Catalog #	Name
Active Motif	Carlsbad, CA, USA	53040	ChIP-IT High Sensitivity® Kit
Agilent Technologies	Santa Clara, CA, USA	200521	QuikChange II Site-Directed Mutagenesis Kit (including DpnI enzyme and PfuUltra High Fidelity polymerase)
Eurofins Genomics	Ebersberg, Germany	n.a.	Mix2Seq kit
Promega Corporation	Madison, WI, USA	E1960	Dual-Luciferase® reporter assay system
Qiagen	Hilden, Germany	158445	Gentra® Puregene® blood kit
		28604	MinElute® Gel Extraction Kit
		51304	QIAamp® DNA Mini Kit
		12162	QIAGEN Plasmid Maxi Kit
		74134	RNeasy Plus Universal Kit
Merck Millipore	St. Louis, MO, USA	PLN350-1KT	Sigma-Aldrich GeneElute™ plasmid miniprep kit
Tecan/ibl international	Männedorf, Switzerland	RE29071	cGMP RIA
Thermo Fisher Scientific	Waltham, MA, USA	M1681	Maxima™ H Minus cDNA Synthesis MasterMix with dsDNase
		23227	Thermo Scientific ™ Pierce™ BCA Protein Assay Kit

2.11.2 Polymerases

Table 24 Polymerases

Manufacturer	Headquarters	Catalog #	Name
Bio-Rad	Hercules, CA, USA	186-3023	ddPCR Supermix for Probes (No dUTP)
New England BioLabs	Ipswich, MA, USA	M0486S	OneTaq® Quick-Load 2x Master Mix with Standard Buffer
		M0491S	Q5® High-Fidelity DNA Polymerase
Quantabio	Gaithersburg, MD, USA	95074-250	PerfeCTa SYBR® Green FastMix (low ROX)

2.12 Consumables

Table 25 Consumables

Manufacturer	Headquarter	Catalog #	Name
5 PRIME GmbH	Hilden, Germany	2302810	Phase lock gel, heavy, 1.5 ml
Becton Dickinson	Franklin Lakes, NJ, USA	762165	PAXgene® Blood RNA Tube
		368861	BD Vacutainer EDTA tube
		364815	BD Vacutainer One-Use Holder
		368975	BD Vacutainer Plus Plastic Serum Tube (Discard Tube)
		367286	BD Vacutainer Safety-Lok™ Blood Collection Set
Bio-Rad	Hercules, CA, USA	#4561023	7.5% Mini-PROTEAN® TGX™ Precast Protein Gels, 10-well
		#1864008	DG8 Cartridges
		#1863009	DG8 Cartridge
Merck Millipore	Billerica, MA, USA	IPVH00010	Immobilon®-P PVDF membrane, 0.45 µm
		PHCC60050	Scepter™ cell counter sensors, 60 µm
		SCGPU01RE	Stericup®-GP, 0.22 µm, polyethersulfone, 150 ml, radio-sterilised
Thermo Fisher Scientific	Waltham, MA, USA	4346907	Applied Biosystems™ MicroAmp® fast optical 96 well reaction plate, 0.1 ml
		4309849	Applied Biosystems™ MicroAmp® optical 384 well reaction plate with barcode
		4311971	Applied Biosystems™ MicroAmp® optical adhesive film

2.13 Devices and utensils

Table 26 Devices and utensils

Manufacturer	Headquarter	Name	Application
Berthold	Bad Wildbad, Germany	Multi Crystal 2111 RIA gamma counter	Radioimmunoassay
Bio-Rad	Hercules, CA, USA	Mini-PROTEAN® tetra cell	Gel electrophoresis
		Mini Trans-Blot® electrophoretic transfer cell	Western blotting
		PX1 PCR Plate Sealer	Sealing 96-well plates
		QX200 Droplet Generator	ddPCR droplet generation
		QX200 Droplet Reader	ddPCR readout
Cytiva	Marlborough, MA, USA	Amersham ImageQuant 800	Western blot and gel documentation
Leica	Wetzlar, Germany	DMRB microscope	Histology documentation
		DFC450C camera	Histology documentation
		CM1850	Cryosectioning
Merck Millipore	Billerica, MA, USA	Milli-Q® Reference	Millipore® water system
		Scepter™ 2.0 Cell Counter	Cell counting
Nikon	Tokyo, Japan	Eclipse TS100	Cell culture microscopy
Olympus	Tokyo, Japan	IX50	Cell culture microscopy
Tecan	Männedorf, Switzerland	Infinite® M200 Pro	Photometric measurements

Manufacturer	Headquarter	Name	Application
		NanoQuant Plate™	DNA/RNA quantification
Thermo Fisher Scientific	Waltham, MA, USA	Applied Biosystems™ Veriti™ Thermal Cycler, 96-Well	cDNA synthesis, endpoint PCR, ddPCR
		Applied Biosystems™ ViiA™ 7 real-time PCR system	qPCR

2.14 Software

Table 27 Software

Manufacturer	Headquarter	Name	Application
Berthold	Bad Wildbad, Germany	LBIS	Radioimmuoassay
Bio-Rad	Herculas, CA, USA	QuantaSoft	ddPCR
Cytiva	Marlborough, MA, USA	IQ800	Western blot and gel documentation
GraphPad Software, Inc	San Diego, CA, USA	GrapPad Prism 9	Statistical analysis
National Institutes of Health	Bethesda, MD, USA	ImageJ 1.52q	Plaque size analysis
Qiagen	Hilden, Germany	CLC Main Workbench 7	Cloning
Tecan	Männedorf, Switzerland	iControl v1.10	Luciferase assay, RNA, DNA, and protein concentration measurement
Thermo Fisher Scientific	Waltham, MA, USA	ViiA™ 7 software v1.2.2	qPCR and genotyping
The R Project, The R foundation	Vienna, Austria	R version 3.6.1	LOD score calculation

2.15 Databases

Ensembl Genome Browser: http://www.ensembl.org

Eukaryotic Promoter Database (EPD): https://epd.epfl.ch//index.php

National Center for Biotechnology Information (NCBI): https://www.ncbi.nlm.nih.gov/

UCSC Genome Browser: *https://genome.ucsc.edu*

2.16 Online tools and resources

AliBaba2.1: http://www.gene-regulation.com/pub/programs/alibaba2/index.html?

Agilent QuikChange Primer Design: https://www.agilent.com/store/primerDesignProgram.jsp

NEBcutter V2.0: http://nc2.neb.com/NEBcutter2/

Protein molecular weight prediction: https://www.bioinformatics.org/sms/prot_mw.html

Servier Medical Art: smart.servier.com

3 Methods

3.1 Ethics statement

The family that was investigated in this study, was identified and biospecimen were collected and analyzed as part of the German MI Family Heart study. Prior to sample collection, all participating individuals gave written informed consent. Study approvals were obtained by the local institutional ethics committees (University of Regensburg, Regensburg, Germany, and University of Lübeck, Lübeck, Germany).

3.2 Molecular cloning

3.2.1 Primer design for molecular cloning

Gateway™ cloning primers: Primers for cloning *ZFX* were designed according to the instruction of the Invitrogen™ Gateway™ gene cloning (Thermo Fisher Scientific) manual. In brief, the forward primer contained the sequence for the Gateway™ *att*B1 site, the Shine-Dalgarno sequence (a ribosomal binding site in prokaryotic mRNA), the Kozak sequence (a ribosomal site in eukaryotic mRNA), plus 18-25 base pairs (bp) of the 5' end of the complete *ZFX* consensus coding sequence (CDS). The *ZFX* consensus CDS was retrieved from NCBI (https://www.ncbi.nlm.nih.gov/). Care was taken to design the forward primer so that the CDS would be in frame with the V5 tag sequence downstream of the CDS insertion site of the Gateway™ pcDNA™-DEST40 vector. Similar to the forward primer, the reverse primer contained the sequence for the Gateway® *att*B2 site together with the 3'end of the ZFX consensus CDS without a stop codon, allowing the *ZFX* CDS to fuse with the V5 tag provided on the vector when expressed. Corresponding forward and reverse primer pairs were chosen based on the similarity of annealing temperature (T_a).

Mutagenesis primers: Primers were designed using the online tool Agilent QuikChange Primer Design (accessed through https://www.agilent.com/store/primerDesignProgram.jsp) according to the website's instructions.

Sequencing primers: 17-28 bp long sequencing primers were designed at 400-800 bp distance along the sequence of interest without considering any primer designing rules.

All primers (Tables 2 to 4) were synthesized by Eurofins Genomics (Ebersberg, Germany) in either HPLC (Gateway™ cloning primers) or salt-free purification grade and provided at a stock concentration of 100 µM (diluted in DNase-/RNase-free water). For downstream applications, primer stocks were diluted 1:10 with DNase-/RNase-free water to create 10 µM working solutions. Stock and working solutions were stored at 4°C for short term and -20°C for long term storage.

3.2.2 Gateway™ cloning

Extraction of ZFX consensus CDS from a cDNA template: Primers for *ZFX* were designed as previously described in chapter 3.2.1. The DNA fragment was then amplified via endpoint PCR using the Q5® High Fidelity DNA Polymerase (New England Biolabs) according to the manufacturer's instructions. In brief, the PCR reaction setup was prepared as outlined in Table 28 using cycling conditions described in Table 29. Therefore, 100 ng of human adult heart cDNA, reverse transcribed from human adult heart mRNA (BioCat GmbH) as described in chapter 3.7.2, served as a DNA template for cloning. The PCR product was loaded onto a 1% agarose gel for band separation via electrophoresis in 1x TBE buffer. Therefore, 1% agarose (w/v) was diluted in 1x TBE buffer and microwaved until the agarose had completely dissolved. After the gel had cooled down, PeqGREEN (VWR) was added (1:20000), and the gel was cast in a gel casting chamber. Upon polymerization, PCR products were each supplemented with 6x Gel Loading Dye Purple (New England Biolabs) at a ratio of 6:1 (25 µl sample with 5µl dye). Thirty microliter of sample was loaded onto the gel. A ladder was included for band size discrimination by loading 5 µl of the 2-log DNA Ladder (New England Biolabs) onto an extra lane. Electrophoresis was performed at 150 V for approximately 30-45 min. DNA bands were visualized using a UV transilluminator. The correct band size (here, 2535 bp) was cut out using a clean disposable scalpel, and the piece of gel was transferred to a 1.5 ml microcentrifuge tube. Then, the DNA fragment was extracted from the gel using the MinElute® Gel Extraction Kit (Qiagen) according to the manufacturer's instruction. Purified *ZFX* PCR products were stored at 4°C for short-term or -20°C for long-term storage.

Table 28 Q5® High Fidelity DNA Polymerase PCR reaction

Component	Concentration of working solution	Final concentration	Volume per reaction
Q5® High Fidelity 2x Master Mix	2x	1x	12.5 µl
Template cDNA	variable	100 ng	1-10 µl
Forward Primer	10 µM	500 nM	1.25 µl
Reverse Primer	10 µM	500 nM	1.25 µl
ddH2O	-	-	up to 25 µl
Total volume			**25 µl**

Table 29 Q5® High Fidelity DNA Polymerase PCR cycling conditions

Cycles	Temperature	Time
1x	98°C	30 s
35x	98°C	10 s
	60°C	30 s
	72°C	30 s/kb of plasmid length
1x	72°C	2 min
Hold	4°C	∞

Insertion of ZFX PCR product into an entry vector: The previously prepared *ZFX* PCR product was transferred into the Invitrogen™ Gateway™ pDONR™221 clone (Thermo Fisher Scientific) using the Invitrogen™ Gateway™ BP Clonase™ II enzyme mix (Thermo Fisher Scientific) according to the manufacturer's instructions. All steps were performed at room temperature unless stated otherwise. In summary, amplicon, entry clone, 1x TE buffer (pH 8.0), and Gateway™ BP Clonase™ II enzyme mix were combined as indicated in Table 30. The required amount of PCR product was calculated using the following equation:

$$(50\ \text{fmol})(\text{PCR product size in bp})\left(\frac{660\ \text{fg}}{\text{fmol}}\right)\left(\frac{1\ \text{ng}}{10^6\ \text{fg}}\right) = X\ \text{ng required PCR product}$$

The mixture was incubated at 25°C for at least 1 h or overnight. Afterward, 1 µl of a 2 µg/µl Proteinase K solution was added to the complete mix and incubated at 37°C for 10 min. Finally, the newly synthesized entry clone was transformed in competent *E.coli* as described in chapter 3.2.4 or was stored until transformation at -20°C.

Table 30 Gateway™ BP Recombination reaction

Component	Concentration of working solution	Final concentration	Volume per reaction
Purified PCR product	-	50 fmol	variable
Entry clone	150 ng/µl (supercoiled)	150 ng	1 µl
1x TE buffer (pH 8.0)	-	-	up to 8 µl
Gateway™ LR Clonase™ II	-	-	2 µl
Total volume			**10 µl**

Transfer of ZFX and PDE5A2 from an entry vector to an expression vector: A Gateway™ pDONR™221 vector containing the complete *PDE5A2* CDS was purchased from PlasmID (HsCD00081701; service is no longer available; the website was formerly accessed through https://plasmid.med.harvard.edu/PLASMID/Home.xhtml). Transfer of the *PDE5A2* or previously subcloned *ZFX* insert from the Gateway™ pDONR™221 vector into an expression clone, here the Invitrogen™ Gateway™ pcDNA™-DEST40 vector (Thermo Fisher Scientific), was performed using the Invitrogen™ Gateway™ LR Clonase™ II enzyme mix (Thermo Fisher Scientific) according to the manufacturer's instructions. All steps were performed at room temperature unless stated otherwise. In summary, entry vector, destination vector, 1x TE buffer (pH 8.0), and Gateway™ LR Clonase™ II enzyme mix were combined as indicated in Table 31 and incubated at 25°C for at least 1 h or overnight. Afterward, 1 µl of a 2 µg/µl Proteinase K solution was added to the complete mix and incubated at 37°C for 10 min. Finally, the expression clone was transformed in competent *E.coli* as described in chapter 3.2.4 or was stored until use at -20°C. For a complete list of Gateway™ plasmids, see Table 13.

Table 31 Gateway™ LR Recombination reaction

Component	Concentration of working solution	Final concentration	Volume per reaction
Entry clone	variable	50-150 ng	variable
Destination vector	150 ng/µl (supercoiled)	150 ng	1 µl
1x TE buffer (pH 8.0)	-	-	up to 8 µl
Gateway™ LR Clonase™ II	-	-	2 µl
Total volume			**10 µl**

3.2.3 Mutagenesis

Correction and alteration of plasmid insert sequences were performed using the Quikchange II XL Site-Directed Mutagenesis Kit (Agilent Technologies) following the manufacturer's instructions. All steps were performed on ice unless stated otherwise. Briefly, the desired mutated plasmid was synthesized by polymerase chain reaction (PCR), using previously designed mutagenesis primers (see Table 3) and a template plasmid containing the sequence to modify. PCR was performed using the PfuUltra High Fidelity polymerase provided by the Quikchange II XL Site-Directed Mutagenesis Kit according to the manufacturer's instructions (for PCR reaction components and cycling conditions, see Tables 32-33) but was scaled down to a final reaction volume of 25 µl (polymerase excluded). After PCR, the original template plasmid was digested using 0.5 µl DpnI (10 U/µl). After 1 h of incubation at 37°C, the newly synthesized mutated plasmid was transformed into competent *E.coli* as described in chapter 3.2.4 or was stored until use at -20°C. All plasmids are listed in Table 13.

Table 32 Quikchange II XL Site-Directed Mutagenesis Kit PCR reaction

Component	Concentration of working solution	Final concentration	Volume per reaction
10x reaction buffer	10x	1x	2.5 µl
Template plasmid	variable	10 ng	1-18.5 µl
Forward Primer	10 µM	400 nM	1 µl
Reverse Primer	10 µM	400 nM	1 µl
dNTP mix	-	-	0.5 µl
QuikSolution reagent	-	-	1.5 µl
ddH2O	-	-	up to 25 µl
Total volume			**25 µl**

Table 33 Quikchange II XL Site-Directed Mutagenesis Kit PCR cycling conditions

Cycles	Temperature	Time
1x	95°C	1 min
18x	95°C	50 s
	60°C	50 s
	68°C	1 min/kb of plasmid length
1x	68°C	7 min
Hold	4°C	∞

3.2.4 Chemical transformation

General chemical transformation: All steps were performed on ice unless stated otherwise. NEB 5-alpha Competent *E.coli* (New England BioLabs) were thawed on ice for approximately 10 min. For one transformation, 50 µl of cells were used. Right after thawing, the cells were gently shaken, and 1 ng of plasmid was added to the cells. After incubation on ice for 30 min, heat shock was performed by incubating the mix at precisely 42°C for 30 s without mixing. Subsequently, the samples were incubated on ice for 5 min. Next, 950 µl of prewarmed SOC medium was added to the cells, followed by incubation in a shaker at 37°C for at least 60 min at 250 rpm. The samples were thoroughly mixed by flicking and inverting before spreading 50 µl of the complete mixture onto prewarmed selection agar plates containing the appropriate antibiotic (see Table 13). The agar plates were incubated overnight at 37°C (maximum 16 h). Alternatively, transformed bacteria could be incubated at 30°C for 24-36 hours or 25°C for 38 hours. After confirming the growth of bacterial colonies, the agar plates were stored at 4°C until further use.

Chemical transformation for mutagenesis: All steps were performed on ice unless stated otherwise. XL10-Gold Ultracompetent Cells (Agilent Technologies) were thawed on ice for approximately 10 min. For one transformation, an aliquot of 45 µl of cells was transferred to a prechilled, sterile 14 ml falcon tube. Then, 2 µl of supplied 2-mercaptoethanol was added to each falcon tube and incubated on ice for a further 10 min. The cells were mixed gently during this incubation step by swirling the tube every 2 min. Then, 2 µl of the DpnI-digested PCR product from chapter 3.2.3 was added to the cells. After incubation on ice for 30 min, heat shock was performed by incubating the mix at precisely 42°C for 30 s without mixing. Subsequently, the samples were incubated on ice for 2 min. 500 µl of prewarmed SOC medium was added to the cells and incubated in a shaker at 37°C at 250 rpm for at least 60 min. Before spreading 250 µl of the complete mixture onto prewarmed selection agar plates containing the appropriate antibiotic, the samples were thoroughly mixed by flicking and inverting. Agar plates were incubated overnight at 37°C (maximum 16 h). Alternatively, transformed bacteria could be incubated at 30°C for 24-36 hours or 25°C for 38 hours. After confirming the growth of bacterial colonies, the plates were stored at 4°C until further use.

3.2.5 Plasmid purification

Small-scale plasmid purification (miniprep): Clones were picked from the agar plates containing the previously transformed bacteria (chapter 3.2.4). Picked clones were cultured in a 14 ml falcon tube containing 5 ml LB medium with the appropriate antibiotic (Table 13) in an incubator at 37°C overnight, followed by miniprep plasmid purification using the GenElute™ Plasmid Miniprep-Kit (Sigma-Aldrich) according to the manufacturer's instructions. The isolated plasmid was eluted in 80 µl DNase/RNase-free water. For short-term storage, the

plasmid was stored at 4°C. For long-term storage, the plasmid was stored at -20°C. Buffer formulations are described in chapter 2.2.4.

Large scale plasmid purification (maxiprep): Clones were picked from the agar plates containing the previously transformed bacteria (chapter 3.2.4). Picked clones were cultured in a conical flask containing 100 ml LB medium with the appropriate antibiotic (Table 13) in an incubator at 37°C overnight, followed by maxiprep plasmid purification using the QIAGEN Plasmid Maxi Kit (Qiagen) according to the manufacturer's instructions. The DNA was resuspended in either 500 µl DNase/RNase-free water or TE buffer (pH 8.0). For short-term storage, the plasmid was stored at 4°C. For long time storage, the plasmid was stored at -20°C. Buffer formulations are described in chapter 2.2.4.

3.2.6 Plasmid control digest

Correct CDS insertion was confirmed via enzymatic digest. Previously purified plasmid (chapter 3.2.5) was submitted to enzymatic digestion as indicated in Table 34 (appropriate enzymes are listed in Table 13), followed by incubation in the buffer and at the temperature specified in Table 15 for 1 h or overnight. Of note, care was taken to choose an enzyme with two cutting regions within the plasmid (one cut in the backbone and one in the insert). Digested plasmids were loaded onto a 1 % agarose gel for band separation via agarose gel electrophoresis in 1x TBE buffer as described earlier (chapter 3.2.2). Expected digest band sizes (Table 13) were predicted using QIAGEN CLC Main Workbench (Qiagen). DNA bands were visualized using UV light and documented using the Amersham ImageQuant 800 with the IQ800 software (both Cytiva).

Table 34 Enzymatic digestion setup for plasmid control digest

Component	Concentration of working solution	Final concentration	Volume per reaction
Plasmid	variable	>20 ng	1-17 µl
Digestion Enzyme	variable	variable	1 µl
10x Digestion buffer	10x	1x	2 µl
ddH_2O	-	-	up to 20 µl
Total volume			**20 µl**

3.2.7 Plasmid sequencing

Correct plasmid sequence was confirmed by the sequencing service of Eurofins Genomics (Ebersberg, Germany) using the Mix2Seq kit (Eurofins Genomics). For each sequencing reaction, the plasmid of interest, one sequencing primer, and DNase/RNase-free water were mixed in a supplied barcoded tube as described in Table 35 and sent to the service provider. Sequences were retrieved on the website of Eurofins Genomics (https://eurofinsgenomics.eu/) and analyzed using QIAGEN CLC Main Workbench (Qiagen).

Table 35 Sequencing reaction setup

Component	Concentration of working solution	Final concentration	Volume per reaction
Plasmid DNA	variable	100 ng/µl	variable
Sequencing primer	10 µM	10 pmol	1 µl
ddH_2O	-	-	up to 17 µl
Total volume			**17 µl**

3.3 Cell culture

3.3.1 Storage of cell line stocks and thawing

Cell line stocks were stored as aliquots in liquid nitrogen tanks for long-term storage. Once a cell aliquot was removed from the liquid nitrogen tank, it was immediately transferred to a preheated water bath (37°C) on dry ice and thawed there for less than 2 min. Then, the cells were transferred into a flask or petri dish under a laminar flow hood and slowly filled up with warm growth medium. Growth medium was exchanged the next day to remove freezing medium remnants. For maintenance, fresh growth medium was exchanged or added every 2-3 days or as required.

3.3.2 Passaging

Immortalized adherent cell lines (HEK293, GC-HEK, HeLa, COS-7) were passaged after reaching up to 90% confluency, human primary cells (HCASMC) at 80-90 % confluency, and suspension cells (MEG-01) held at a concentration of 1-2 x 10^5 cells/ml. Before passaging, growth media (for medium formulations of different cell types, see chapter 2.2.3), washing buffers, and trypsin were warmed to 37°C. Immortalized adherent cell lines (HEK293E, HEK293A, GC-HEK, HeLa, COS-7) were washed once with 5 ml Dulbecco's PBS (Biochrom). Then, cells were detached using 5 ml of a 0.25 % trypsin-EDTA solution (Sigma Aldrich) for 3-5 min in a humidified incubator at 37 °C and 5 % CO_2. After confirming complete cell detachment under a microscope, the trypsinization process was stopped by adding 10 ml of growth medium. For trypsin removal, the cell suspension was transferred to a falcon tube and centrifuged at 1000 rpm at room temperature for 2 min. After removing the supernatant, the cell pellet was resuspended by flicking the falcon tube and adding growth medium as desired. For maintenance, 1:10 of the cell suspension was transferred into a fresh flask containing warm growth medium. Human primary cells (HCASMC) were treated as described above but using the DetachKit (PromoCell). In brief, primary cells were washed using 5 ml HEPES BSS (PromoCell), trypsinized using 5 ml of a 0.04 % trypsin-EDTA solution (PromoCell), and the enzymatic digest was stopped using 5 ml of a trypsin neutralization solution (TNS; PromoCell). For maintenance, HCASMC were split at a ratio of 1:3. Suspension cells (MEG-01) were

passaged either by adding enough growth medium or taking a fraction of the cell suspension and diluting it in fresh medium to reach a concentration of 1-2 x 10^5 cells/ml.

3.3.3 Cell counting

After trypsinization, as described earlier, HEK293, GC-HEK, COS-7, and HeLa cells were counted using the Scepter™ 2.0 Cell Counter (Merck Millipore). HCASMC and MEG-01 were counted using a conventional Neubauer counting chamber.

3.3.4 Cell freezing

HEK293, GC-HEK, HeLa, COS-7, and Meg-01 were frozen as aliquots in cryovials in their respective growth medium containing an additional 5 % (v/v) DMSO. HCASMC were frozen in Cryo-SFM (PromoCell). The cryovials were first stored at -80°C within a freezing container filled with isopropanol, ensuring a freezing rate of 1 °C/min. After 1-3 days, the cryovials were taken out of the freezing container and stored in a liquid nitrogen tank for long-term storage.

3.4 Transfection

3.4.1 Overexpression

Genes of interest were overexpressed in cell lines using FuGENE® HD (Promega) according to the manufacturer's instructions. Briefly, cells were seeded in 24-well plates to achieve 70-80% confluency on the day of transfection. Per 24-well plate, 500 ng plasmid DNA, Opti-MEM™ I Reduced Serum Medium (Gibco), and FuGENE® HD were combined as indicated in Table 36. For other well plate or dish formats, the plasmid amount and reagent volumes were scaled up or down according to the ratio of the seeding areas. After incubation at room temperature for 15 min, the mixture was added to the cells in the well plate little by little. Transfected cells were incubated in a humidified incubator at 37°C and 5% CO_2 for up to 72 h before harvesting.

Table 36 FuGENE® HD reagent volumes or final concentration per well or petri dish

Component	96-well	24-well	15 cm dish
Opti-MEM™ I Reduced Serum Medium	up to 10 µl	up to 50 µl	up to 2550 µl
Plasmid	0.1 µg	0.5 µg	51 µg
FuGENE® HD	0.29 µl	1.47 µl	255 µl
Transfection volume	**10 µl**	**50 µl**	**2550 µl**

3.4.2 siRNA knock-down

Small interfering RNA (siRNA) knock-down was conducted utilizing the Invitrogen™ Lipofectamine RNAiMAX Transfection Reagent (Thermo Fisher Scientific) to deliver siRNA

according to the manufacturer's instructions. Silencer Select siRNAs were purchased from Thermo Fisher Scientific (Waltham, MA, USA) (Table 9). The lyophilized siRNA (5 nmol) was dissolved in 50 µl DNase-/RNase-free water to achieve a 100 µM stock solution. Stocks were stored at -20°C. Cells were seeded in 24-well plates to achieve 70-80% confluency on the day of transfection. For siRNA knock-down, 100 µM siRNA stocks were diluted 1:10 in DNase-/RNase-free water to obtain a 10 µM working solution. Transfection reagents and siRNA were mixed as outlined in Table 37. After 5 min incubation at room temperature, 50 µl reaction mix was added to each well little by little. Transfected cells were incubated in a humidified incubator at 37°C and 5% CO_2 for up to 72 h before harvesting.

Table 37 Lipofectamine RNAiMAX reagent volumes for one well of a 24-well plate

Step	Reagents	Volume
Step A	Opti-MEM™ I Reduced Serum Medium	25 µl
	Lipofectamine RNAiMAX	1.5 µl
Step B	Opti-MEM™ I Reduced Serum Medium	24.5 µl
	10 µM siRNA	0.5 µl
Transfection volume	**Combined A + B**	**50 µl**

3.5 DNA/RNA sampling

3.5.1 DNA extraction

For DNA extraction from cultured cells, the QIAamp® DNA Mini Kit (Qiagen) was used according to the manufacturer's instructions. The DNA was eluted into 200 µl DNase-/RNase-free water and stored at 4°C for short-term storage and -20°C for long-term storage.

3.5.2 RNA extraction

Cell culture: Total RNA from cultured cells was extracted using Invitrogen™ TRIzol (Thermo Fisher Scientific) after a modified protocol from Chomczynski and Sacchi (1993). In brief, cells were cultured in 24-well cell culture plates in a humidified incubator at 37°C with 5% CO_2. After experimental treatment, the 24-well cell culture plate was placed on ice and rinsed once with 500 µl chilled PBS. Then, the cells were harvested using 500 µl TRIzol per well. Cells were detached from the cell culture plate with a cell scraper and transferred into a 1.5 ml microcentrifuge tube. Then, the tubes were placed into a -80°C freezer until solid frozen and thawed again, submitting the cells to a freeze-thaw cycle. If necessary, this step was repeated several times. Thawed samples were incubated at room temperature for an additional 10 min. After vortexing, 120 µl DNase-/RNase-free water and 100 µl chloroform were added to each sample. The tubes were mixed by inverting and incubated at room temperature for 10 min. Meanwhile, 2 ml tubes containing 5PRIME phase-lock gel (heavy; Quantabio) were prepared by centrifugation at 7500 rpm at 4°C for 30 s. These tubes were kept at 4°C until further use. Post incubation, samples were mixed by carefully pipetting and transferred into previously

prepared 2 ml tubes containing the 5PRIME phase-lock gel. Samples were mixed by inverting five times and centrifuged at 13000 rpm at 4°C for 10 min, resulting in an organic and aqueous phase separation. The aqueous phase (380 µl) was transferred into a new 1.5 ml microcentrifuge tube. In addition, 280 µl ice-cold isopropanol and 1.5 µl Invitrogen™ GlycoBlue™ coprecipitant (Thermo Fisher Scientific) were added. The samples were mixed well by vortexing and incubated at -20°C for at least 30 min or overnight. After incubation, the samples were centrifuged at 14000 rpm at 4°C for 30 min, and the supernatant was discarded. Then, the RNA pellets were washed twice using 1 ml 75% ethanol. After each washing step, samples were centrifuged at 14000 rpm at 4°C for 5 min, and the supernatant was discarded. The remaining alcohol was removed using a pipette without disturbing the pellet, then air-dried for 1-5 min. Finally, the RNA pellets were resuspended in at least 12 µl DNase-/RNase-free water, depending on the pellet size. Resuspended RNA was immediately placed on ice and either used right away or stored at -80°C until further use.

Mouse tissue: Mouse aortas were cut into small pieces using a clean scalpel on a clean surface on dry ice. The pieces were transferred into a prechilled 14 ml falcon tube, adding 500 µl QIAzol Lysis Reagent (part of the RNeasy Plus Universal Kit; Qiagen) to each sample. Next, samples were homogenized using a tissue disruptor probe. Homogenized samples were incubated at room temperature for 5 min before freezing them at -80°C until solid frozen. RNA samples were submitted to several freeze-thaw cycles prior to extracting total RNA using the RNeasy Plus Universal Kit (Qiagen) following the manual's instructions. Extracted RNA was immediately placed on ice and stored at -80°C until use.

3.6 Nucleic acid concentration quantification

DNA and RNA concentration measurements were carried out with the NanoQuant Plate™ (Tecan) and the Infinite M200Pro (Tecan) by measuring the 260 nm to 280 nm ratio.

3.7 Polymerase chain reaction

3.7.1 Primer design for polymerase chain reaction

For qualitative real-time PCR (qPCR) or endpoint PCR, 17-28 bp long primers were designed using the online tools NCBI Primer Blast (accessed through https://www.ncbi.nlm.nih.gov/tools/primer-blast/) or Primer3 (accessed through https://www.bioinformatics.nl/cgi-bin/primer3plus/primer3plus.cgi). As far it was applicable for the gene of interest, qPCR primers were designed considering the criteria outlined in Table 38. All primers are listed in Table 5.

Table 38 Primer design criteria

Primer length	17-28 bp
Amplicon length	maximum 150 bp; not necessary for endpoint PCR and ddPCR
GC content	40-60 %
GC clamp at 3' end	yes (maximum of three G's or C's)
Annealing temperature (T_a)	T_a (similar for forward and reverse primer)
Melting temperature (T_m)	52-58 °C (lower than T_a)
Exon-exon span	yes
QC secondary structures	each primer sequence within itself and forward and reverse primer sequences to each other may not be complimentary at the 5' or 3' end
QC template secondary structures	primer binding sites should be located at sites with little to no secondary structures (ΔG of -6-0 kcal/mol is generally tolerated); checked template sequence using the online tool *mfold* (not available anymore; formerly accessed at http://mfold.rna.albany.edu/?q=mfold/download-mfold)
QC off-target binding	checked for potential off-target binding using the online tools *NCBI Primer BLAST* (https://www.ncbi.nlm.nih.gov/tools/primer-blast) and *UCSC in silico PCR* (https://genome.ucsc.edu/cgi-bin/hgPcr)

All primers were synthesized by Eurofins Genomics (Ebersberg, Germany) in salt-free purification grade and provided at a stock concentration of 100 µM (diluted in DNase-/RNase-free water). For downstream applications, primer stocks were diluted 1:10 with DNase-/RNase-free water to create 10 µM working solutions. Stock and working solutions were stored at 4°C for short-term and -20°C for long-term storage.

3.7.2 cDNA synthesis

cDNA was synthesized from previously extracted or commercially purchased mRNA (Table 8) using the Maxima™ H Minus cDNA Synthesis MasterMix with dsDNase (Thermo Fisher Scientific) according to the manufacturer's instructions using a thermal cycler. In order to achieve a cDNA equivalent of at least 10 ng/µl, 200-2000 ng total RNA was reverse transcribed. cDNA was stored at 4°C for short-term and -20°C for long-term storage.

3.7.3 Endpoint PCR

Endpoint PCR was conducted using the OneTaq® Quick-Load 2x Master Mix with Standard Buffer (New England Biolabs) according to the manufacturer's instructions using a thermal cycler. Per PCR reaction, 20-50 ng cDNA was applied (for complete reaction setup and cycling conditions, see Tables 39 and 40). PCR products (25 µl) were separated by size on a 1% agarose gel in 1x TBE buffer as previously described in chapter 2.3.1. DNA bands were visualized using UV light and documented using the Amersham ImageQuant 800 and the IQ800 software (both Cytiva).

Table 39 OneTaq® Quick-Load 2x Master Mix with Standard Buffer PCR reaction

Component	Concentration of working solution	Final concentration	Volume per reaction
OneTaq Quick-Load 2x Mastermix	2x	1x	12.5 µl
Template cDNA	variable	20-50 ng	variable
Forward Primer	10 µM	250 nM	0.5 µl
Reverse Primer	10 µM	250 nM	0.5 µl
ddH_2O	-	-	up to 25 µl
Total volume			**25 µl**

Table 40 OneTaq® Quick-Load 2x Master Mix with Standard Buffer PCR cycling conditions

Cycles	Temperature	Time
1x	94°C	30 s
30x	94°C	15 s
	45-68°C	30 s
	68°C	1 min/kb
1x	68°C	5 min
Hold	4°C	∞

3.7.4 Quantitative real-time PCR

Relative mRNA expression levels were assessed via quantitative real-time PCR (qPCR) using PerfeCTa SYBR® Green FastMix (low ROX; Quantabio) according to the manufacturer's instructions. Briefly, 1-20 ng cDNA were applied in each qPCR reaction using primer pairs against the target gene of interest, including one housekeeping gene, e.g., *RPLP0* (for a complete list of sequences, see Table 5). Samples were measured as duplicates for each target gene, and a melting curve analysis was included at the end of the qPCR measurement. All measurements were carried out using the ViiA 7 Real-Time PCR System with the ViiA 7 software v.1.2.2 (both Applied Biosystems). Gene expression of each sample was normalized against individual housekeeping gene expression (ΔCt). Relative expression levels between samples were assessed using the ΔΔCt method and plotted as fold change of $2^{-\Delta\Delta Ct}$ relative to the control group. Comparison of gene expression levels between different cell lines was plotted as "relative copy number", i.e., $2^{-\Delta Ct} \cdot 100$. Reaction setup and cycling conditions are outlined in Tables 41 and 42.

Table 41 PerfeCTa SYBR® Green FastMix (low ROX) qPCR reaction

Component	Concentration of working solution	Final concentration	Volume per reaction
2x PerfeCTa SYBR® Green FastMix	2x	1x	10 µl
Template cDNA	variable	1-20 ng	variable
Forward Primer	10 µM	100 nM	0.2 µl
Reverse Primer	10 µM	100 nM	0.2 µl
ddH_2O	-	-	up to 20 µl
Total volume			**20 µl**

Table 42 PerfeCTa SYBR® Green FastMix (low ROX) qPCR cycling conditions

Cycles	Temperature	Time
1x	95°C	30 s
40x	95°C	15 s
	60°C	1 min
	95°C	15 s
1x	60°C	1 min
1x	95°C	15 s

3.7.5 Droplet digital PCR

Allelic imbalance was analyzed with droplet digital PCR (ddPCR) using the digital PCR supermix for probes (No dUTP) (Bio-Rad) according to the manufacturer's instructions. Probes were made using the probe design service of Bio-Rad (Hercules, CA, USA) (see chapter 2.3.7). Custom-made gBlocks™, containing the alternative promoter sequence flanking rs201005905 with either the non-effect/wild-type (WT) or risk/mutant allele (MUT), were purchased from Integrated DNA Technologies (Coralville, IA, USA) (Table 10). In order to create a stock solution, 250 ng lyophilized gBlock™ was dissolved in 250 µl 1x TE buffer containing 100 ng/µl Poly(A) carrier (Roche). Stocks were stored in a post-PCR environment at -20°C. gBlocks™ were used as controls to assess the primer binding efficiency. Before each ddPCR, gBlock™ stocks were diluted 1:400000 in 1x TE buffer containing 100 ng/µl Poly(A) carrier to achieve a final copy number of approximately 40000 copies/µl. For ddPCR, samples were prepared in duplicates as outlined in Table 43. Per reaction, 1 ng of cDNA or diluted gBlock™ was applied. Furthermore, for optimal accuracy of the copy number analysis, HaeIII enzyme (New England Biolabs) was added to the reaction. The complete ddPCR reaction mixture was then transferred to a DG8 Cartridge (Bio-Rad) and supplemented with the Droplet Generation Oil for Probes (Bio-Rad) for the generation of nanodroplets using the QX200 droplet generator (Bio-Rad). Generated nanodroplets were carefully transferred to a 96-well plate, sealed with an aluminum foil, and cycled in a thermal cycler according to the conditions indicated in Table 44. Finally, nanodroplets were read out using the QX200 droplet reader and analyzed using the QuantaSoft software (both from Bio-Rad). Data are expressed as copies/µl.

Table 43 Droplet digital PCR supermix for probes (No dUTP) ddPCR reaction

Component	Concentration of working solution	Final concentration	Volume per reaction
2x ddPCR Supermix for Probes (No dUTP)	2x	1x	10 µl
Template	variable	diluted gBlock or 1 ng cDNA	1-8 µl
HaeIII enzyme	2 u/µl	2 u	1 µl
20x custom probe	20x	1x	1 µl
ddH_2O	-	-	up to 20 µl
Total volume			**20 µl**

Table 44 Droplet digital PCR supermix for probes (No dUTP) ddPCR cycling conditions

Cycles	Temperature	Time
1x	95°C	10 min
40x	94°C	30 s
	55°C	1 min
1x	98°C	10 min
Hold	4°C	∞

(note: ramp rate was set to 40% for all cycling steps)

3.7.6 Genotyping

The rs201005905 genotype was assessed via genotyping, using custom-made probes by Thermo Fisher Scientific (Waltham, MA, USA) (chapter 2.3.7). Briefly, 10 ng of DNA was submitted to PCR as described in Tables 45-46 using the ViiA 7 Real-Time PCR System with the ViiA 7 software v.1.2.2 (both Applied Biosystems).

Table 45 Taqman™ genotyping reaction

Component	Concentration of working solution	Final concentration	Volume per reaction
Universal Master Mix II, no UNG	2x	1x	12.5 µl
Plasmid	variable	10 ng	variable
20x Custom probe	20x	1x	1.25 µl
ddH2O	-	-	up to 25 µl
Total volume			**25 µl**

Table 46 Taqman™ genotyping cycling conditions

Cycles	Temperature	Time
1x	95°C	10 min
40x	95°C	15 s
	60°C	1 min
1x	60°C	30 s

3.8 Protein sampling from cultured cells

All steps were performed on ice unless stated otherwise. Cells were washed once by replacing the growth medium with ice-cold 1x PBS (20 ml per 15 cm petri dish, 500 µl per well of a 24-well plate). After discarding the supernatant, cells were harvested in 1x RIPA buffer (1 ml per 15 cm petri dish, 50 µl per well of a 24-well plate) supplemented 1:100 with Invitrogen™ HALT™ protease inhibitor (100x) (Thermo Fisher Scientific) by using a clean cell scraper. Then, cell lysates were transferred to a prechilled 1.5 ml microcentrifuge tube. Prior to further processing, the samples were submitted to a freeze-thaw cycle at -80°C. Thawed cells were lysed using an ultrasonic bath three times for 30 s with incubation steps on ice for 30 s following each sonification step. Then, the lysate was centrifuged at maximum speed (~13000 rpm) for 30 min, and the supernatant was transferred to a new prechilled 1.5 ml microcentrifuge tube

to remove any cell debris. Purified lysates were either stored at -20°C for short-term, -80°C for long-term storage or subsequently submitted to gel electrophoresis. For buffer formulations, refer to chapter 2.2.6.

3.9 *In vitro* transcription/translation

In vitro protein translation was performed using the TNT® Quick Coupled Transcription/Translation System (Promega) according to the manufacturer's instructions. For each reaction, 1 µg of plasmid was employed. The resulting protein lysates were either stored at -20°C or subsequently submitted to western blot analysis. Therefore, 20 µl undiluted lysate was supplemented with 20 µl 2x Laemmli buffer and boiled at 95°C for 5 min prior to gel electrophoresis as described in chapter 3.11.2.

3.10 Protein concentration quantification

Protein concentration was measured using the Pierce™ BCA Protein Assay Kit (Thermo Fisher Scientific) according to the manufacturer's instructions using the M200Pro reader (Tecan) with the i-control software (Tecan). Absorbance was measured at 562 nm, and sample concentration was assessed by comparing against a standard curve which was included in each concentration measurement.

3.11 Western blot analysis

3.11.1 Sample preparation

For standard western blot applications of protein samples derived from cell harvest (chapter 3.8), 10-20 µg protein was supplemented with 1x RIPA buffer to a volume of 20 µl, followed by the addition of 20 µl 2x Laemmli buffer. Supplemented protein mixes were boiled at 95°C for 5 min. If desired, samples were centrifuged at maximum speed at 4°C for 10 min to decrease DNA or salt remnants interfering with protein band formation in the gel. Sample preparation of protein samples from other applications is described in respective method chapter sections. All buffer formulations are listed in chapter 2.2.6.

3.11.2 Gel electrophoresis and western blotting

For gel electrophoresis, the Mini-PROTEAN® system (Bio-Rad) was used according to the manufacturer's instructions. Thirty µl of the previously prepared sample was loaded onto the gel. In addition, 10 µl of a broad range color prestained protein standard (New England Biolabs) or 5 µl of Novex™ MagicMark™ XP Western protein standard (Thermo Fisher Scientific) was loaded onto an extra well for size discrimination. Gel chambers were filled up with 1x TRIS/glycine/SDS running buffer (Bio-Rad), and gel electrophoresis was performed at

300 V for approximately 15 min. Meanwhile, Immobilon®-P polyvinylidene difluoride (PVDF) membranes (Merck Millipore) were activated by incubation in 10 ml methanol on a rocker for 5 min, followed by incubation in transfer buffer until use. Next, the gel was placed on the previously prepared PDFV membrane for blotting, and protein lanes were transferred to the membrane by wet blotting at 100 V for 50 min in ice-cold transfer buffer. Afterward, the membrane was briefly rinsed in 1x PBS, followed by a blocking step in 5% w/v milk in 1x PBS on a rocker. Primary antibody was diluted in 5 ml 2.5% milk w/v in PBS-T buffer according to the manufacturer's recommendation. Blots were incubated with the primary antibody in a 50 ml falcon tube on a rotator at 4°C overnight. The next day, blots were washed with PBS-T buffer five times for 5 min. Meanwhile, secondary antibody was diluted in 30 ml 2.5% milk w/v in PBS-T buffer in a 1:100000 ratio. Blots were incubated with secondary antibody on a rocker at room temperature for 1 h, followed by washing with PBS-T buffer five times for 5 min. During that time, SuperSignal™ West Dura Extended Duration Substrate (Thermo Fisher Scientific) was prepared to the manufacturer's instructions, and blots were incubated therein for 5 min prior to band visualization using the Amersham ImageQuant 800 (Cytiva) with the preinstalled IQ800 control software (Cytiva). For all buffer formulations, refer to chapter 2.2.6.

3.12 Luciferase assay

Putative gene regulatory function of the familial *PDE5A* variant was examined via gene reporter assays, using the Dual-Luciferase™ reporter assay system (Promega) according to the manufacturer's protocol. Therefore, the alternative promoter region of *PDE5A*, containing either the wild-type or mutant allele, was cloned into the pGL4.10 backbone (Promega) (insert sequences are listed in Supplementary Table 1). This was conducted in collaboration with the Institute of Cardiogenetics (University of Lübeck, Lübeck, Germany). For the assay, HEK293E, HeLa, or COS-7 cells were seeded in 24-well plates and incubated in a humidified incubator at 37°C and 5% CO_2. After reaching 70-80% confluency, cells were co-transfected in triplicates with 450 ng of one of the pGL4.10 constructs and 50 ng of the pRL-TK vector (as described in chapter 3.4.1). Transfected cells were placed back into an incubator with 37°C and 5% CO_2. Twenty-four hours post-transfection, the cells were placed on ice and carefully washed once with 500 µl ice-cold 1x PBS, followed by a lysis step using 50 µl 1x PLB. Cells were immediately detached from the 24-well plate using a scratcher and transferred to a 1.5 ml microcentrifuge tube. After one freeze-thaw cycle, 20 µl of the cell lysate was transferred to a white 96-well plate at room temperature. Supplied LARII and Stop & Glow® buffer were prepared as proposed by the kit's instructions at room temperature. Luciferase activity was measured using the Infinite M200Pro (Tecan) and the i-control software (Tecan). For analysis, a ratio was computed from the firefly luciferase activity signal and *Renilla* luciferase activity signal. Values were displayed as arbitrary light units of the firefly luciferase/*Renilla* luciferase ratio.

3.13 Chromatin immunoprecipitation

The binding of transcription factor ZFX to the *PDE5A* alternative promoter site was confirmed via chromatin immunoprecipitation (ChIP) using the ChIP-IT High Sensitivity® Kit (Active Motif) according to the manufacturer's instructions. Therefore, HeLa cells were seeded in 15 cm petri dishes to achieve 70-80% confluency on the day of transfection. Full-length ZFX-V5 (ZFX with a C-terminal V5 tag) was transfected as described in chapter 3.4.1. For one ChIP assay, one 15 cm petri dish was sufficient. Chromatin was pulled down using a ChIP certified antibody targeting the V5 epitope (ab15828; abcam) or rabbit IgG (PP64; Merck Millipore) as a negative control, and presence of the alternative promoter site was detected by qPCR as described in chapter 3.7.4 (primers are listed in Table 5). Values were expressed as fold change of the chromatin enrichment relative to input.

3.14 Oligonucleotide pull-down assay

3.14.1 Bait oligonucleotide concatemerization and biotinylation

Briefly, oligonucleotide sequences targeting the familial *PDE5A* variant were kindly provided by Martin Dichgans (Institute for Stroke and Dementia, LMU Munich, Munich, Germany) (Table 11). Desthiobiotinylated bait oligonucleotides for pull-down were synthesized by oligo concatemerization using adapter-based conjugation with polynucleotide kinase (PNK) and T4 ligase (both Thermo Fisher Scientific). Buffers used for the reactions were supplied with both enzymes. In brief, corresponding bait oligonucleotide pairs or desthiobiotinylated adapter oligonucleotide pairs (5'-desthiobiotin-CAGGCTCCGAATTCGCCCTT-3' and 5'-TTAAGGGCGAATTCGGAGCCTG-3') were annealed in a 1.5 ml microcentrifuge tube as indicated in Table 47 at 95°C for 5 min. The annealed oligonucleotides and adapter oligonucleotides were phosphorylated as described in Table 48 and incubated at 37°C for 2 h. Phosphorylated oligonucleotides and adapter oligonucleotides were then ligated as indicated in Table 49 at room temperature for 1 h or overnight. Excess adapter oligonucleotides were removed using G50 columns (GE Healthcare) according to the manufacturer's instructions. Successful concatemerization was confirmed on a 1% agarose gel as described in chapter 3.2.2.

Table 47 Bait oligo concatemerization: annealing reaction

Component	Concentration of working solution	Final concentration	Volume per reaction
Forward oligo or adapter	100 µM	45 µM	45 µl
Reverse oligo or adapter	100 µM	45 µM	45 µl
Annealing buffer	10x	1x	10 µl
Total volume			**100 µl**

Table 48 Bait oligo concatemerization: phosphorylation reaction

Component	Concentration of working solution	Final concentration	Volume per reaction
Annealed oligos or adapter	45 µM	22.5 µM	100 µl
T4 ligase buffer	10x	1x	20 µl
PEG 4000	50% (w/v)	-	10 µl
dATP	100 mM	5 mM	10 µl
DTT	1 M	5 mM	2 µl
ddH_2O	-	-	50 µl
PNK	10 u/µl	100 u	10 µl
Total volume			**200 µl**

Table 49 Bait oligo concatemerization: ligation and biotinylation reaction (adapter-based conjugation)

Component	Concentration of working solution	Final concentration	Volume per reaction
Phosphorylated oligos	22.5 µM	11.25 µM	50 µl
Phosphorylated adapter	45 µM	5.63 µM	12.5 µl
T4 ligase buffer	10x	0.5x	5 µl
PEG 4000	50% (w/v)	-	2.5 µl
ddH_2O	-	-	50 µl
T4 ligase	5 u/µl	20 u	4 µl
Total volume			**100 µl**

3.14.2 Oligonucleotide pull-down in HeLa nuclear lysates

Pull-downs were performed following a modified protocol from Hubner *et al.* (Hubner *et al.*, 2015). First, 1.5 ml microcentrifuge tubes were rinsed with 200 µl DBB twice before adding 10 µl Invitrogen™ streptavidin beads (Thermo Fisher Scientific) to 200 µl DBB. The beads were washed once, followed by immediate resuspension in 150 µl DBB buffer and 50 pmol (here, 3 µl) of biotinylated bait oligos for coupling at room temperature at 600 rpm for 1 h. Subsequent steps were carried out on ice. Coupled beads were washed twice with DBB and twice with PBB. For each pull-down, 200 µg HeLa nuclear lysate (Ipracell) was diluted in a total volume of 200 µl PBB and supplemented with 2 µl EDTA-free HALT™ protease inhibitor (100x) (Thermo Fisher Scientific). After incubation at 4°C for 1.5 h on a shaker, beads were washed three times with PBB and three times with wash buffer. Pulled-down proteins were reduced by adding 30 µl of 1x Laemmli buffer and boiled at 95°C for 5 min. Then, samples were centrifuged at 7000 rpm at 4°C for 10 min, and the supernatant containing the pull-down was transferred to a fresh 1.5 ml tube. The sample was either stored at -20°C for long-term storage or subsequently submitted to gel electrophoresis and western blot analysis (chapter 3.11.2). All buffer formulations are listed in chapter 2.2.5.

3.15 Radioimmunoassay

3.15.1 Sample preparation

PDE5A2 catalytic activity was assessed by measuring the cGMP content of cells after *PDE5A2* overexpression in a cell model of stable sGC expression (GC-HEK cell line) (Mullershausen *et al.*, 2004). This cell line was a kind gift by Andreas Friebe (Department of Physiology I, University of Würzburg, Würzburg, Germany).

Comparison PDE5A2 wild-type (PDE5A2^{WT}) to the familial PDE5A2 variant p.Lys7Ter isoform (PDE5A2$^{p.Lys7Ter}$): GC-HEK cells were seeded in 24-well plates. After reaching 70-80% confluency, 500 ng plasmid containing PDE5A2$^{p.Lys7Ter}$ or PDE5A2$^{p.Lys7Ter}$ was transfected in duplicates as previously described (chapter 3.4.1). In addition, a No-PDE5 negative control (untransfected GC-HEK cells) was included. Twenty-four hours post-transfection, cells were submitted to sGC stimulation by 100 µM GSNO for 1 min.

Characterization of rare PDE5A variants from the discovery study: Rare *PDE5A* variants identified in the discovery study: GC-HEK cells were seeded in 96-well plates. After reaching 70-80% confluency, of each *PDE5A2* construct, 100 ng plasmid was transfected in duplicates as previously described (chapter 3.4.1). Additionally, a No-PDE5 negative control (untransfected GC-HEK cells) and positive control (PDE5A2^{WT}) were included. Forty-eight hours post-transfection, cells were submitted to sGC stimulation by 100 µM GSNO for 5 min.

sGC stimulation: The 24-well (96-well) plate was placed on a heating plate at 37°C. First, cells were carefully rinsed with 500 µl (90 µl) room temperature 1x PBS. Then, cells were incubated in 450 µl (45 µl) room temperature 30 mM HEPES (Lonza) on the heating plate at 37°C for 15 min. Meanwhile, 1 mM GSNO solution was prepared as described in chapter 2.2.7. GSNO had to be prepared freshly for each measurement. When the incubation time was over, 50 µl (5 µl) 500 µM GSNO was added to each well and stimulated cells were incubated for precisely 1 min (5 min). For establishing purposes, other time points (0 s [“stimulated” with 30 mM HEPES], 10 s, 20 s, 30 s, 40 s, 50 s, 2 min, 3 min) were tested as well. The stimulation was stopped using 100 µl (10 µl) ice-cold 60 mM HCl, and samples were subsequently placed on ice. Furthermore, samples were submitted to one freeze-thaw cycle, then transferred into a 1.5 ml microcentrifuge tube and either measured right away as described in chapter 3.15.2 or stored at -20°C. All buffer and solution formulations are described in chapter 2.2.7.

3.15.2 cGMP detection

Measurements were conducted utilizing the cGMP radioimmunoassay (IBL international) according to the manufacturer’s instructions using the Multi Crystal 2111 RIA gamma counter (Berthold) with the LBIS software (Berthold). Before the experiment, samples were diluted at 1:50 in assay buffer provided by the kit. The cGMP concentration was assessed by comparison to a standard curve included in each measurement. Lower cGMP concentration

indicated high PDE5 activity. For simplicity, data were either displayed as fold change cGMP concentration relative to the No-PDE5 control or fold change cGMP degradation relative to the No-PDE5 control (untransfected GC-HEK cells). For the latter, cGMP concentrations were inverted by subtracting them from the mean value of the No-PDE5 control (since the No-PDE5 control did not reveal any cGMP degradation activity, cGMP levels were the highest in this sample), followed by normalization relative to the No-PDE5 control.

3.16 Animal experiment

3.16.1 Experiment setup

Eight- to twelve-week-old B6.129P2-Apoe^{tm1Unc}/J mice (male and female), in the following called *Apoe* KO mice, were treated with 40 mg/kg sildenafil citrate (Fagron GmbH & Co. KG) per day for 12 weeks. Sildenafil citrate was provided in the drinking water for *ad libitum* intake at a concentration of 260 mg/L. Control animals were given normal drinking water. In addition, all animals received a high-fat diet (Envigo). All experiments were approved by the local animal welfare authority (Regierung Oberbayern).

3.16.2 Mouse sacrifice and sample collection

After 12 weeks of treatment, animals were sacrificed by isoflurane inhalation followed by exsanguination via the retrobulbar plexus. Blood was collected using Microvette 500 EDTA tubes (Sarstedt) with the help of a glass capillary. One blood-filled capillary was set aside in a clear microtube for subsequent fluorescence-activated cell sorter (FACS) analysis in collaboration with Hendrik Sager (Deutsches Herzzentrum München, Munich, Germany). For plasma extraction, blood samples were centrifuged at 4000 rpm at 4°C for 15 min, and the upper transparent layer (blood plasma) was transferred into a 1.5 ml microcentrifuge. Plasma samples were stored at -80°C or immediately submitted to total cholesterol, HDL, and LDL measurement. This was conducted by the in-house department of Laboratory Medicine (Deutsches Herzzentrum München, Munich, Germany) as part of their routine work. Next, the aorta was isolated from the mice, using a modified protocol of Robins *et al*. (Robbins *et al.*, 2014). Briefly, to open up the abdominal cavity, mice were placed on the back on a surgical board, and the abdominal area was sanitized using wipes with 70% ethanol. First, a cut was made inferior to the xiphoid process of the sternum. The skin in this area was removed to reveal the superior portion of the peritoneum and inferior section of the thoracic cavity. Then, the xiphoid process was lifted by lateral incisions below the xiphoid process along the subcostal margins. The thoracic cavity was opened by dissecting up through the diaphragm to the neck, taking care not to damage the heart or blood vessels in the process. Lateral incisions were extended by cranial incisions to remove the anterior section of the ribcage. Thyroid glands, esophagus, and lungs were removed to view the aorta better. The right atrium was cut

prior to slow injection of 10 ml ice-cold 1x PBS to the left ventricle with a 10 cc syringe and a 25 gauge needle. Gastrointestinal contents were exposed by caudal incisions through the abdominal wall to the lower limbs. Liver and spleen were transferred to 1.5 ml microcentrifuge tubes and frozen in liquid nitrogen. The abdominal fat, organs, and intestines were removed to view the aorta better. The aorta was separated from the spine dorsally and the esophagus ventrally by blunt dissection under a dissection microscope. Then, the aorta was dissected starting by caudal dissection from the carotids until the iliac bifurcation. When reaching the perirenal area, care was taken not to injure the aorta when working around the renal arteries. The kidneys were carefully removed and frozen in a 1.5 ml microcentrifuge tube in liquid nitrogen. Finally, the aorta was removed (with the aortic root remaining in the heart) and placed in a petri dish filled with 1x PBS on ice. The aorta was further processed for qPCR (chapters 3.5.2 and 3.7.4) or FACS analysis. The latter was performed in collaboration with Hendrik Sager (Deutsches Herzzentrum München, Munich, Germany). Aortic roots were carefully dissected out of the heart and placed in molds filled with Tissue-Tek® O.C.T.™ compound (Sakura Finetek) for histological analyses. The molds were subsequently frozen by placing into the liquid nitrogen vapor phase and stored at -80°C until further use.

3.16.3 Histology

Embedded aortic roots were sectioned using the CM1850 cryostat (Leica). A series of five µm thick transversal sections (every 30 µm) were stained using hematoxylin (Carl Roth) and eosin stain (Carl Roth) (H&E staining). First, sections were submitted to a decreasing alcohol dilution series (100% xylol twice, 100% ethanol twice, 96% ethanol once, and 70% once) for 1 min each, briefly washed in Millipore, and incubated in hematoxylin (Carl Roth) for 3 min. Then, sections were briefly dipped in a 0.1 % HCl solution, followed by incubation in flowing tap water for 5 min. Furthermore, sections were submitted to a second staining step in 0.5% v/v eosin (Carl Roth) for 3 min. Next, the excess stain was removed by incubating in Millipore water for 30 s. Finally, stained sections were dehydrated in an increasing alcohol dilution series (reverse order of previously described decreasing alcohol series; for a complete list of staining formulations and solutions, refer to chapter 2.2.8). Sections were mounted using Pertex® (HistoLab) and analyzed utilizing the Leica DMRB microscope (Leica) together with the Leica DFC450C (Leica) camera and the LAS4.5 software (Leica). Plaque size was assessed using Image J (Schneider *et al.*, 2012). Data are expressed as the average plaque size of a complete series (here defined as the onset of the aortic valves to the disappearance of the valves) in mm^2.

3.17 Statistical analysis

Odds ratio (OR) was calculated using the Chi-square test. Confidence interval (CI) was calculated using the Baptista-Pike method. ORs are given as OR ± 95% CI. Data normality was tested using the D'Agostino-Pearson omnibus normality test or Shapiro-Wilk normality test. Data are displayed as mean ± standard error mean (SEM) or standard deviation (SD) for grouped data. Normally distributed data were analyzed using Student's unpaired/paired t-test (comparison of two groups). Grouped data were analyzed using multiple t-tests. Comparison of more than two groups was conducted using ordinary/RM one-way analysis of variance (ANOVA) followed by correction for multiple testing by either Bonferroni's, Turkey's, or Dunn's multiple comparison testing. Data that were not normally distributed were analyzed using the Mann-Whitney test (comparison of two groups) or the Kruskal-Wallis test (more than two groups).

Statistical significance was defined as $p<0.05$. All statistical calculations were performed using the GraphPad Prism® software version 9.0 for Mac OS X.

4 Results

4.1 Investigation of rare *PDE5A* variants

4.1.1 Identification and selection of rare *PDE5A* variants

In collaboration with the Center for Genomic Medicine (Massachusetts General Hospital, Boston, MA, USA), 67 rare coding variants in *PDE5A* were detected in a subset of a discovery study with 5090 controls and 4703 cases of European ancestry (Myocardial Infarction Genetics *et al.*, 2016) (Table 50). None of these variants had been reported to associate with CAD before. Six variants with a minor allele frequency (MAF) equal to or above 0.1% were chosen for further analysis (highlighted in white in Table 50). Figure 4 depicts the location of those chosen variants within the functional units of the PDE5 enzyme.

Table 50 Identified rare PDE5A variants in the discover study

The discovery study (Myocardial Infarction Genetics et al., 2016) comprised 5090 controls and 4703 cases. Variants are sorted by decreasing minor allele frequency (MAF). All variants with a MAF<0.1% are highlighted in grey. Polyphen prediction: +, benign; (+), benign or not available, (-), possibly damaging, -, probably damaging or loss of function. *: only affecting *PDE5A1*. †: only affecting *PDE5A3*. Note: variant locations are mapped to the GRCh37 assembly.

ID	Variant	Amino acid	MAF	Polyphen prediction
M45	4:120427058_C/T	p.Arg688Lys	0,006385	(+)
M13	4:120423809_A/G	p.Ile726Thr	0,002604	(-)
M50	4:120463748_T/G	p.Lys428Gln	0,002349	(+)
M38	4:120419776_C/T	p.Gly818Ser	0,002195	(+)
M1	4:120419806_G/A	p.Gln808Ter	0,002144	-
M61	4:120528249_T/A	p.Glu119Val	0,001583	(+)
M54	4:120484068_A/C	p.Leu299Val	0,000919	(+)
M18	4:120440278_A/G	p.Leu589Pro	0,000613	-
M42	4:120422407_T/G	p.Asp751Ala	0,000562	(+)
M34	4:120528040_G/A	p.Leu137Phe	0,000460	-
M36*	4:120549819_C/G	p.Arg3Pro	0,000306	(-)
M19	4:120442215_C/A	p.Val542Phe	0,000204	-
M52	4:120474818_C/T	p.Ser376Asn	0,000204	(+)
M47	4:120446722_G/C	p.Asn535Lys	0,000153	(+)
M31	4:120527940_C/T	p.Arg170His	0,000153	(-)
M37*	4:120549822_T/C	p.Glu2Gly	0,000102	(-)
M62	4:120528331_T/C	p.Ser40Gly	0,000102	(+)
M68*	4:120549687_C/G	p.Arg47Thr	0,000102	(+)
M3	4:120446851_CT/C	intronic	0,000102	-
M16	4:120425748_C/G	p.Met706Ile	0,000102	-
M23	4:120463721_C/T	p.Glu437Lys	0,000102	(-)
M59	4:120528213_T/G	p.Lys131Thr	0,000102	(+)
M48	4:120460116_G/A	p.Ala492Val	0,000102	(+)
M63	4:120528342_C/T	p.Arg36His	0,000102	(+)
M21	4:120460167_G/A	p.Ser475Leu	0,000102	-
M22	4:120463711_A/G	p.Leu440Pro	0,000102	-

M24	4:120474830_A/C	p.Ile372Ser	0,000102	-
M26	4:120486510_T/C	p.Tyr268Cys	<0.0001	(-)
M2	4:120423733_T/TA	intronic	<0.0001	-
M6*	4:120549735_T/TCGACCGA	p.Glu31ValfsTer19	<0.0001	-
M7*	4:120549748_G/A	p.Gln27Ter	<0.0001	-
M8*	4:120549755_C/CT	p.Arg25GlufsTer23	<0.0001	-
M9	4:120419763_C/T	p.Arg822Gln	<0.0001	(-)
M10	4:120419788_T/C	p.Asn814Asp	<0.0001	(-)
M27	4:120488245_T/C	p.Thr244Ala	<0.0001	-
M35	4:120528092_T/G	p.Lys119Asn	<0.0001	(-)
M39	4:120419853_T/C	p.Asp792Gly	<0.0001	(+)
M40	4:120419881_C/T	p.Val783Met	<0.0001	(+)
M41	4:120422327_C/G	p.Glu778Gln	<0.0001	(+)
M43	4:120423733_T/TA	intronic	<0.0001	-
M44	4:120423746_A/G	p.Ile747Thr	<0.0001	(+)
M51	4:120463760_C/T	p.Glu424Lys	<0.0001	(+)
M53	4:120481454_G/A	p.Thr347Ile	<0.0001	(+)
M57	4:120528181_C/G	p.Asp100His	<0.0001	(+)
M72*	4:120549793_G/C	p.Arg12Gly	<0.0001	(+)
M4	4:120481449_A/T	intronic	<0.0001	-
M14	4:120425692_C/T	p.Arg725Gln	<0.0001	(-)
M28	4:120488257_C/G	p.Gly240Arg	<0.0001	(-)
M29	4:120517735_A/C	p.Ile206Met	<0.0001	(-)
M32	4:120527989_C/G	p.Asp154His	<0.0001	-
M33	4:120527998_G/A	p.Arg151Cys	<0.0001	-
M46	4:120432252_T/C	p.Ile628Val	<0.0001	(+)
M49	4:120463726_T/C	p.Asn435Ser	<0.0001	(+)
M56	4:120527967_A/G	p.Leu161Pro	<0.0001	(+)
M64	4:120528393_C/A	p.Gly19Val	<0.0001	(+)
M66	4:120528448_T/G	p.Met11Leu	<0.0001	(+)
M67†	4:120548323_G/T	p.Pro3His	<0.0001	(+)
M69*	4:120549706_T/A	p.Thr41Ser	<0.0001	(+)
M70*	4:120549742_A/G	p.Ser29Pro	<0.0001	(+)
M71*	4:120549792_C/T	p.Arg12Gln	<0.0001	(+)
M5	4:120528250_C/A	p.Glu119Ter	<0.0001	-
M11	4:120422353_A/G	p.Ile769Thr	<0.0001	-
M12	4:120423777_G/C	p.Gln737Glu	<0.0001	-
M30	4:120527922_C/A	p.Gly176Val	<0.0001	-
M15	4:120425738_C/T	p.Ala710Thr	<0.0001	-
M17	4:120425750_T/C	p.Met706Val	<0.0001	-
M20	4:120446754_G/A	p.Arg525Trp	<0.0001	-

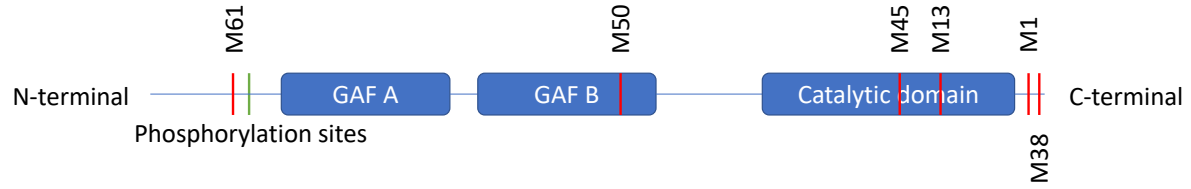

Figure 4 Location of the six selected rare *PDE5A* variants within the PDE5 enzyme

The variants (marked in red) are spread across several functional units of PDE5. For example, one of the variants, p.Glu119Val (M61), can be found nearby phosphorylation sites Ser92 and Ser102 (green; both are too close to discriminate, hence represented by one line here). None of the selected variants is located in the GAF A domain, while one (p.Lys428Gln; M50) is in the GAF B domain. However, most variants can be found within the catalytic or post-catalytic domain. For simplicity reasons, variants were named after the IDs given in Table 50. GAF: cGMP-specific phosphodiesterases, adenylyl cyclases and FhlA.

4.1.2 Effect of the selected rare *PDE5A* variants on PDE5 function

First, we attempted to study the putative effects of the variants on the PDE5 function. Therefore, plasmids containing each variant were overexpressed in GC-HEK cells. GC-HEK cells stably overexpress the α_1 and β_1 subunit of the sGC, synthesizing cGMP upon stimulation with an NO donor (Mullershausen *et al.*, 2004). For this experiment, we assessed the capability of these variants to degrade cGMP in GC-HEK cells 24 hours post-transfection and 1 min stimulation with 100 µM GSNO. A No-PDE5 negative control (untransfected GC-HEK cells) and a wild-type PDE5A2 positive control were included in the measurements. Unexpectedly, the variants did not act as predicted by Polyphen (Table 50). Instead, two previously predicted loss-of-function variants were functional (M1 and M13), whereas three other variants, which had been predicted as benign, were loss-of-function variants (M45, M50, and M38). Only M61 had been predicted correctly (Figure 5).

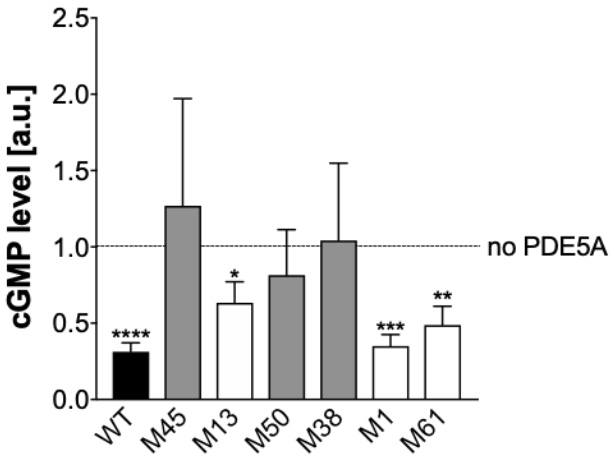

Figure 5 Activity of PDE5A^{WT} and PDE5A variants

Overexpression of the *PDE5A* variants in GC-HEK cells revealed that variants M13, M1, and M61 are able to catalyze cGMP. All three variants significantly decreased cGMP levels in the GC-HEK cells compared to the No-PDE control (indicated by the line). M45, M50, and M38 are loss-of-function variants. WT: PDE5A2 WT. Data are mean ± SEM of 7 independent experiments. One sample t-test. *: p<0.05. **: p<0.01, ***: p<0.001, ****: p<0.0001.

4.1.3 Influence of the selected rare *PDE5A* variants on CAD risk

We chose the three loss-of-function variants for further analysis (M45, M50, and M38). Therefore, we compared the allele counts of these variants in the cases (n=4643) and controls (n=5016) of the discovery study (Table 51). More loss-of-function variants were found in the control group (2.6%) than in the case group (1.8%) (Table 51), i.e., carriers of inactivating *PDE5A* variants featured reduced risk for CAD (OR 0.69 [95% CI 0.52-0.91], p<0.01) (Figure 6).

Table 51 Frequency of *PDE5A* loss-of-function variants with a MAF≥0.1% in cases and controls

Mutation	Type of mutation	Controls (n=5,016)	Cases (n=4,643)
M45	p.Arg688Lys	69 (1.5)	56 (1.1)
M50	p.Lys428Gln	31 (0.6)	15 (0.3)
M38	p.Gly818Ser	30 (0.6)	13 (0.3)
Σ		**130 (2.6)**	**84 (1.8)**

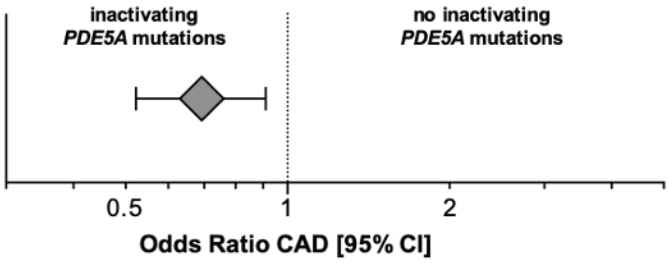

Figure 6 Loss-of-function *PDE5A* variants and CAD risk

Carriers of loss-of-function variants with a MAF≥0.1% reveal reduced risk for CAD (OR 0.69 [95% CI 0.52-0.91], p<0.01).

Furthermore, in collaboration with the Center for Genomic Medicine (Massachusetts General Hospital, Boston, MA, USA), we aimed to replicate our findings in the MIGen study (n cases=24747, n controls=29704) (Myocardial Infarction Genetics Consortium *et al.*, 2009) and two further datasets from UK Biobank (UKB_13K: n_{cases}=6382, $n_{controls}$=6343; UKB_50K n_{cases}=1930, $n_{controls}$=44597) (https://www.ukbiobank.ac.uk/). However, after correction for principal components (PCs) and covariates, the previously observed signal was lost (Figure 7). While our initial results suggest that loss-of-function *PDE5A* variants may be associated with reduced CAD risk, we were not able to replicate this finding in UK Biobank. Why the signal was lost and whether the adjustment for covariates, which are themselves influenced by PDE5 function, influenced this analysis remains to be studied.

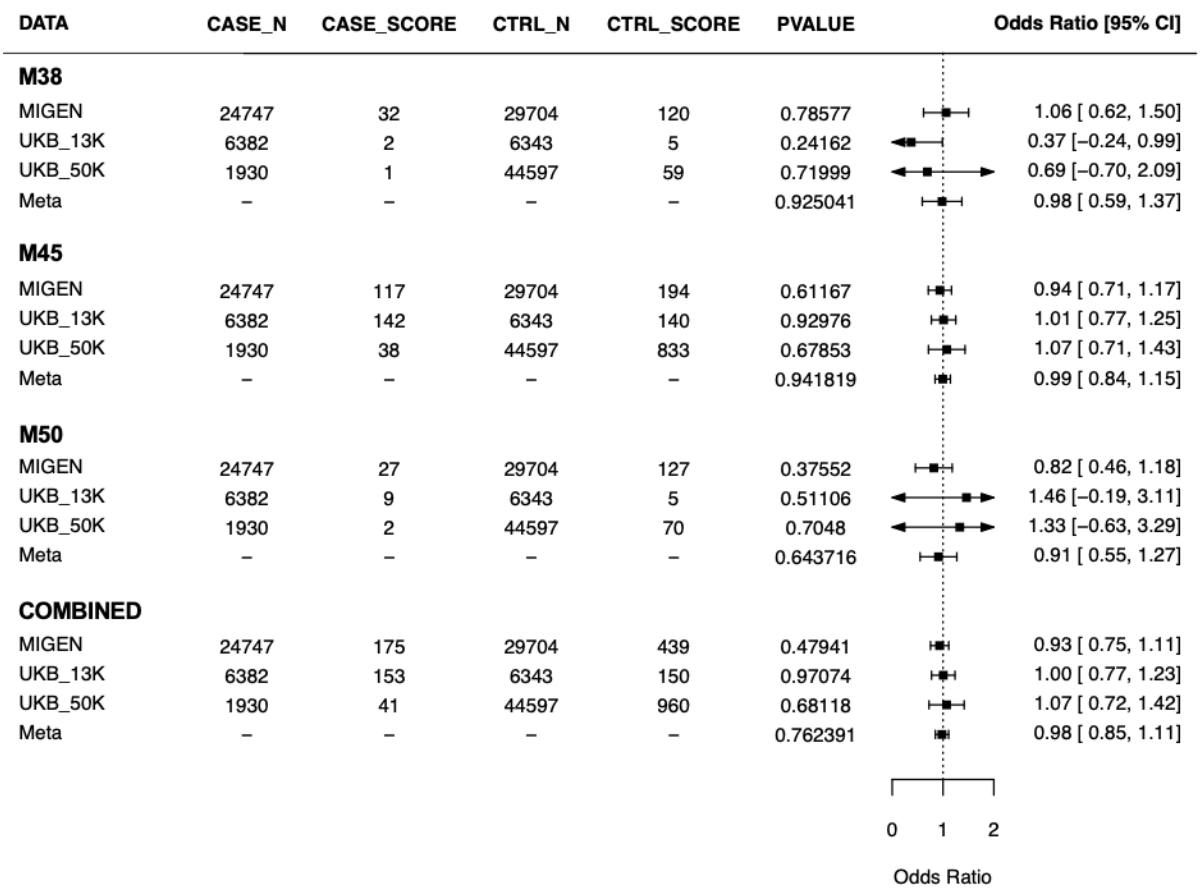

Figure 7 Replication in the MIGen study and UK Biobank cohorts

The previously observed signal for reduced CAD risk disappeared after correction for PCs and covariates. Data analysis and data visualization were conducted by Sekar Kathiresan/Amit Khera (Center for Genomic Medicine, Massachusetts General Hospital, Boston, MA, USA). MIGEN: Myocardial Infarction Genetics Consortium. UKB: UK Biobank.

4.2 Investigation of an extended family suffering from premature CAD and MI

4.2.1 Identification of the putative causal variant in the CAD/MI family

An extended family with a high prevalence of premature CAD and MI was identified as part of the German Heart Family Heart study. This family displayed a relatively moderate cardiovascular risk profile (Supplementary Table 2). Preceding this study, DNA samples of three family members were submitted to whole-exome sequencing (WES) (Figure 8A) (Brænne *et al.*, 2012). In addition, stringent bioinformatic filtering and Sanger sequencing were applied (outlined in Figure 8B), leading to the identification of a *PDE5A* variant (dbSNP: rs201005905; ClinGen Allele Registry: NM_033430.3:c.19A>T, NP_236914.2:p.Lys7Ter; gnomAD: 4-120548312-T-A, MAF $2.1*10^{-4}$) (Brænne *et al.*, 2012). Genotyping of the other family members revealed that 33.3% (10 of 30) of the non-founders, i.e., individuals with parents in the pedigree, carried the identified *PDE5A* variant. Notably, all variant carriers were heterozygotes, indicating autosomal dominant inheritance. Fifty percent (5 of 10) were affected

by CAD/MI. As opposed to this, only 5% (1 of 20) of non-variant carriers were affected by CAD/MI. The maximum LOD score for the *PDE5A* variant in this family was 3.16 at a recombination fraction of θ=0.17 (Figure 8C). Furthermore, it was located in a particular genetic region, harboring two different functional aspects. On the one hand, it was located in the first exon of *PDE5A2*, leading to a presumable stop codon by exchange of lysine at the seventh amino acid position. On the other hand, it was in the first intron of *PDE5A1* and *PDE5A3*, which had been reported to be an alternative promoter site (Figure 8D) (Lin *et al.*, 2000b).

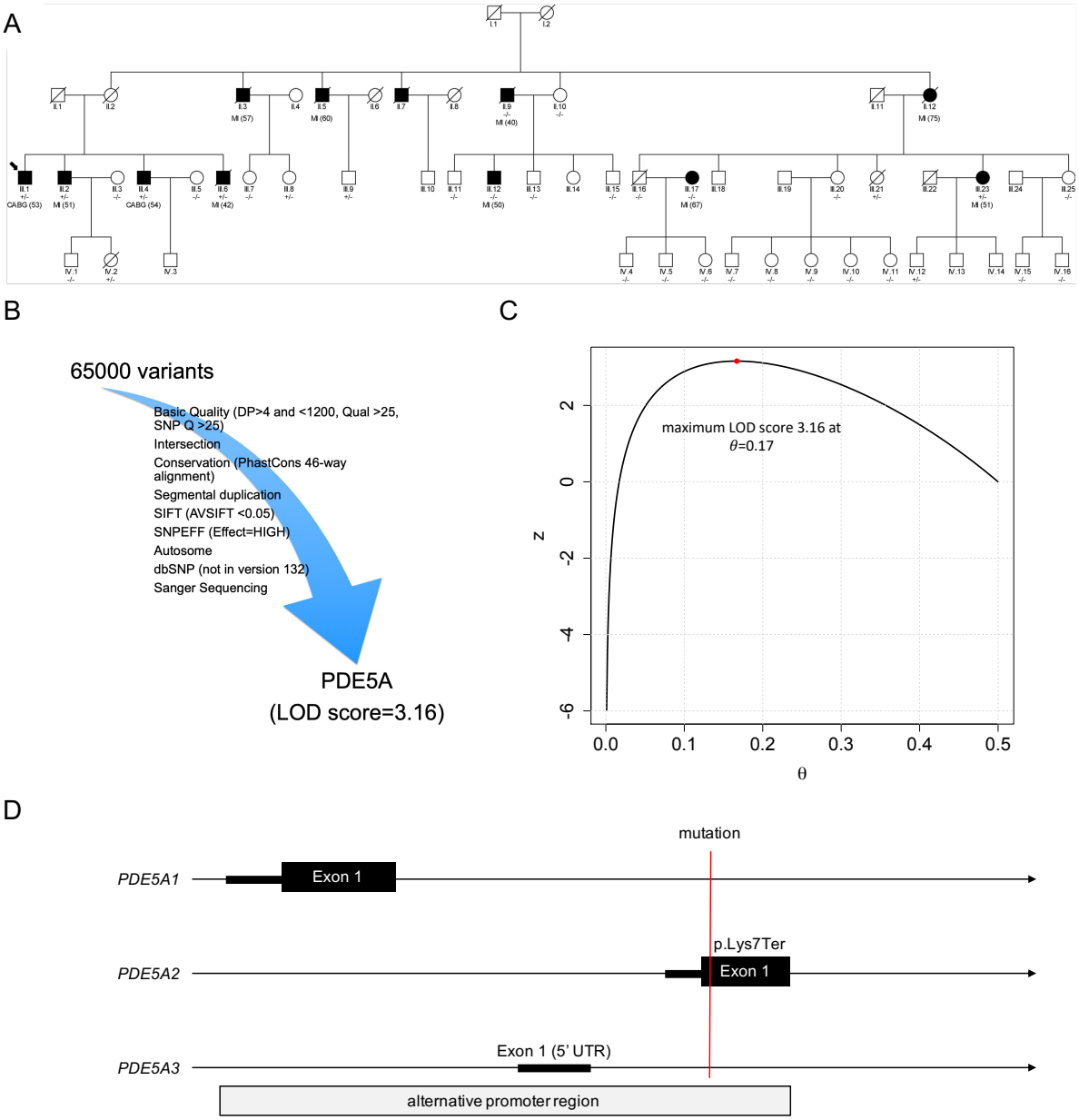

Figure 8 Association of a *PDE5A* variant with CAD in an extended family

A. Family pedigree. The arrow denotes the index patient (III.1). Individuals III.6, III.23, and the index patient underwent whole-exome sequencing. Other family members were genotyped. Variant carrier status is displayed as +/- or -/- in case of heterozygous carrier status or wild-type (WT) *PDE5A*, respectively. **B**. Bioinformatic filtering strategy that led to the identification of the *PDE5A* variant. **C**. Logarithm of the odds (LOD). The maximum LOD

score was z=3.16 at a recombination fraction of θ=0.17. **D**. Location of the variant in the *PDE5A* gene (red line). Figures **A** and **D** were reprinted with permission: Figures 1A and 1B, respectively, from "Identification of a Functional *PDE5A* variant at the Chromosome 4q27 Coronary Artery Disease Locus in an Extended Myocardial Infarction Family" by Dang *et al.*, *Circulation* 2021. 144: 662-665. Copyright © 2021 by Wolters Kluwer Health, Inc.

4.2.2 Effect of the familial *PDE5A* variant on the *PDE5A2* isoform.

4.2.2.1 Investigation of the stop codon in PDE5A2

We first attempted to examine the effect of this particular variant on the first exon of *PDE5A2*. Here, the variant seemed to lead to a stop codon (p.Lys7Ter) (Figure 9A). Thus, we expected a loss-of-function. Due to lack of an antibody that was able to detect overexpressed PDE5, we used V5-tagged PDE5A2 (PDE5A2-V5) for western blot analysis, which could be detected using a V5 antibody (Cell Signaling). Overexpression of the mutant *PDE5A2* sequence in HEK293 cells, however, unexpectedly revealed the expression of a truncated protein in HEK293 cells ($PDE5A2^{p.Lys7Ter}$) (Figure 9B). This result could be replicated by *in vitro* transcription/translation of the mutant *PDE5A2* sequence, although, the wild-type PDE5A2 isoform was also strongly expressed with the mutant sample (Figure 9C). Next, we sought to analyze the putative start codon of the truncated isoform. Hence, we exchanged contemplable methionine candidates downstream of p.Lys7Ter with a stop codon using *in vitro* mutagenesis. Overexpression of these constructs in HEK293 cells showed that the third methionine is required to express the truncated $PDE5A2^{p.Lys7Ter}$ isoform (Figure 9B). Consequently, $PDE5A2^{p.Lys7Ter}$ has a predicted molecular weight of 89.5 kDa, hence resembling PDE5A3 (according to https://www.bioinformatics.org/sms/prot_mw.html).

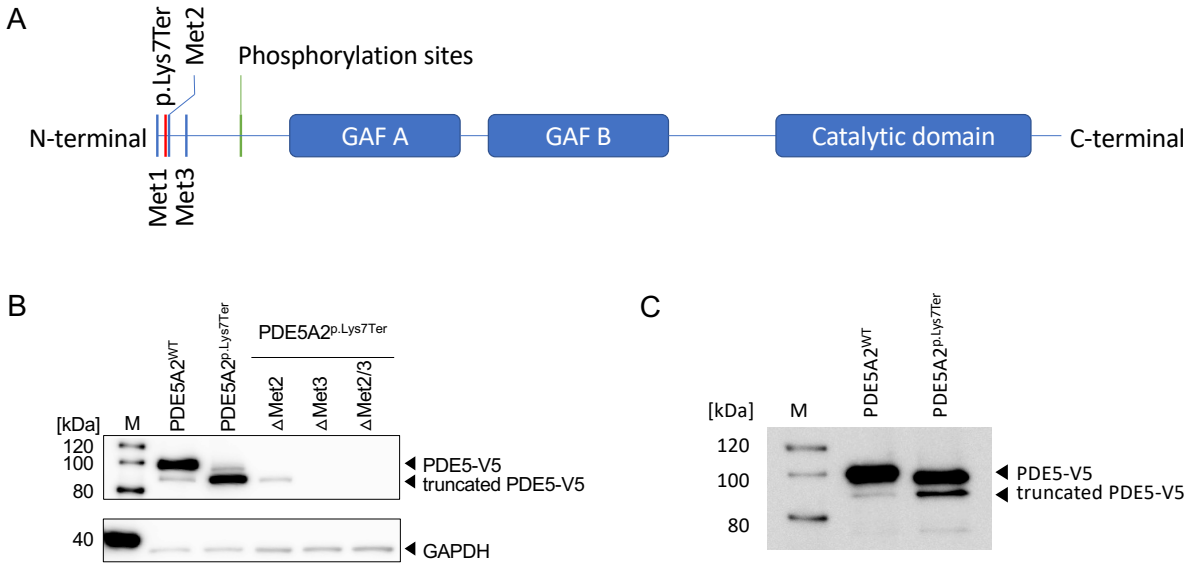

Figure 9 The effect of the p.Lys7Ter variant on the PDE5A2 isoform

A. Position of p.Lys7Ter within the PDE5 enzyme (red line). Met: methionine. GAF: cGMP-specific phosphodiesterases, adenylyl cyclases and FhlA. Adapted from Dang *et al.* (2021). **B**. Representative western blot showing the truncated $PDE5A2^{p.Lys7Ter}$. HEK293 cells overexpressing $PDE5A2^{WT}$ or $PDE5A2^{p.Lys7Ter}$. To identify alternative starts of translation, two methionines downstream of p.Lys7Ter were mutated. ΔMet2: 2nd methionine

mutated. ΔMet3: 3rd methionine mutated. ΔMet2/3: methionines 2 and 3 mutated. M: marker. **C**. Representative western blot showing the truncated PDE5a2$^{p.Lys7Ter}$ after *in vitro* transcription/translation. Adapted Figure **A** and reprinted Figure **B** with permission: Figures 1C and 1D, respectively, from "Identification of a Functional *PDE5A* variant at the Chromosome 4q27 Coronary Artery Disease Locus in an Extended Myocardial Infarction Family" by Dang *et al.*, *Circulation* 2021. 144: 662-665. Copyright © 2021 by Wolters Kluwer Health, Inc.

4.2.2.2 Activity of the truncated PDE5A2 isoform

Having excluded the formation of nonsense PDE5A2 isoform, we investigated the activity of PDE5A2$^{p.Lys7Ter}$. GC-HEK cells overexpressing PDE5A2^{WT} or PDE5A2$^{p.Lys7Ter}$ were submitted to stimulation with 100 µM GSNO for 1 min. Thereafter, the cellular cGMP concentration was assessed via radioimmunoassay. We could demonstrate that the truncated PDE5A2$^{p.Lys7Ter}$ is active. Additionally, p.Lys7Ter does not alter the activity of PDE5A2$^{p.Lys7Ter}$ compared to its wild-type isoform (Figure 10).

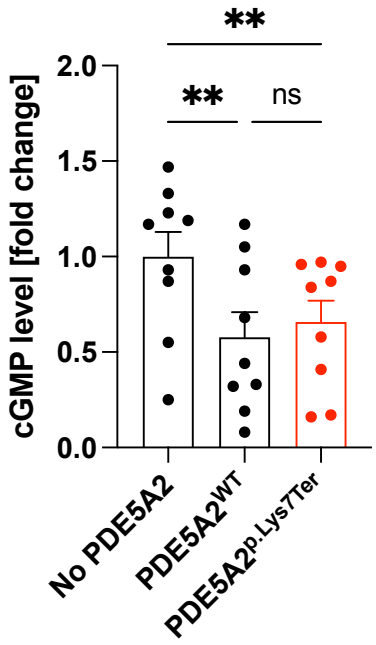

Figure 10 PDE5A2$^{p.Lys7Ter}$ activity

PDE5A2$^{p.Lys7Ter}$ is equally active as PDE5A^{WT}. Data are mean ± SEM of 9 individual experiments. RM one-way ANOVA with Turkey's multiple comparison test. **: p<0.01. ns: not significant. Adapted with permission from: Figure 1E from "Identification of a Functional *PDE5A* variant at the Chromosome 4q27 Coronary Artery Disease Locus in an Extended Myocardial Infarction Family" by Dang *et al.*, *Circulation* 2021. 144: 662-665. Copyright © 2021 by Wolters Kluwer Health, Inc.

Thus, the p.Lys7Ter mutation does not lead to a loss-of-function but the expression of a truncated yet active PDE5A2 isoform.

4.2.3 Effect of the familial *PDE5A* variant on the intronic region of *PDE5A*

4.2.3.1 Investigation of the *PDE5A* alternative promoter

As mentioned before, the variant identified in the family was also located in the first intron of *PDE5A1* and *PDE5A3* (Figure 8D). Interestingly, this region had been reported to be an alternative promoter region (Lin *et al.*, 2000b). Since we could exclude the formation of a nonsense protein in chapter 4.2.2 but did not detect any other alteration in the enzyme function, we continued to study the putative regulatory effects of the variant on the alternative *PDE5A* promoter site. Indeed, reporter gene assays confirmed promoter activity at the region flanking the variant (±300 nucleotides 5' and 3' of the variant) (Supplementary Table 1). Furthermore, alternative promoter sequence containing the mutant/risk allele (alt. promoter^{MUT}) led to increased promoter activity compared to the wild-type/non-risk allele (alt. promoter^{WT}) (Figure 11).

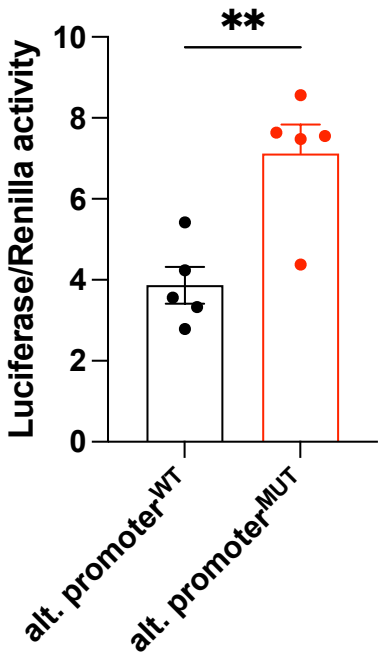

Figure 11 Alternative promoter activity

Reporter gene assays using HEK293 overexpressing the *PDE5A* alternative promoter with the wild-type/non-risk (alt. promoter^{WT}) or mutant/risk allele (alt. promoter^{MUT}). Student's paired t-test. Data are mean ± SEM **: p<0.01. Adapted with permission from: Figure 1F from "Identification of a Functional *PDE5A* variant at the Chromosome 4q27 Coronary Artery Disease Locus in an Extended Myocardial Infarction Family" by Dang *et al.*, *Circulation* 2021. 144: 662-665. Copyright © 2021 by Wolters Kluwer Health, Inc.

4.2.3.2 Allelic imbalance

Next, we examined putative allelic imbalance effects since the mutant allele increased promoter activity. Therefore, we established an allelic imbalance assay using ddPCR to study the expression of both alleles in whole blood mRNA of heterozygous mutation carriers. Indeed, we could demonstrate significant preferential expression of the mutant/risk allele in the heterozygous mutation carriers (Figure 12).

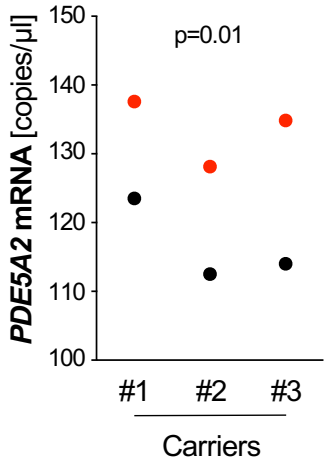

Figure 12 Allelic imbalance assay

Copy numbers of *PDE5A2* mRNA in whole blood of heterozygous p.Lys7Ter variant carriers (n=3). The copy number was significantly higher for the mutant allele (red dots) than the wild-type allele (black dots) (133.5±2.8 vs. 116.7±3.4 [copies/µl], respectively, p=0.01). Student's paired t-test. Reprinted with permission from: Figure 1G from "Identification of a Functional *PDE5A* variant at the Chromosome 4q27 Coronary Artery Disease Locus in an Extended Myocardial Infarction Family" by Dang *et al.*, *Circulation* 2021. 144: 662-665. Copyright © 2021 by Wolters Kluwer Health, Inc.

4.2.3.3 Transcription factor binding site analysis

To further investigate the reason for the changes in the promoter activity, we sought to analyze putative transcription factors that might be involved in the variant region. *In silico* analysis of the variant using the online tool Alibaba 2.1 (http://www.gene-regulation.com/pub/programs/alibaba2/index.html?), however, did not predict any promising differentially binding transcription factor candidates (data not shown).

In collaboration with the Max-Planck-Institute of Biochemistry (Martinsried, Germany), stable isotope labeling of amino acids in cell culture (SILAC) analysis was performed using HeLa cells. Therefore, oligonucleotides containing either the wild-type allele (alt. promoter^{WT}) or mutant allele (alt. promoter^{MUT}) were utilized. The SILAC experiment revealed differential binding of transcription factor ZFX to the wild-type allele (Figure 13A), suggesting a repressive function of ZFX in the context of *PDE5A* regulation. In addition, we further confirmed the preferential binding of ZFX to the wild-type allele of the alternative promoter by oligonucleotide pull-down and western blot analysis (Figure 13B). According to the eukaryotic promoter database (https://epd.epfl.ch//index.php), the *PDE5A* promoter indeed features several ZFX binding motifs (Figure 13C). Nevertheless, we sought to validate ZFX binding to the alternative *PDE5A* promoter. Thus, we performed a ChIP analysis. Due to the lack of a ChIP-certified ZFX antibody, we overexpressed ZFX containing a C-terminal V5 tag (ZFX-V5) in HeLa cells and conducted immunoprecipitation using a ChIP certified V5 antibody (abcam). This way, we demonstrated the binding of ZFX-V5 to the alternative *PDE5A* promoter site by ChIP (Figures 13D and E).

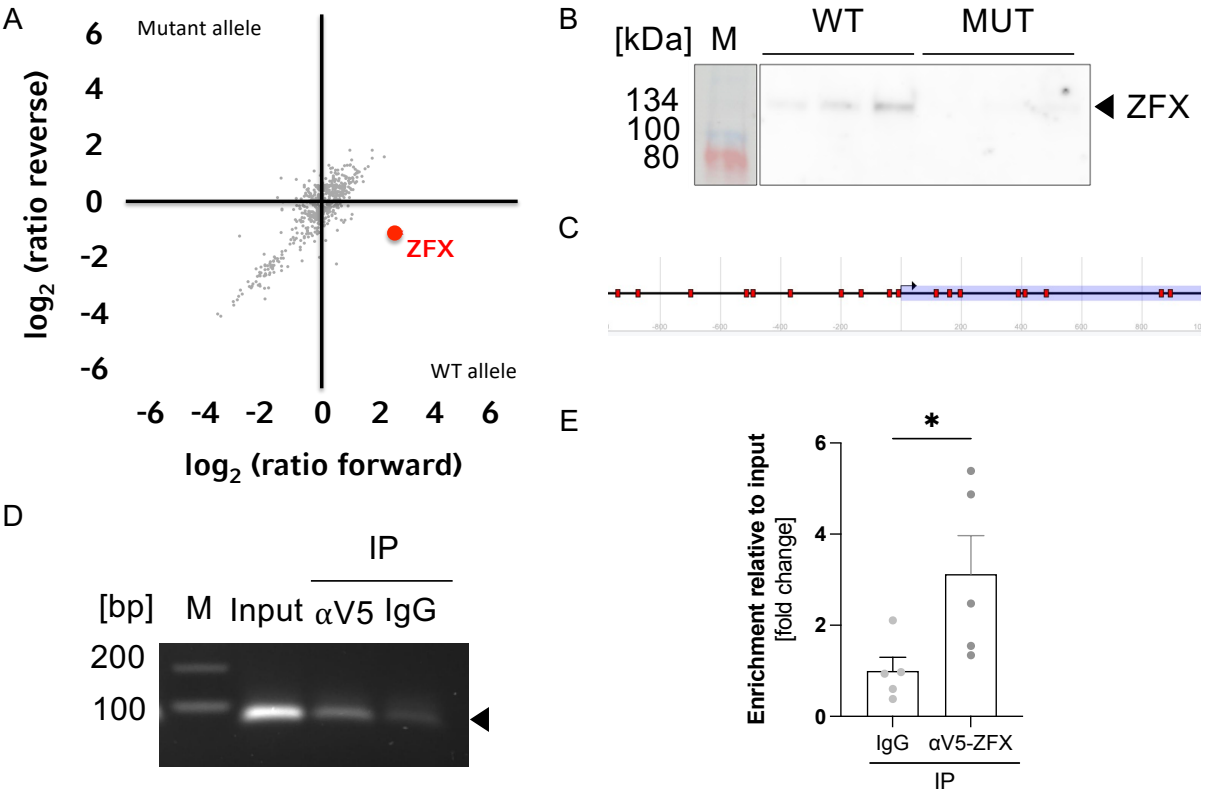

Figure 13 Differential protein-DNA interaction at the mutation site

A. SILAC analysis. The transcription factor ZFX preferentially binds to the WT allele of the variant. The SILAC experiment was conducted, analyzed, and visualized by Martin Dichgans/Manuel Lehm (Institute for Stroke and Dementia, LMU Munich, Martinsried, Germany) **B**. Replication of the SILAC experiment. Oligonucleotide pull-down using HeLa nuclear lysate, followed by western blot analysis, confirmed the preferential binding of ZFX (arrow) with the wild-type (WT) allele of the variant. WT: wild-type. MUT: mutant. M: marker **C**. Predicted ZFX binding sites (red boxes) at the *PDE5A* locus according to the Eukaryotic Promoter Database (https://epd.epfl.ch/). **D-E**. ChIP experiments demonstrated the binding of ZFX to the alternative promoter site. **D**. Agarose gel electrophoresis of the PDE5A2 alternative promoter sequences after immunoprecipitation of either V5 (αV5) or control (immunoglobulin G [IgG]). M: marker. **E**. Quantification of n=5 individual ChIP experiments (p=0.03). Data are mean ± SEM of 5 individual experiments. Student's paired t-test. *: p<0.05. Figures **B**-**E** were adapted with permission from: Figures 1H-K from "Identification of a Functional *PDE5A* variant at the Chromosome 4q27 Coronary Artery Disease Locus in an Extended Myocardial Infarction Family" by Dang *et al.*, *Circulation* 2021. 144: 662-665. Copyright © 2021 by Wolters Kluwer Health, Inc.

4.2.3.4 Identification of relevant cell types

After discovering the differentially binding transcription factor ZFX to the mutation site, we first assessed whether ZFX is present in relevant cell types. PDE5 function is best described in vascular smooth muscle cells (VSMCs) and platelets. Hence, these became our primary targets. qPCR analysis showed *ZFX* mRNA expression in human coronary artery smooth muscle cells (HCASMCs) and megakaryoblasts (MEG-01 cell line), which are platelet progenitors (Figure 14). In MEG-01, however, *ZFX* is expressed to a much lower magnitude than in HCASMCs, suggesting that the mechanism involving differential binding of ZFX to the *PDE5A* alternative promoter may be more relevant in VSMCs.

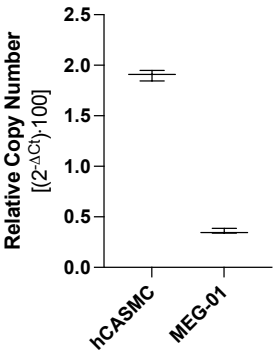

Figure 14 *ZFX* mRNA expression in relevant cell types

ZFX mRNA is expressed in human coronary artery smooth muscle cells (HCASMCs) and in megakaryoblasts (MEG-01), which are platelet progenitor cells. qPCR was performed in triplicates. Data are displayed as minimum to maximum, one sample each.

4.2.3.5 Establishing a ZFX knock-down assay

Next, we established a small interference ribonucleic acid (siRNA) knock-down assay (Figure 15) in HCASMCs and MEG-01. We could detect significantly decreased *ZFX* mRNA levels 24-72 h post-knock-down in both cell types by qPCR (Figure 15). However, the knock-down efficiency was not as high in MEG-01 as in HCASMCs (50% compared to 80%, respectively).

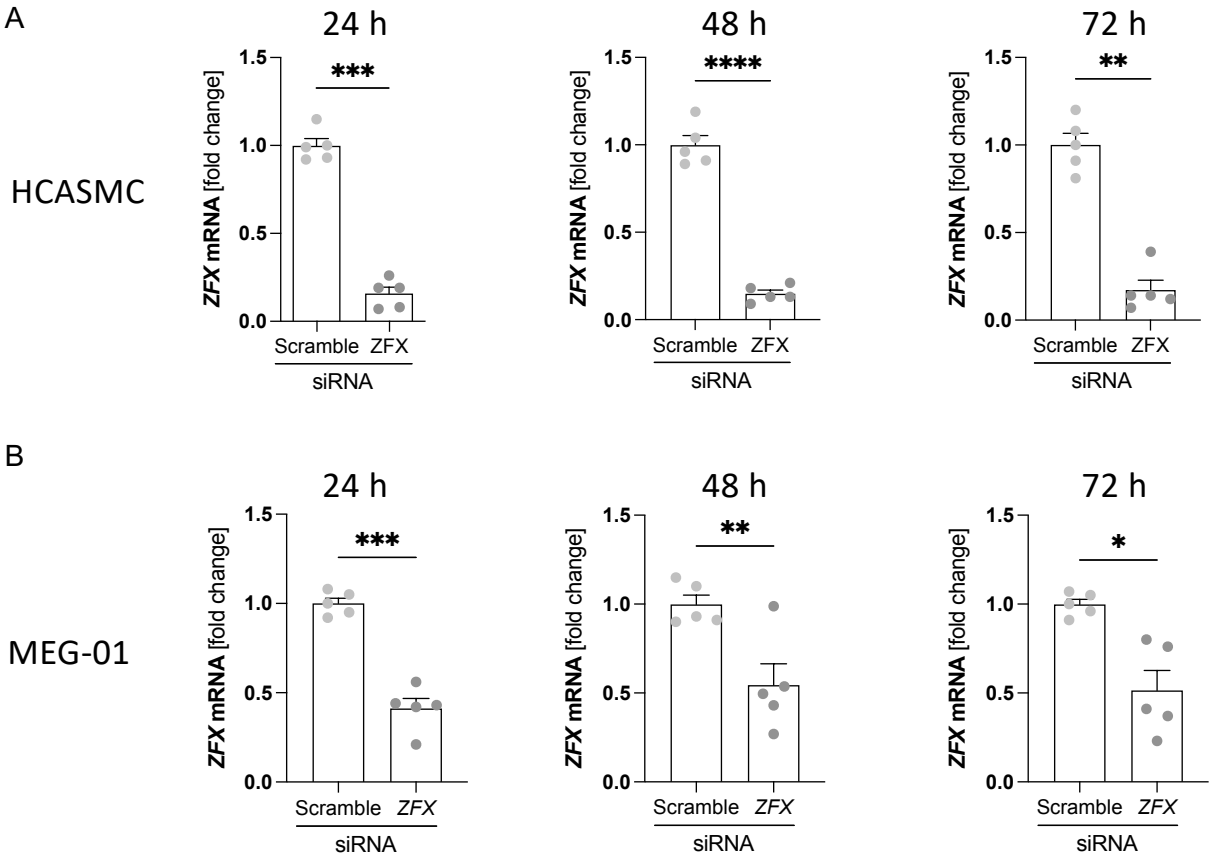

Figure 15 *ZFX* siRNA knock-down efficiency

A. *ZFX* mRNA levels after 24 h, 48 h, or 72 h *ZFX* siRNA knock-down in human coronary artery smooth muscle cells (HCASMCs). Student's paired t-test. Data are mean ± SEM of 5 individual experiments. **: p<0.01. ***: p<0.001. ****: p<0.0001. **B**. *ZFX* mRNA levels after 24 h, 48 h, or 72 h *ZFX* siRNA knock-down in megakaryoblasts (MEG-01). Data are mean ± SEM of 5 individual experiments. Student's paired t-test. *: p<0.05. **: p<0.01. ***: p<0.001. Figure **A** is adapted with permission from: Partial Figure 1L from "Identification of a Functional *PDE5A* variant at the Chromosome 4q27 Coronary Artery Disease Locus in an Extended Myocardial Infarction Family" by Dang *et al.*, *Circulation* 2021. 144: 662-665. Copyright © 2021 by Wolters Kluwer Health, Inc.

4.2.3.6 Influence of ZFX on PDE5A regulation/expression

Further analyzing the consequence of a *ZFX* knock-down in human coronary artery smooth muscle cells (HCASMCs) and MEG-01 cells, we performed qPCR targeting *PDE5A* after knock-down of *ZFX* in the individual cell types. That way, we demonstrated increased *PDE5A* mRNA expression in HCASMCs after 72 h *ZFX* siRNA knock-down (Figure 16A). However, despite a recognizable trend with MEG-01 cells, no significant increase of *PDE5A* expression was reached.

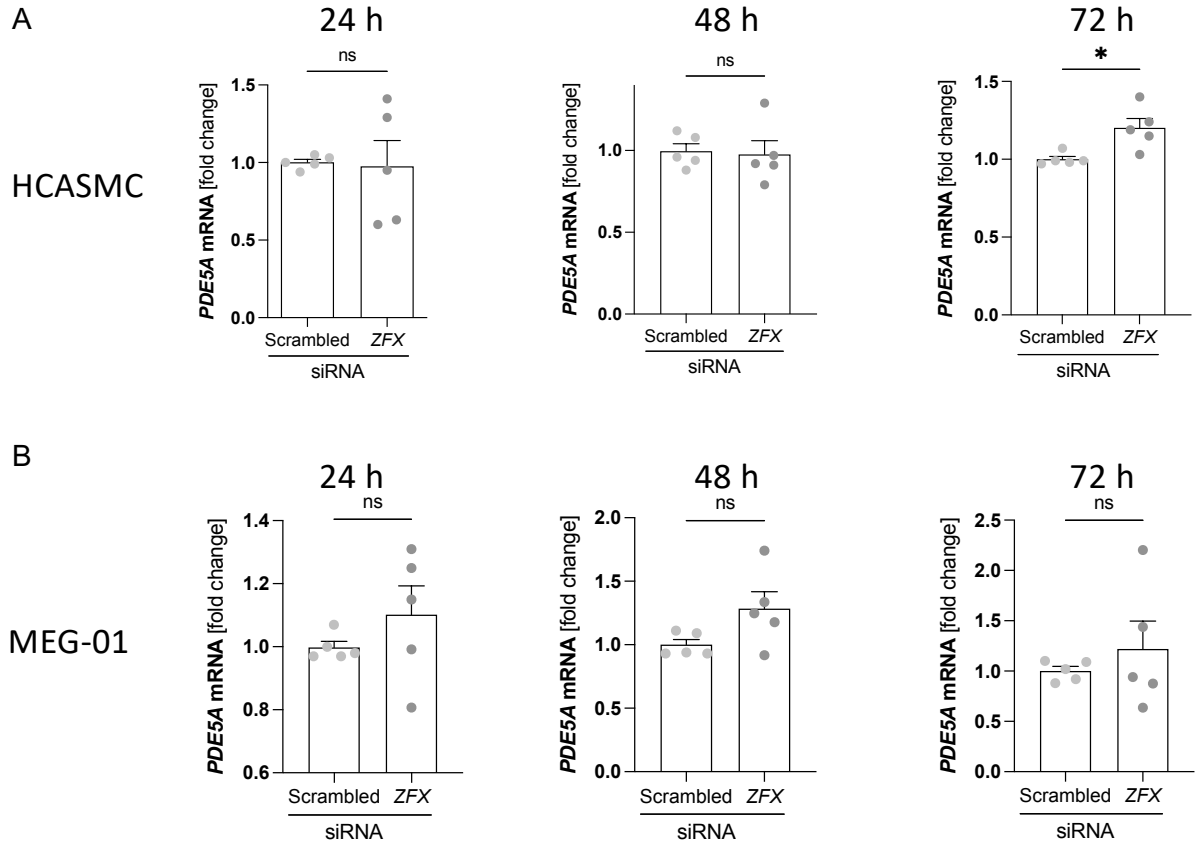

Figure 16 *PDE5A* mRNA expression in absence of ZFX

A. *PDE5A* mRNA expression after ZFX knock-down in HCASMCs. Lack of ZFX leads to increased *PDE5A* mRNA expression in HCASMCs after 72 h. Data are mean ± SEM of 5 individual experiments. Student's paired t-test. *: p<0.05. ns: not significant. **B**. *PDE5A* mRNA expression after ZFX knock-down in MEG-01 cells. Data are mean ± SEM of 5 individual experiments. Student's paired t-test. ns: not significant. Figure **A** is adapted with permission from: Partial Figure 1L from "Identification of a Functional *PDE5A* variant at the Chromosome 4q27 Coronary Artery Disease Locus in an Extended Myocardial Infarction Family" by Dang *et al.*, *Circulation* 2021. 144: 662-665. Copyright © 2021 by Wolters Kluwer Health, Inc.

Consequently, our findings hint towards a higher expression of *PDE5A* due to differential binding of the transcription factor ZFX to the mutation site in heterozygous mutation carriers of the presented CAD/MI family. Furthermore, VSMCs are likely to be the affected cell type of the discovered mechanism. However, more functional studies and patient data are required to validate these observations.

4.3 Effect of chronic PDE5 inhibition in an atherosclerotic mouse model

Since our data suggested that increased PDE5 expression might worsen CAD risk, we set out to study the potential of PDE5 inhibition to attenuate or even prevent atherosclerosis in an atherosclerotic mouse model. Therefore, we chose to utilize *Apoe* knockout (KO) mice, which feature tremendously increased blood cholesterol levels, leading to cholesterol-driven atherogenesis. For our experimental setup, 8–12-week-old *Apoe* KO mice received a high-fat diet and the PDE5 inhibitor sildenafil (approximately 40 mg/kg per day) for 12 weeks (Figure 17). Sildenafil was administered through the drinking water, and drinking behavior was controlled daily to ensure appropriate sildenafil intake. Control animals (also *Apoe* KO) received a high-fat diet but normal drinking water. The experimental groups contained equally mixed genders, and mice were held in groups of four animals per cage.

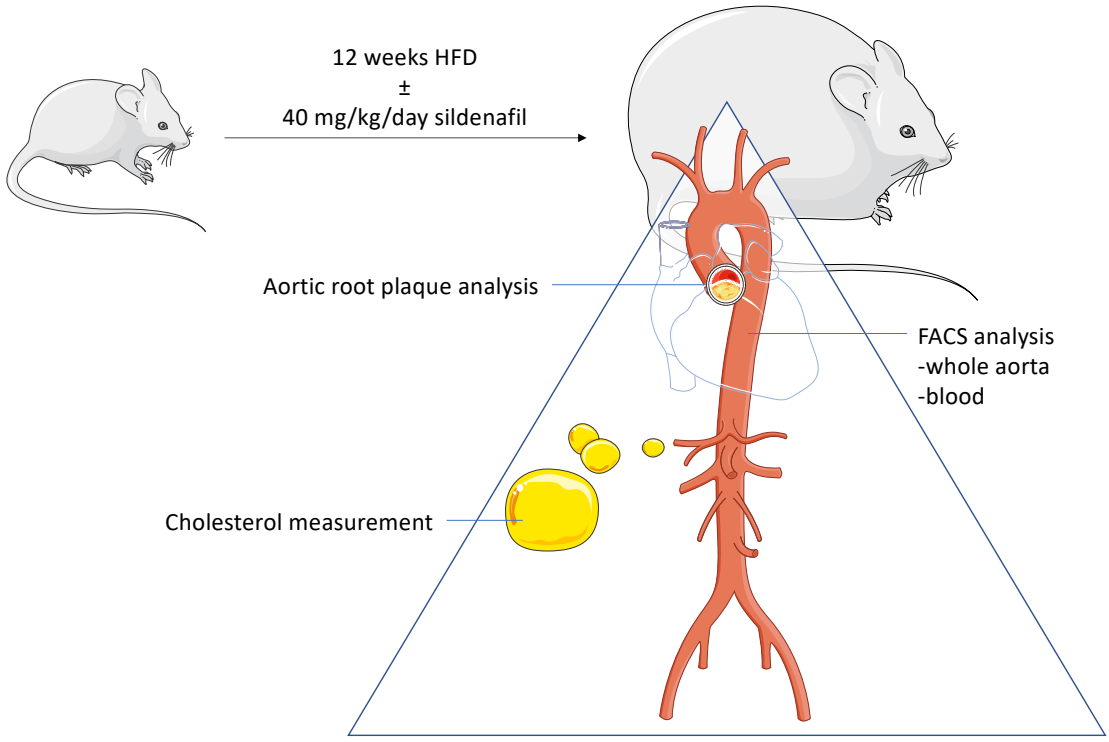

Figure 17 Experimental setup

Apoe KO were fed with high-fat diet and received sildenafil for 12 weeks. At the end of the experiment, animals were sacrificed to collect blood, the aorta, and other organs for further analysis. The figure was created using Servier Medical Art (smart.servier.com) (Les Laboratoires Servier, SAS, Suresnes, France). FACS: fluorescence-activated cell sorter.

4.3.1 General phenotype

Throughout the experiment, mouse weights were assessed weekly until the end of the experiment. Both the treatment and the control group presented similar growth and weight progression (Figure 18).

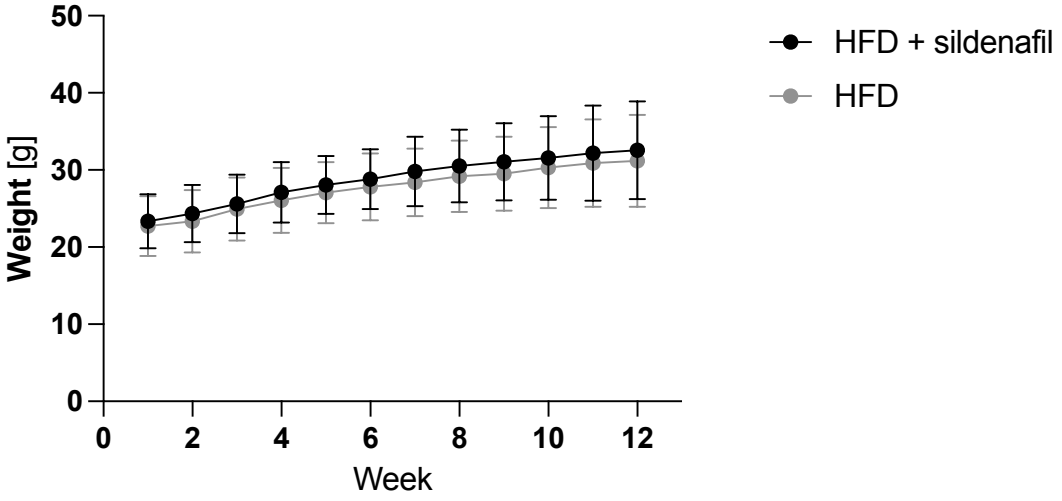

Figure 18 Weight progression

Weight of *Apoe* KO animals throughout 12 weeks of HFD ± sildenafil treatment. Data are mean ± SD of n=45 sildenafil treated animals and n=43 controls. Multiple unpaired t-tests (not significant). HFD: high-fat diet.

Furthermore, we measured total cholesterol levels at the end of the experiment. As expected, sildenafil treatment did not lead to any difference in cholesterol levels (Figure 19).

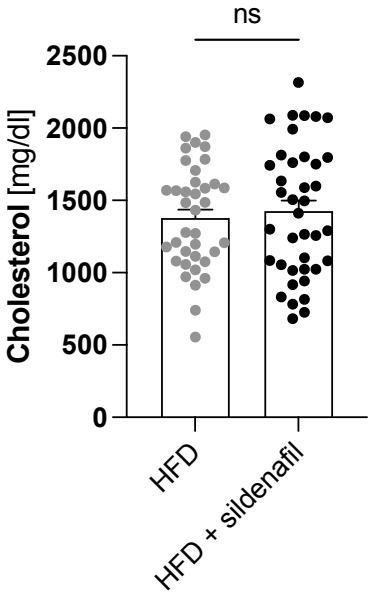

Figure 19 Cholesterol levels

Cholesterol levels in *Apoe* KO mice after 12 weeks of HFD ± sildenafil treatment. Data are mean ± SEM of n=37 controls and n=39 sildenafil treated *Apoe* KO mice. Student's unpaired t-test. ns: not significant.

4.3.2 Plaque phenotype

Since we expected the involvement of VSMCs, we examined putative alterations in atherosclerotic plaque phenotype. In collaboration with Hendrik Sager (Deutsches Herzzentrum München, Munich, Germany), FACS analysis was performed using whole blood and whole aorta. However, despite gross plaque formation in the control and treatment groups, no difference in the inflammatory cell composition was detected (Figure 20).

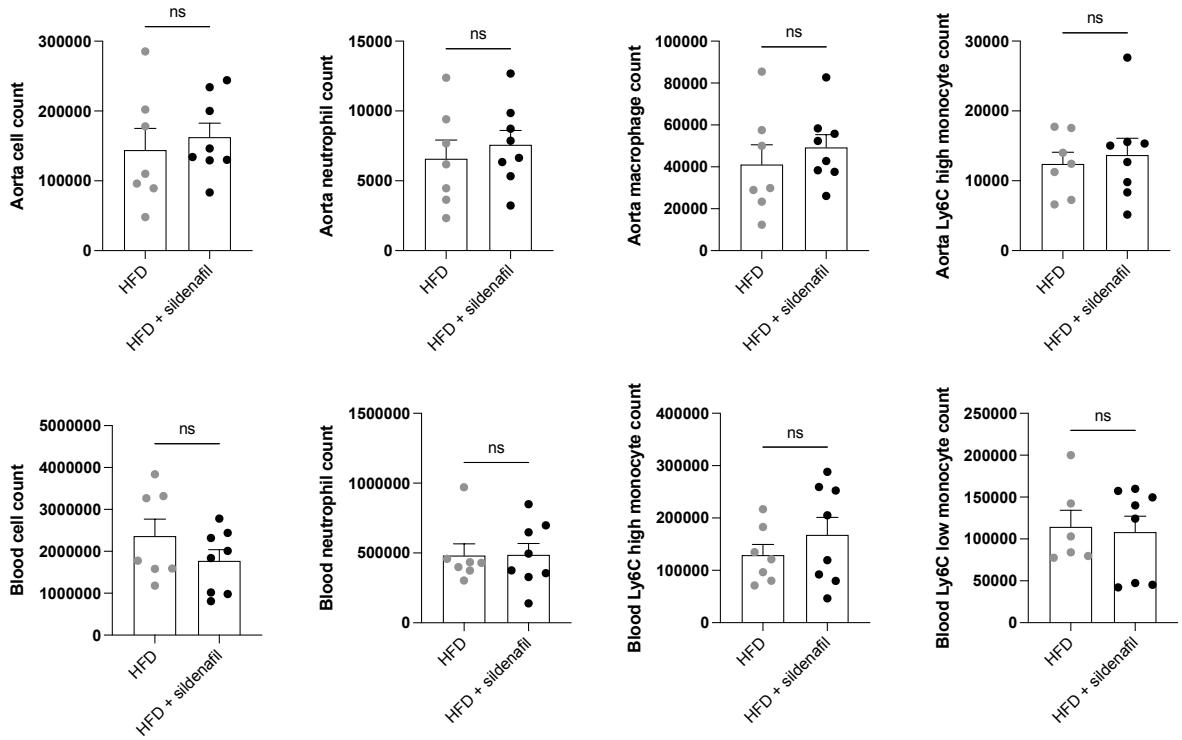

Figure 20 Absolute numbers of inflammatory cell counts in aorta and whole blood

FACS analysis did now show any difference regarding the inflammatory cell composition in aorta or blood (plotted as absolute numbers). Samples were processed, measured, and analyzed by Hendrik Sager/Julia Hinterdobler (Deutsches Herzzentrum München, Munich, Germany). Data are mean ± SEM of n=7 control animals and n=8 sildenafil treated animals. Mann-Whitney test. ns: not significant.

Additionally, we analyzed the plaque sizes within the aortic root. Therefore, a series of five µm thick transversal sections (every 30 µm) were stained with H&E, and atherosclerotic lesion sizes were assessed. However, unexpectedly, no differences between the control and treatment groups could be spotted (Figure 21).

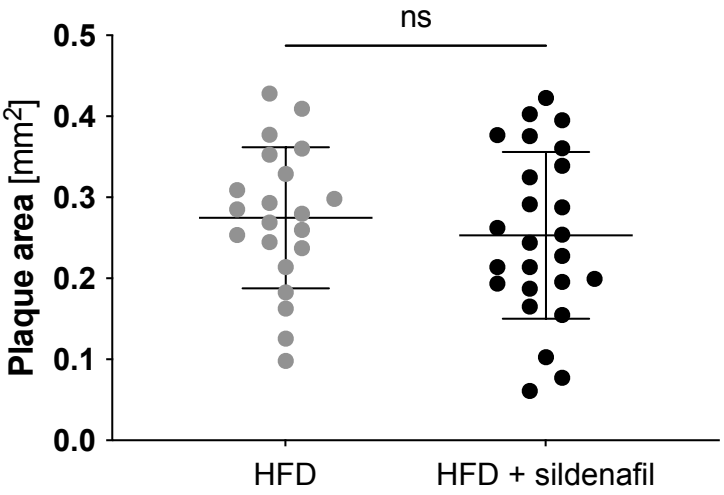

Figure 21 Sizes of atherosclerotic lesions found in the aortic root

Sildenafil did not lead to alterations in plaque sizes. Data are mean ± SEM of n=21 controls and n=25 sildenafil treated *Apoe* KO animals. Student's unpaired t-test. ns: not significant.

4.3.3 Influence of chronic sildenafil treatment on the expression of members of the NO-cGMP pathway

We then examined whether the chronic sildenafil treatment modulated the expression of members of the NO-cGMP pathway. For this, we extracted total mRNA from the mouse aortas and performed qPCR targeting murine *Nos3*, *Gucy1a1*, *Pde5a*, and *Irag*. All those targets could be detected in the aorta except for *Gucy1a1*. Furthermore, no significant difference could be detected with *Nos3*, *Pde5a, and Nos3* in sildenafil-treated *Apoe* KO mice (Figure 22).

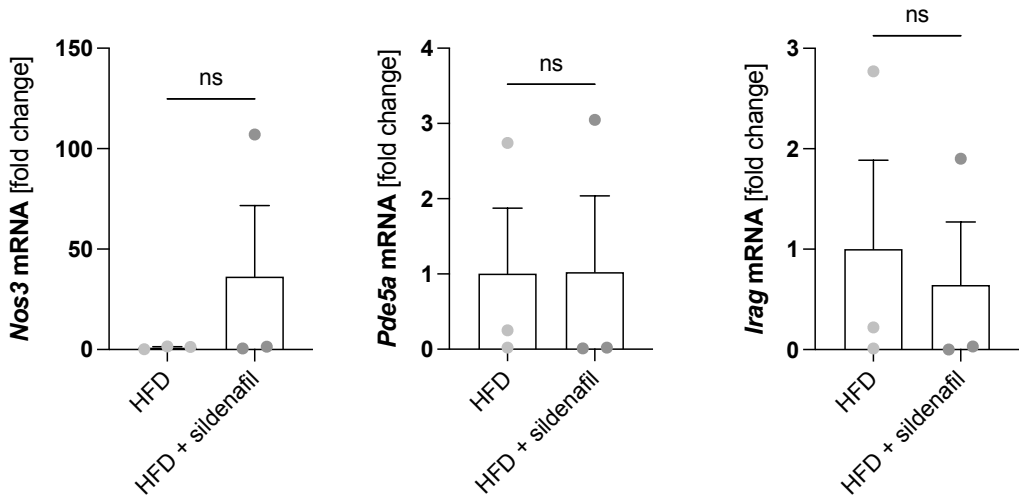

Figure 22 Expression of members of the NO-cGMP pathway in aortas of Apoe KO mice treated with high-fat diet and sildenafil

qPCR analysis of *Nos3*, *Pde5a*, and *Irag*. Sildenafil did not lead to changes in the expression of those genes. Data are mean ± SEM of n=3 per group. Mann-Whitney test. ns: not significant.

In summary, our approach to studying the effect of sildenafil on atherosclerosis did not reveal any benefits of sildenafil treatment in the context of cholesterol-driven atherogenesis. Neither did the treatment prevent the development of atherosclerotic plaques nor attenuate plaque formation. Thus, further study is required to assess the potential use of PDE5 inhibitors regarding CAD.

5 Discussion

Our study investigated the presumable role of PDE5 in CAD, considering several genetic and pharmacological aspects. First, we sought to functionally validate rare *PDE5A* variants identified in a discovery study. These variants were further examined by association analysis, calculating their putative genetic impact on CAD by comparing their presence in case and control cohorts of different studies. Next, we assessed the impact of another rare *PDE5A* variant (dbSNP: rs201005905; ClinGen Allele Registry: NM_033430.3:c.19A>T, NP_236914.2:p.Lys7Ter; gnomAD: 4-120548312-T-A, MAF $2.1*10^{-4}$) that had been identified in a family with a high prevalence for CAD and MI. Furthermore, we finally investigated the effect of chronic PDE5 inhibition on CAD in an atherosclerotic mouse model. All over, our findings suggest that PDE5 overexpression may promote CAD risk. In the following, implications and limitations of this study on the role of PDE5 in CAD risk will be discussed.

5.1 Rare coding variants of *PDE5A* and CAD risk

In order to investigate the presumable role of PDE5 in CAD, we studied rare *PDE5A* variants with presumed loss-of-function. Due to the distinctive nature of such rare variants, their analysis may deliver information on gene causality and targets that can be examined functionally and maybe pharmacologically (Momozawa and Mizukami, 2021). In addition, insights from rare variants with defined functional implications can help understand and interpret common variants identified by GWAS (Myocardial Infarction Genetics Consortium Investigators *et al.*, 2014, Bomba *et al.*, 2017, Stitziel *et al.*, 2017).

In collaboration with the Center for Genomic Medicine (Massachusetts General Hospital, Boston, MA, USA), we identified 67 rare coding variants in *PDE5A* in a subset of a discovery study with 5090 controls and 4703 cases of European ancestry (Myocardial Infarction Genetics *et al.*, 2016) (Table 50). Only variants with a MAF≥0.1% were chosen for association testing. Due to the number of cases and controls used in this study, variants with a lower MAF would have resulted in allele counts of n≤3, which would not have contributed to the test but rather diluted the statistical power.

In addition, we sought to increase statistical power by selecting for variants within a defined functional unit, e.g., gain-of-function or loss-of-function. Therefore, *in silico* prediction presents a helpful tool. However, missing functional knowledge about the gene or lack of accuracy of the prediction method (as seen with *GUCY1A1* in Wobst *et al.* (2016)) can exacerbate the selection or lead to the inclusion of variants that may decrease power. Therefore, we assessed the ability of the chosen rare *PDE5A* variants on cGMP degradation prior to inclusion into the association analysis. Using a stable sGC overexpression cell model

producing cGMP upon stimulation with a NO donor (Mullershausen *et al.*, 2004), every *PDE5A* variant was overexpressed individually, and the cGMP degradation capability of each variant was examined using a cGMP radioactive immunoassay. Out of six coding variants with a MAF≥0.1%, two previously predicted loss-of-function variants were functional. In contrast, three other variants, predicted as benign, were loss-of-function variants (Figure 5). Only one variant had been predicted correctly, emphasizing the importance of functional validation prior to association analysis since this can be a source for false conclusions later on. However, functional study of the variants of interest may not always be possible or feasible, either (i) because no functional assay is available for the variant of interest, or (ii) the number of variants to test is too high, making the process extremely laborious. Our study was limited to coding *PDE5A* variants since we would not have been able to test the functional consequence of intronic variants in an overexpression approach. Although the selection of variants is meant to increase statistical power and create meaningful association data, limited means to test the variant function may also lead to oversight of relevant variants, potentially weakening the association estimate.

We focused on the three identified loss-of-function *PDE5A* variants for the association analysis. The presence of those selected variants was significantly associated with reduced CAD risk in the discovery study dataset (OR, 0.69; 95% CI, 0.52-0.91; p<0.01) (Figure 6), proposing a protective effect of inactivating *PDE5A* variants on CAD. Replication of these suggestive variants in the MIGen study (n cases=24747, n controls=29704; (Myocardial Infarction Genetics Consortium *et al.*, 2009)) and two other datasets from UK Biobank (UKB_13K: n cases=6382, n controls=6343; UKB_50K n cases=1930, n controls=44597; https://www.ukbiobank.ac.uk/) in collaboration with the Center for Genomic Medicine (Massachusetts General Hospital, Boston, MA, USA), however, led to a loss of signal after adjusting for covariates and principal components (PCs) (Figure 7).

PCs display a small set of uncorrelated variables derived from a large set of variables, which try to explain as much of the total variance as possible (Abegaz *et al.*, 2019). In statistical genetics, PC regression is an established tool to discriminate possible confounders, i.e., population stratification, which may give rise to false positives or false negatives (Freedman *et al.*, 2004). For example, population stratification occurs if the genetic risk depends on ethnic background, the variants are unequally distributed among different ethnic subgroups, and cases and control groups feature study participants of different ethnic backgrounds. Hence, observed associations may be due to sampling differences and not the disease (Thomas and Witte, 2002, Wacholder *et al.*, 2002, Liu *et al.*, 2013, Abegaz *et al.*, 2019). Therefore, adjusting for PCs helps remove traits that correlate with the disease, ideally guaranteeing that observed associations are independent of other interacting factors (Aschard *et al.*, 2015). Compared to PC analysis (PCA) with common variants, PCA for rare variants remains challenging (Ma and

Shi, 2020). Typically, rare variant analyses display systematically different stratification than GWAS, which PCA cannot easily correct (Mathieson and McVean, 2012, Abegaz *et al.*, 2019, Ma and Shi, 2020). Furthermore, Mathieson and McVean demonstrated that correcting rare variant data using PCs can mitigate signals of truly associated variants (Mathieson and McVean, 2012, Abegaz *et al.*, 2019). Besides confounding factors, association studies can also be adjusted for demographic, environmental, and heritable covariates to find variants exclusively associated with the disease. However, by nature, genetic variants can potentially interact with both the disease and heritable covariates used for correction. If that is the case, the association estimates for the unadjusted and adjusted association will result in different outcomes (Aschard *et al.*, 2015). PDE5 expression, for example, is linked to diseases such as hypertension (Thieme *et al.*, 2017). Suppose one or more covariates used for adjustment also affect blood pressure. In that case, correction for these covariates may introduce a bias to the adjusted association estimate, explaining the loss of signal in our study. Hence, PC testing and reconsideration of the adjustment strategy are necessary for making a valid conclusion regarding the association of rare *PDE5A* variants with CAD.

To our knowledge, our rare variant analysis provides the first hint that inactivating *PDE5A* variants presumably exhibit protective effects against CAD. Apart from the limitations discussed above, our hypothesis must also be tested in populations of other ancestries than European since ethnicity-dependent differences had been reported regarding NO response (Cardillo *et al.*, 1999). Besides the functional insights derived from such analyses, these findings may provide potential markers for patient screening to assess individual CAD risk.

5.2 Implications of a familial *PDE5A* variant on CAD

In collaboration with the Institute of Cardiogenetics (University of Lübeck, Lübeck, Germany), whole-exome sequencing (WES) led to the identification of another rare *PDE5A* variant (dbSNP: rs201005905; ClinGen Allele Registry: NM_033430.3:c.19A>T, NP_236914.2:p.Lys7Ter; gnomAD: 4-120548312-T-A, MAF $2.1*10^{-4}$) in three members of a family with a high prevalence for premature CAD and MI (Figure 8) (Brænne *et al.*, 2012). In contrast to whole-genome approaches, WES focuses on analyzing the protein-coding genomic regions (exome). Since approximately 85% of disease-causing mutations are believed to be located in coding and functional genomic regions (Botstein and Risch, 2003, Majewski *et al.*, 2011), studying the exome by WES presents a promising approach to identify causal variants, especially in rare, often monogenic, genetic disorders (Rabbani *et al.*, 2014).

The familial *PDE5A* variant rs201005905 cosegregated with the disease phenotype. The maximum LOD score was 3.16 at a recombination fraction of θ=0.17 (Figure 8C). LOD scores indicate a logarithmic ratio of the “probability of linkage” and the “probability of non-

linkage" between a variant and a trait. For example, a LOD score of 3 means that if the possibility of linkage were 1000, the possibility of non-linkage would be 1. Hence, LOD scores above 3, as presented in this CAD/MI family, indicate a very high linkage probability (Morton, 1955), emphasizing a causal role of this particular *PDE5A* variant with CAD and MI.

Apart from the association of rs201005905 with CAD and MI, there is also the possibility that traditional risk factors may interfere with the phenotype in the family. However, based on the available background data, the family displayed a relatively moderate cardiovascular risk profile, which cannot explain the high prevalence of CAD and MI in this family alone (Supplementary Table 2).

The identified familial *PDE5A* variant rs201005905 was initially predicted to lead to a loss of function due to the stop codon (p.Lys7Ter) in the first exon of the *PDE5A2* isoform. However, on closer examination, overexpression of *PDE5A2* containing the stop codon followed by western blot analysis revealed the expression of a truncated PDE5A2 isoform (Figure 9). Due to the lack of a reliable PDE5 antibody, we had used V5-tagged PDE5A2 constructs (wild-type and variant form) for the western blot analysis. Although this approach may seem artificial, overexpression of PDE5-V5 utilizing *in vitro* transcription/translation resulted in similar protein bands (Figures 9B and C, respectively).

We then investigated the mechanisms that might lead to the truncated PDE5A2 isoform. Regarding PDEs, alternative transcription has only been reported for *PDE3A* (Wechsler *et al.*, 2002). Interestingly, mutagenesis experiments showed that the truncated PDE5A2 isoform resembles PDE5A3, which expression is usually restricted to tissues with cardiac or smooth muscle cell content (Lin *et al.*, 2000b, Lin, 2004) (Figure 9B). Thus, the alternative *PDE5A2* start codon seems to be a regular transcription initiation site in the proper cell-specific context, i.e., cardiac and smooth muscle cells. For a long time, the phenomenon of alternative transcription sites has been understood to be of adaptive nature. However, Xu *et al.* hypothesized that although multiple transcriptional initiation sites may exist within a gene, each gene would favor one optimal transcription start site (Xu *et al.*, 2019). Furthermore, they postulated that alternative transcriptional initiation would instead result from molecular errors (Xu *et al.*, 2019). The stop codon in *PDE5A2* may display such an error, leading to the alternative transcription from the *PDE5A3* transcriptional start and expression of the truncated PDE5A2 isoform. Unfortunately, it was not possible to analyze biospecimen of mutation carriers to investigate whether this truncated isoform also is produced *in vivo*.

Next, we attempted to study the activity of the truncated PDE5A2 isoform. However, functional evaluation of the previously used PDE5A2-V5 constructs was not possible since the C-terminal V5 tag, which was close to the catalytic domain, seemed to interfere with the catalytic function of the enzyme. Thus, untagged PDE5A2 was tested in the activity assay,

which revealed similar activity properties of the truncated PDE5A2 isoform like its wild-type counterpart (Figure 10).

Taken together, the p.Lys7Ter variant did neither lead to a loss of the PDE5A2 isoform nor alter PDE5A2 enzyme activity.

Having excluded a loss-of-function, we sought to investigate possible regulatory changes. Apart from the first exon of *PDE5A2*, the variant was also located in the first intron of *PDE5A1* and *PDE5A3* (Figure 8D). Interestingly, this region had already been described to exhibit promoter function (Lin *et al.*, 2000b). Alternative promoters, besides alternative splicing, contribute to the generation of protein and regulatory diversity (Landry *et al.*, 2003). The *PDE5A* alternative promoter is positioned downstream of the *PDE5A1* transcription initiation site (first exon of *PDE5A1*) and upstream of the transcription start of *PDE5A2* (first exon of *PDE5A2*) and *PDE5A3* (second *PDE5A* exon). Thus, only the latter two variants can be affected by the alternative promoter. So far, this has not been shown. Promoter sequences harbor great potential to give rise to polymorphisms involved in gene expression (Hoogendoorn *et al.*, 2003). Our reporter gene assays verified promoter activity at the intronic region encompassing the variant (Figure 11). Moreover, the promoter activity increased with the mutant allele of rs201005905, suggesting differential expression of *PDE5A*. Indeed, allelic imbalance assays demonstrated preferential transcription of the risk allele in mRNA from whole blood of the heterozygous variant carriers (Figure 12). Demonstrating true differential *PDE5A* expression in different tissues of interest would have been desirable. However, only blood samples were available, limiting how this variant could be studied in the variant carriers. Moreover, *PDE5A* is not as abundantly expressed in whole blood, where it is mainly found in platelets, as in SMCs. Rapid degradation of mRNA in platelets (Alhasan *et al.*, 2016), in addition to observed degradation of *PDE5A* mRNA in the blood samples starting 2 h after blood collection, even in the presence of RNA stabilizer (data not shown), made an inter-individual comparison of *PDE5A* mRNA levels difficult and unreliable. Consequently, we only compared differential allele transcription within the heterozygous variant carriers.

SNPs can influence the regulation of gene expression in various ways. Cis-acting regulatory polymorphisms mainly influence transcription initiation, directly affecting the regulated gene. On the one hand, cis-acting SNPs can disrupt transcription factor binding sites or alter transcription factor binding affinity to the DNA. On the other hand, SNPs may alter splicing patterns by resulting in exon skipping, activation of cryptic splice sites, or changing the balance of alternatively spliced isoforms (Pagani and Baralle, 2004, Johnson *et al.*, 2005, Knight, 2005). Trans-acting regulatory polymorphisms include changes in proteins involved in gene regulatory activity, like polymerases, transcription factors, co-factors, and RNAs involved in gene regulation, e.g., long non-coding RNAs (Johnson *et al.*, 2005). Since we had observed promoter activity at the SNP region (Figure 11), we investigated possible cis-acting

mechanisms. *In silico* analysis of the SNP did not hint towards altered transcription factor binding (data not shown). Regardless, SILAC analysis, which was performed in collaboration with the Max-Planck-Institute of Biochemistry (Martinsried, Germany), revealed preferential binding of the transcription factor ZFX to the wildtype allele in HeLa cells (Figure 13A). SILAC is an advanced mass spectrometric method for functional and quantitative proteome analysis (Mann, 2006). It allows the direct comparison of two proteomes in one measurement by labeling one proteome with stable isotopes. This method tremendously increases the comparability of two individual proteome samples, decreasing the probability of false-positive associations (Mann, 2006). Nevertheless, we sought to validate our findings. Repeating the SILAC pull-down in unlabeled HeLa nucleic lysates, we analyzed the presence of ZFX by western blot instead of mass spectrometry (Figure 13B). Similar to the SILAC result, differential binding of ZFX to the wildtype allele was detected. Comparison with the Eucaryotic Promoter Database (https://epd.epfl.ch/) further approved ZFX binding sites around the SNP site (Figure 13C). Moreover, ChIP analysis in HeLa cells overexpressing recombinant ZFX-V5 protein (full-length ZFX protein including a 3'-terminal V5 tag) demonstrated binding of ZFX-V5 to the wildtype allele of the alternative *PDE5A* promoter site (Figures 13D-E). These experiments were conducted using HeLa cells or HeLa nuclear lysates. Although this may appear artificial, HeLa cell lysates are commonly used as a transcription factor provider since they express many DNA binding proteins, enabling a simple environment to study DNA-protein interactions. Introduction of the rs201005905 mutant allele would have been desirable to further show the non-binding of ZFX in an endogenous environment. However, due to the lack of suitable protospacer adjacent motif (PAM) sites, the mutation could not be inserted into a cell line for advanced functional study of the variant.

In order to analyze the functional consequence of a lack of ZFX at the *PDE5A* promoter, we studied *PDE5A* expression in the context of *ZFX* siRNA knock-down. ZFX is expressed in different vascular cells but is most abundant in vascular SMCs. Since PDE5 seems to act mainly through SMCs and platelets in the vasculature, we chose VSMCs and megakaryoblasts, which are platelet progenitor cells, for further functional investigation (Figure 14). *ZFX* siRNA knock-down led to a significant increase of *PDE5A* expression in vascular SMCs (Figure 15A), implicating that ZFX usually exhibits repressive function at the *PDE5A* promoter. Although megakaryoblasts also exhibited increased PDE5 expression after ZFX knock-down, the effect was insignificant. Hence, the mechanism underlying the phenotype in the family may be mediated through SMCs rather than platelets. Of note, ZFX is more considered to be a transcriptional activator (Schneider-Gadicke *et al.*, 1989). Nevertheless, some studies have also shown the repressive function of ZFX, for example, with histone H1 gene expression (Gokhman *et al.*, 2013). In *Zfx* KO mice, more genes were found to be upregulated than downregulated in cell types unrelated to this study, i.e., hematopoietic and

embryonic stem cells (Galan-Caridad *et al.*, 2007). While some of the observed regulatory effects might be indirect, there is a chance that ZFX does not exclusively exhibit its function as an activator.

Taken together, the risk allele of rs201005905 interferes with ZFX binding, thereby amplifying *PDE5A* expression. Thus, enhanced PDE5 expression seems to be the mechanism in this family. Beyond that, this insight may also explain the effect of the common *PDE5A* variant (rs7678555), which had been discovered by GWAS (Nelson *et al.*, 2017). As discussed in chapter 5.1, functional interpretation of common variants remains challenging, particularly for variants found in non-coding genomic regions. Besides insights from WES variants, strategies to determine the biological function and relevance of common variants for diseases include the “closest gene approach”, incorporation of expression data, and investigating transgenic animal models (Kessler and Schunkert, 2021). Here, the discovery of the familial *PDE5A* variant helped to understand the presumable causal role of *PDE5A* at the 4q27 locus. When the common variant rs7678555 was discovered at that specific locus (Nelson *et al.*, 2017), it was first assigned to the closely encoded *MAD2L1* gene. However, this gene had neither been mentioned in context with CVD nor did it seem functionally relevant in the vasculature. Intriguingly, the risk allele of this SNP was significantly associated with increased *PDE5A* expression in human aortic tissue, despite its great distance to *PDE5A*. Preliminary data suggest that rs7678555 influences *PDE5A* expression through the long non-coding RNA *LINC02502* encoded near the SNP site. *LINC02502* was shown to interact with the RE1-silencing transcription factor (REST), another GWAS candidate for CAD (Nikpay *et al.*, 2015, Nelson *et al.*, 2017), which usually represses *PDE5A* expression. *In vitro* knock-down and overexpression approaches with *LINC02502* and *PDE5A* in VSMCs, followed by RNA immunoprecipitation, suggested that *LINC02502* interacts with REST, inhibiting its binding to the *PDE5A* promoter and thereby influencing *PDE5A* expression (Hegge *et al.*, 2020, Hoehne *et al.*, 2020). Since the familial *PDE5A* variant identified by WES also acts through increased *PDE5A* expression, a causal role of *PDE5A* at the 4q27 locus is highly probable. Indeed, increased PDE5 expression had long been suspected of playing a role in CVDs (Corbin *et al.*, 2005, Pokreisz *et al.*, 2009, Shan *et al.*, 2012, Mergia and Stegbauer, 2016, Thieme *et al.*, 2017). However, those studies did not go beyond observations, therefore, lacked causality (Mergia and Stegbauer, 2016).

Although we show a strong association between the familial *PDE5A* variant rs201005905 with CAD/MI in a family suffering from CAD/MI, the immediate functional consequence of this variant is less clear and remains to be investigated. We demonstrated that a lack of ZFX affects *PDE5A* expression in vascular SMCs rather than platelets (Figure 16). In VSMCs, PDE5 may control cellular phenotypes such as SMC phenotype switch (Lincoln *et al.*, 2006), migration (Brown *et al.*, 1999), proliferation (Wharton *et al.*, 2005), and apoptosis

(Zhu *et al.*, 2005). Other relevant cell types for cardiovascular function include endothelial cells. Although PDE5 is expressed in endothelial cells, little is known about its function. Some studies suggest roles in cell growth, apoptosis, and NOS activity modulation (Zhu *et al.*, 2005, Gebska *et al.*, 2011). However, the role of PDE5 in endothelial cells is debatable since the magnitude of PDE5 expression in endothelial cells is not comparable to VSMCs. Studying a *Pde5a* transgenic mouse model would have been desirable to understand the pathophysiological consequence of alterations in PDE5 expression and involved cell types. However, unlike other members of the NO-cGMP pathway, *Pde5a* cannot be studied in a KO mouse model since *Pde5a* KO mice have never been successfully generated (Francis *et al.*, 2010). Hence, studying the effect of PDE5 on the pathology of CAD and MI so far relied on the use of PDE5 inhibitors and observations thereof, which will be discussed in more detail in chapter 5.3.

In summary, this is the first report about a distinct rare variant in *PDE5A* (rs201005905), cosegregating with the disease phenotype observed in a family suffering from premature CAD/MI. Furthermore, this variant exhibits its effect by increasing PDE5 expression, complementing the previous observation that PDE5 loss-of-function may exert protective effects (chapter 5.1). Furthermore, our finding endorses a causal role of *PDE5A* in CAD at the 4q27 locus.

5.3 Effect of chronic PDE5 inhibition in an atherosclerotic mouse model

Based on the presumable protective effect of a lack of PDE5 in the vasculature, we sought to investigate the potential of the PDE5 inhibitor sildenafil to prevent atherosclerosis. Therefore, we analyzed atherosclerosis progression of *Apoe* KO mice in the context of chronic sildenafil treatment. *Apoe KO* mice, lacking the ApoE protein, are an established model for studying atherosclerosis (Getz and Reardon, 2012). In contrast to wild-type mice, *Apoe* KO animals form atherosclerotic plaques with age, which can be accelerated by administering a high-fat diet. In this study, the high-fat diet was administered for 12 weeks, which is more than sufficient for the development of gross plaques. Mouse atherosclerotic plaques differ slightly from human plaque development and pathophysiology (Getz and Reardon, 2012, von Scheidt *et al.*, 2017). Nevertheless, plaques from *Apoe* and *Ldlr* KO mice feature properties seen in patients with FH (Getz and Reardon, 2012).

As expected, all mice developed obesity throughout the experiment (Figure 18). Sildenafil was diluted in the drinking water (260 mg/L) and provided *ad libitum*. Water consumption was monitored daily, ensuring that the sildenafil treatment group received approximately 4 ml per day, corresponding to a dose of 40 mg/kg per day. This dose was chosen based on findings in the literature (Dussault *et al.*, 2009, Balarini *et al.*, 2013, Rodrigues *et al.*, 2013). In order to characterize atherosclerotic phenotypes, we examined total plasma cholesterol content (Figure 19). Aortic plaque phenotype and putative inflammatory alterations

in the blood were investigated using FACS analysis (Figure 20). Furthermore, plaque size was assessed by histologic analysis of the aortic root (Figure 21), aortic arch, and whole aorta (data not shown). Controversially, our study did not reveal any differences between *Apoe* KO mice and *Apoe* KO mice treated with sildenafil in any regard. We noticed a high variability in the control and treatment groups alike. Some of the mice (in both control and treatment groups) hardly developed atherosclerotic plaques, which is untypical for *Apoe* KO mice after receiving a high-fat diet for 12 weeks. Since all mice became heavily obese and exhibited strongly enhanced total cholesterol levels in plasma, responsiveness to the diet did not seem to be the problem. Hence, differences in plaque size could have been affected by other factors than sildenafil treatment. We also assessed the expression of several members of the NO-cGMP pathway in the aortas of control and sildenafil-treated animals to exclude effects due to differential expression. However, we could not detect any noteworthy differences (Figure 22).

Opposite to our findings, Balarini *et al.* demonstrated diminished plaque size in the aortic root after chronic sildenafil treatment in *Apoe* KO mice (Balarini *et al.*, 2013). Unlike our study, in which we simultaneously administered a high-fat diet and sildenafil for 12 weeks, Balarini *et al.* first initiated plaque formation using a high-fat diet for 7 weeks before adding sildenafil administration for 3 weeks (Balarini *et al.*, 2013). Similarly, other studies investigating chronic sildenafil administration in *Apoe* KO mice chose 7 days to 3 weeks of chronic sildenafil medication (Dussault *et al.*, 2009, Rodrigues *et al.*, 2013). However, comparability of these studies is difficult since the extension of sildenafil administration time might also result in a different outcome in the other studies (Rodrigues *et al.*, 2013).

From this, we made two conclusions: (i) either the atherosclerotic phenotype in our *Apoe* KO mice was too strong after receiving a high-fat diet for 12 weeks, overshadowing possibly subtle effects, or (ii) long-term continuous intake of sildenafil does not prevent or lessen lipoprotein-driven atherogenesis, while medium-term chronic administration after the onset of atherosclerosis progression may attenuate plaque progression. The inclusion of a non-high-fat *Apoe* KO control could have been helpful to answer some of the questions. Also, examining plaque phenotype at earlier time points might deliver further insights. Furthermore, blood pressure may be another interesting phenotype to look at. Addressing these points, however, was beyond reach for this study.

Although the effect of PDE5 inhibition on atherosclerosis remains to be resolved, PDE5 inhibition may still be interesting for patients carrying gain-of-function *PDE5A* variants or variants modulating other members of the NO-cGMP pathway.

5.4 Conclusion

As indicated by GWAS analyses and exome sequencing studies, solid genetic evidence hinted towards a crucial role of the NO-cGMP pathway in CAD. Despite this

prominent association, signals for *PDE5A* were unexpectedly underrepresented. Apart from the familial variant (rs201005905) reported in this study, only one more variant (rs7678555) has been identified, linking CAD risk with increased *PDE5A* expression. While other studies successfully explained the role of, for example, sGC in CAD, the role of PDE5 in CAD remained elusive. Here, we present the first study demonstrating a putative causal role of *PDE5A* in CAD. On the one hand, we showed that rare loss-of-function *PDE5A* variants exhibit a presumable protective effect against CAD risk. On the other hand, we characterized a rare gain-of-function *PDE5A* variant in a family suffering from premature CAD and MI, which led to increased *PDE5A* expression in vascular SMCs through differential ZFX binding to the *PDE5A* promoter.

In summary, we provide evidence of a putative causal effect of PDE5 on CAD and MI, suggesting that increased PDE5 expression may have detrimental effects on cardiovascular health. Thus, our data coincide with the previous notion derived from other genetic evidence that increased cGMP bioavailability in the vasculature may have a protective effect on atherosclerosis and CAD. Although an attractive pharmacological target, PDE5 inhibition may rather be effective in individuals carrying *PDE5A* risk variants or other variants that reduce cGMP bioavailability. Thus, this study may hold promising implications for assessing genetic CAD risk and personalized medicine approaches.

6 Acknowledgements

First of all, I would like to express my utmost gratitude towards Prof. Heribert Schunkert and Thorsten Kessler for allowing me to work on this project, their knowledgeable guidance and advice, culminating in this study's successful publication.

Furthermore, I thank Prof. Johannes Beckers for his full support throughout my thesis.

I am incredibly thankful for every team member of the Schunkert Lab and all collaborators who brought life and light into this project. I especially thank Jana Wobst and Julia Werner, who have accompanied this journey from the beginning and have tremendously contributed to my work scientifically and emotionally.

Most importantly, I am beyond grateful for the wholehearted and unconditional support of my family, close friends, and my fiancé David during this defining chapter of my life.

7 Bibliography

Abegaz, F., Chaichoompu, K., Genin, E., Fardo, D. W., Konig, I. R., Mahachie John, J. M. and Van Steen, K. Principals about principal components in statistical genetics. *Brief Bioinform* 2019. 20 (6): 2200-2216.

Abifadel, M., Varret, M., Rabes, J. P., Allard, D., Ouguerram, K., Devillers, M., Cruaud, C., Benjannet, S., Wickham, L., Erlich, D., Derre, A., Villeger, L., Farnier, M., Beucler, I., Bruckert, E., Chambaz, J., Chanu, B., Lecerf, J. M., Luc, G., Moulin, P., Weissenbach, J., Prat, A., Krempf, M., Junien, C., Seidah, N. G. and Boileau, C. Mutations in PCSK9 cause autosomal dominant hypercholesterolemia. *Nat Genet* 2003. 34 (2): 154-156.

Aicher, A., Heeschen, C., Mildner-Rihm, C., Urbich, C., Ihling, C., Technau-Ihling, K., Zeiher, A. M. and Dimmeler, S. Essential role of endothelial nitric oxide synthase for mobilization of stem and progenitor cells. *Nat Med* 2003. 9 (11): 1370-1376.

Alhasan, A. A., Izuogu, O. G., Al-Balool, H. H., Steyn, J. S., Evans, A., Colzani, M., Ghevaert, C., Mountford, J. C., Marenah, L., Elliott, D. J., Santibanez-Koref, M. and Jackson, M. S. Circular RNA enrichment in platelets is a signature of transcriptome degradation. *Blood* 2016. 127 (9): e1-e11.

Alves, A. C., Etxebarria, A., Soutar, A. K., Martin, C. and Bourbon, M. Novel functional APOB mutations outside LDL-binding region causing familial hypercholesterolaemia. *Hum Mol Genet* 2014. 23 (7): 1817-1828.

Ammendola, A., Geiselhoringer, A., Hofmann, F. and Schlossmann, J. Molecular determinants of the interaction between the inositol 1,4,5-trisphosphate receptor-associated cGMP kinase substrate (IRAG) and cGMP kinase Ibeta. *J Biol Chem* 2001. 276 (26): 24153-24159.

Antl, M., von Bruhl, M. L., Eiglsperger, C., Werner, M., Konrad, I., Kocher, T., Wilm, M., Hofmann, F., Massberg, S. and Schlossmann, J. IRAG mediates NO/cGMP-dependent inhibition of platelet aggregation and thrombus formation. *Blood* 2007. 109 (2): 552-559.

Aschard, H., Vilhjalmsson, B. J., Joshi, A. D., Price, A. L. and Kraft, P. Adjusting for heritable covariates can bias effect estimates in genome-wide association studies. *Am J Hum Genet* 2015. 96 (2): 329-339.

Aszodi, A., Pfeifer, A., Ahmad, M., Glauner, M., Zhou, X. H., Ny, L., Andersson, K. E., Kehrel, B., Offermanns, S. and Fassler, R. The vasodilator-stimulated phosphoprotein (VASP) is involved in cGMP- and cAMP-mediated inhibition of agonist-induced platelet aggregation, but is dispensable for smooth muscle function. *Embo j* 1999. 18 (1): 37-48.

Balarini, C. M., Leal, M. A., Gomes, I. B., Pereira, T. M., Gava, A. L., Meyrelles, S. S. and Vasquez, E. C. Sildenafil restores endothelial function in the apolipoprotein E knockout mouse. *J Transl Med* 2013. 11: 3.

Bartels, E. D., Christoffersen, C., Lindholm, M. W. and Nielsen, L. B. Altered metabolism of LDL in the arterial wall precedes atherosclerosis regression. *Circ Res* 2015. 117 (11): 933-942.

Bautista, L. E. Inflammation, endothelial dysfunction, and the risk of high blood pressure: epidemiologic and biological evidence. *J Hum Hypertens* 2003. 17 (4): 223-230.

Bekkering, S., Quintin, J., Joosten, L. A., van der Meer, J. W., Netea, M. G. and Riksen, N. P. Oxidized low-density lipoprotein induces long-term proinflammatory cytokine production and foam cell formation via epigenetic reprogramming of monocytes. *Arterioscler Thromb Vasc Biol* 2014. 34 (8): 1731-1738.

Benjamin, E. J., Muntner, P., Alonso, A., Bittencourt, M. S., Callaway, C. W., Carson, A. P., Chamberlain, A. M., Chang, A. R., Cheng, S., Das, S. R., Delling, F. N., Djousse, L., Elkind, M. S. V., Ferguson, J. F., Fornage, M., Jordan, L. C., Khan, S. S., Kissela, B. M., Knutson, K. L., Kwan, T. W., Lackland, D. T., Lewis, T. T., Lichtman, J. H., Longenecker, C. T., Loop, M. S., Lutsey, P. L., Martin, S. S., Matsushita, K., Moran, A. E., Mussolino, M. E., O'Flaherty, M., Pandey, A., Perak, A. M., Rosamond, W. D., Roth, G. A., Sampson, U. K. A., Satou, G. M., Schroeder, E. B., Shah, S. H., Spartano, N. L., Stokes, A., Tirschwell, D. L., Tsao, C. W., Turakhia, M. P., VanWagner, L. B., Wilkins, J. T., Wong, S. S., Virani, S. S., American Heart Association Council on, E., Prevention Statistics, C. and Stroke Statistics, S. Heart Disease and Stroke Statistics-2019 Update: A Report From the American Heart Association. *Circulation* 2019. 139 (10): e56-e66.

Bennett, M. R., Sinha, S. and Owens, G. K. Vascular Smooth Muscle Cells in Atherosclerosis. *Circ Res* 2016. 118 (4): 692-702.

Benz, P. M., Blume, C., Seifert, S., Wilhelm, S., Waschke, J., Schuh, K., Gertler, F., Munzel, T. and Renne, T. Differential VASP phosphorylation controls remodeling of the actin cytoskeleton. *J Cell Sci* 2009. 122 (Pt 21): 3954-3965.

Bischoff, E. Potency, selectivity, and consequences of nonselectivity of PDE inhibition. *Int J Impot Res* 2004. 16 Suppl 1: S11-14.

Bogdan, C. Nitric oxide and the regulation of gene expression. *Trends Cell Biol* 2001. 11 (2): 66-75.

Bomba, L., Walter, K. and Soranzo, N. The impact of rare and low-frequency genetic variants in common disease. *Genome Biol* 2017. 18 (1): 77.

Boren, J., Chapman, M. J., Krauss, R. M., Packard, C. J., Bentzon, J. F., Binder, C. J., Daemen, M. J., Demer, L. L., Hegele, R. A., Nicholls, S. J., Nordestgaard, B. G., Watts, G. F., Bruckert, E., Fazio, S., Ference, B. A., Graham, I., Horton, J. D., Landmesser, U., Laufs, U., Masana, L., Pasterkamp, G., Raal, F. J., Ray, K. K., Schunkert, H., Taskinen, M. R., van de Sluis, B., Wiklund, O., Tokgozoglu, L., Catapano, A. L. and Ginsberg, H. N. Low-density lipoproteins cause atherosclerotic cardiovascular disease: pathophysiological, genetic, and therapeutic insights: a consensus statement from the European Atherosclerosis Society Consensus Panel. *Eur Heart J* 2020. 41 (24): 2313-2330.

Botstein, D. and Risch, N. Discovering genotypes underlying human phenotypes: past successes for mendelian disease, future approaches for complex disease. *Nat Genet* 2003. 33 Suppl: 228-237.

Braenne, I., Kleinecke, M., Reiz, B., Graf, E., Strom, T., Wieland, T., Fischer, M., Kessler, T., Hengstenberg, C., Meitinger, T., Erdmann, J. and Schunkert, H. Systematic analysis of variants related to familial hypercholesterolemia in families with premature myocardial infarction. *Eur J Hum Genet* 2016. 24 (2): 191-197.

Brænne, I., Medack, A., Stark, K., Field, S., Tuna, S., null, n., Deloukas, P., Samani, N. J., Hengstenberg, C., Schunkert, H. and Erdmann, J. Abstract 19823: Whole-Exome Sequencing in an Extended Family with Myocardial Infarction Identified a Potential Functional Mutation in PDE5A. *Circulation* 2012. 126 (suppl_21): A19823-A19823.

Brown, C., Pan, X. and Hassid, A. Nitric oxide and C-type atrial natriuretic peptide stimulate primary aortic smooth muscle cell migration via a cGMP-dependent mechanism: relationship to microfilament dissociation and altered cell morphology. *Circ Res* 1999. 84 (6): 655-667.

Brune, B., Schmidt, K. U. and Ullrich, V. Activation of soluble guanylate cyclase by carbon monoxide and inhibition by superoxide anion. *Eur J Biochem* 1990. 192 (3): 683-688.

Cardillo, C., Kilcoyne, C. M., Cannon, R. O., 3rd and Panza, J. A. Attenuation of cyclic nucleotide-mediated smooth muscle relaxation in blacks as a cause of racial differences in vasodilator function. *Circulation* 1999. 99 (1): 90-95.

CARDIoGRAMplusC4D Consortium, Deloukas, P., Kanoni, S., Willenborg, C., Farrall, M., Assimes, T. L., Thompson, J. R., Ingelsson, E., Saleheen, D., Erdmann, J., Goldstein, B. A., Stirrups, K., Konig, I. R., Cazier, J. B., Johansson, A., Hall, A. S., Lee, J. Y., Willer, C. J., Chambers, J. C., Esko, T., Folkersen, L., Goel, A., Grundberg, E., Havulinna, A. S., Ho, W. K., Hopewell, J. C., Eriksson, N., Kleber, M. E., Kristiansson, K., Lundmark, P., Lyytikainen, L. P., Rafelt, S., Shungin, D., Strawbridge, R. J., Thorleifsson, G., Tikkanen, E., Van Zuydam, N., Voight, B. F., Waite, L. L., Zhang, W., Ziegler, A., Absher, D., Altshuler, D., Balmforth, A. J., Barroso, I., Braund, P. S., Burgdorf, C., Claudi-Boehm, S., Cox, D., Dimitriou, M., Do, R., DIAGRAM Consortium, CARDIOGENICS Consortium, Doney, A. S., El Mokhtari, N., Eriksson, P., Fischer, K., Fontanillas, P., Franco-Cereceda, A., Gigante, B., Groop, L., Gustafsson, S., Hager, J., Hallmans, G., Han, B. G., Hunt, S. E., Kang, H. M., Illig, T., Kessler, T., Knowles, J. W., Kolovou, G., Kuusisto, J., Langenberg, C., Langford, C., Leander, K., Lokki, M. L., Lundmark, A., McCarthy, M. I., Meisinger, C., Melander, O., Mihailov, E., Maouche, S., Morris, A. D., Muller-Nurasyid, M., MuTHER Consortium, Nikus, K., Peden, J. F., Rayner, N. W., Rasheed, A., Rosinger, S., Rubin, D., Rumpf, M. P., Schafer, A., Sivananthan, M., Song, C., Stewart, A. F., Tan, S. T., Thorgeirsson, G., van der Schoot, C. E., Wagner, P. J., Wellcome Trust Case Control Consortium, Wells, G. A., Wild, P. S., Yang, T. P., Amouyel, P., Arveiler, D., Basart, H., Boehnke, M., Boerwinkle, E., Brambilla, P., Cambien, F., Cupples, A. L., de Faire, U., Dehghan, A., Diemert, P., Epstein, S. E., Evans, A., Ferrario, M. M., Ferrieres, J., Gauguier, D., Go, A. S., Goodall, A. H., Gudnason, V., Hazen, S. L., Holm, H., Iribarren, C., Jang, Y., Kahonen, M., Kee, F., Kim, H. S., Klopp, N., Koenig, W., Kratzer, W., Kuulasmaa, K., Laakso, M., Laaksonen, R., Lee, J. Y., Lind, L., Ouwehand, W. H., Parish, S., Park, J. E., Pedersen, N. L., Peters, A., Quertermous, T., Rader, D. J., Salomaa, V., Schadt, E., Shah, S. H., Sinisalo, J., Stark, K., Stefansson, K., Tregouet, D. A., Virtamo, J., Wallentin, L., Wareham, N., Zimmermann, M. E., Nieminen, M. S., Hengstenberg, C., Sandhu, M. S., Pastinen, T., Syvanen, A. C., Hovingh, G. K., Dedoussis, G., Franks, P. W., Lehtimaki, T., Metspalu, A., Zalloua, P. A., Siegbahn, A., Schreiber, S., Ripatti, S., Blankenberg, S. S., Perola, M., Clarke, R., Boehm, B. O., O'Donnell, C., Reilly, M. P., Marz, W., Collins, R., Kathiresan, S., Hamsten, A., Kooner, J. S., Thorsteinsdottir, U., Danesh, J., Palmer, C. N., Roberts, R., Watkins, H., Schunkert, H. and Samani, N. J. Large-scale association analysis identifies new risk loci for coronary artery disease. *Nat Genet* 2013. 45 (1): 25-33.

Carvajal, J. A., Germain, A. M., Huidobro-Toro, J. P. and Weiner, C. P. Molecular mechanism of cGMP-mediated smooth muscle relaxation. *J Cell Physiol* 2000. 184 (3): 409-420.

Chen, Z. and Schunkert, H. Genetics of coronary artery disease in the post-GWAS era. *J Intern Med* 2021.

Chistiakov, D. A., Sobenin, I. A. and Orekhov, A. N. Vascular extracellular matrix in atherosclerosis. *Cardiol Rev* 2013. 21 (6): 270-288.

Chomczynski, P. and Sacchi, N. Single-step method of RNA isolation by acid guanidinium thiocyanate-phenol-chloroform extraction. *Anal Biochem* 1987. 162 (1): 156-159.

Clarke, M. and Bennett, M. The emerging role of vascular smooth muscle cell apoptosis in atherosclerosis and plaque stability. *Am J Nephrol* 2006. 26 (6): 531-535.

Clarkson, P. B., Lim, P. O. and MacDonald, T. M. Influence of basal nitric oxide secretion on cardiac function in man. *Br J Clin Pharmacol* 1995. 40 (4): 299-305.

Cooper, T. J., Guazzi, M., Al-Mohammad, A., Amir, O., Bengal, T., Cleland, J. G. and Dickstein, K. Sildenafil in Heart failure (SilHF). An investigator-initiated multinational randomized controlled clinical trial: rationale and design. *Eur J Heart Fail* 2013. 15 (1): 119-122.

Corbin, J. D. Mechanisms of action of PDE5 inhibition in erectile dysfunction. *Int J Impot Res* 2004. 16 Suppl 1: S4-7.

Corbin, J. D., Beasley, A., Blount, M. A. and Francis, S. H. High lung PDE5: a strong basis for treating pulmonary hypertension with PDE5 inhibitors. *Biochem Biophys Res Commun* 2005. 334 (3): 930-938.

Corbin, J. D., Zoraghi, R. and Francis, S. H. Allosteric-site and catalytic-site ligand effects on PDE5 functions are associated with distinct changes in physical form of the enzyme. *Cell Signal* 2009. 21 (12): 1768-1774.

Corinaldesi, C., Di Luigi, L., Lenzi, A. and Crescioli, C. Phosphodiesterase type 5 inhibitors: back and forward from cardiac indications. *J Endocrinol Invest* 2016. 39 (2): 143-151.

Dang, T. A., Schunkert, H. and Kessler, T. cGMP Signaling in Cardiovascular Diseases: Linking Genotype and Phenotype. *J Cardiovasc Pharmacol* 2020. 75 (6): 516-525.

Dang, T. A., Kessler, T., Wobst, J., Wierer, M., Braenne, I., Strom, T. M., Tennstedt, S., Sager, H. B., Meitinger, T., Erdmann, J. and Schunkert, H. Identification of a Functional PDE5A Variant at the Chromosome 4q27 Coronary Artery Disease Locus in an Extended Myocardial Infarction Family. *Circulation* 2021. 144 (8): 662-665.

Dangel, O., Mergia, E., Karlisch, K., Groneberg, D., Koesling, D. and Friebe, A. Nitric oxide-sensitive guanylyl cyclase is the only nitric oxide receptor mediating platelet inhibition. *J Thromb Haemost* 2010. 8 (6): 1343-1352.

Das, A., Durrant, D., Salloum, F. N., Xi, L. and Kukreja, R. C. PDE5 inhibitors as therapeutics for heart disease, diabetes and cancer. *Pharmacol Ther* 2015. 147: 12-21.

Davignon, J. and Ganz, P. Role of endothelial dysfunction in atherosclerosis. *Circulation* 2004. 109 (23 Suppl 1): III27-32.

Degerman, E., Belfrage, P. and Manganiello, V. C. Structure, localization, and regulation of cGMP-inhibited phosphodiesterase (PDE3). *J Biol Chem* 1997. 272 (11): 6823-6826.

Desch, M., Sigl, K., Hieke, B., Salb, K., Kees, F., Bernhard, D., Jochim, A., Spiessberger, B., Hocherl, K., Feil, R., Feil, S., Lukowski, R., Wegener, J. W., Hofmann, F. and Schlossmann, J. IRAG determines nitric oxide- and atrial natriuretic peptide-mediated smooth muscle relaxation. *Cardiovasc Res* 2010. 86 (3): 496-505.

Deschatrettes, E., Jouvert, P. and Zwiller, J. Overexpression of cyclic GMP-dependent protein kinase reduces MeCP2 and HDAC2 expression. *Brain Behav* 2012. 2 (6): 732-740.

Ding, B., Abe, J. I., Wei, H., Huang, Q., Walsh, R. A., Molina, C. A., Zhao, A., Sadoshima, J., Blaxall, B. C., Berk, B. C. and Yan, C. Functional role of phosphodiesterase 3 in cardiomyocyte apoptosis: implication in heart failure. *Circulation* 2005. 111 (19): 2469-2476.

Doshi, S. N., McDowell, I. F., Moat, S. J., Lang, D., Newcombe, R. G., Kredan, M. B., Lewis, M. J. and Goodfellow, J. Folate improves endothelial function in coronary artery disease: an effect mediated by reduction of intracellular superoxide? *Arterioscler Thromb Vasc Biol* 2001. 21 (7): 1196-1202.

Doshi, S. N., McDowell, I. F., Moat, S. J., Payne, N., Durrant, H. J., Lewis, M. J. and Goodfellow, J. Folic acid improves endothelial function in coronary artery disease via mechanisms largely independent of homocysteine lowering. *Circulation* 2002. 105 (1): 22-26.

Dussault, S., Maingrette, F., Menard, C., Michaud, S. E., Haddad, P., Groleau, J., Turgeon, J., Perez, G. and Rivard, A. Sildenafil increases endothelial progenitor cell function and improves ischemia-induced neovascularization in hypercholesterolemic apolipoprotein E-deficient mice. *Hypertension* 2009. 54 (5): 1043-1049.

Emdin, C. A., Khera, A. V., Klarin, D., Natarajan, P., Zekavat, S. M., Nomura, A., Haas, M., Aragam, K., Ardissino, D., Wilson, J. G., Schunkert, H., McPherson, R., Watkins, H., Elosua, R., Bown, M. J., Samani, N. J., Baber, U., Erdmann, J., Gormley, P., Palotie, A., Stitziel, N. O., Gupta, N., Danesh, J., Saleheen, D., Gabriel, S. and Kathiresan, S. Phenotypic Consequences of a Genetic Predisposition to Enhanced Nitric Oxide Signaling. *Circulation* 2018. 137 (3): 222-232.

Erdmann, J., Stark, K., Esslinger, U. B., Rumpf, P. M., Koesling, D., de Wit, C., Kaiser, F. J., Braunholz, D., Medack, A., Fischer, M., Zimmermann, M. E., Tennstedt, S., Graf, E., Eck, S., Aherrahrou, Z., Nahrstaedt, J., Willenborg, C., Bruse, P., Braenne, I., Nothen, M. M., Hofmann, P., Braund, P. S., Mergia, E., Reinhard, W., Burgdorf, C., Schreiber, S., Balmforth, A. J., Hall, A. S., Bertram, L., Steinhagen-Thiessen, E., Li, S. C., Marz, W., Reilly, M., Kathiresan, S., McPherson, R., Walter, U., CardioGram, Ott, J., Samani, N. J., Strom, T. M., Meitinger, T., Hengstenberg, C. and Schunkert, H. Dysfunctional nitric oxide signalling increases risk of myocardial infarction. *Nature* 2013. 504 (7480): 432-436.

Erdmann, J., Kessler, T., Munoz Venegas, L. and Schunkert, H. A decade of genome-wide association studies for coronary artery disease: the challenges ahead. *Cardiovasc Res* 2018. 114 (9): 1241-1257.

Fagan, K. A., Fouty, B. W., Tyler, R. C., Morris, K. G., Jr., Hepler, L. K., Sato, K., LeCras, T. D., Abman, S. H., Weinberger, H. D., Huang, P. L., McMurtry, I. F. and Rodman, D. M. The pulmonary circulation of homozygous or heterozygous eNOS-null mice is hyperresponsive to mild hypoxia. *J Clin Invest* 1999. 103 (2): 291-299.

Fernandez-Friera, L., Fuster, V., Lopez-Melgar, B., Oliva, B., Sanchez-Gonzalez, J., Macias, A., Perez-Asenjo, B., Zamudio, D., Alonso-Farto, J. C., Espana, S., Mendiguren, J., Bueno, H., Garcia-Ruiz, J. M., Ibanez, B., Fernandez-Ortiz, A. and Sanz, J. Vascular Inflammation in Subclinical Atherosclerosis Detected by Hybrid PET/MRI. *J Am Coll Cardiol* 2019. 73 (12): 1371-1382.

Forstermann, U. and Munzel, T. Endothelial nitric oxide synthase in vascular disease: from marvel to menace. *Circulation* 2006. 113 (13): 1708-1714.

Forstermann, U. and Sessa, W. C. Nitric oxide synthases: regulation and function. *Eur Heart J* 2012. 33 (7): 829-837, 837a-837d.

Francis, S. H., Bessay, E. P., Kotera, J., Grimes, K. A., Liu, L., Thompson, W. J. and Corbin, J. D. Phosphorylation of isolated human phosphodiesterase-5 regulatory domain induces an apparent conformational change and increases cGMP binding affinity. *J Biol Chem* 2002. 277 (49): 47581-47587.

Francis, S. H., Busch, J. L., Corbin, J. D. and Sibley, D. cGMP-dependent protein kinases and cGMP phosphodiesterases in nitric oxide and cGMP action. *Pharmacol Rev* 2010. 62 (3): 525-563.

Francis, S. H., Blount, M. A. and Corbin, J. D. Mammalian cyclic nucleotide phosphodiesterases: molecular mechanisms and physiological functions. *Physiol Rev* 2011. 91 (2): 651-690.

Freedman, M. L., Reich, D., Penney, K. L., McDonald, G. J., Mignault, A. A., Patterson, N., Gabriel, S. B., Topol, E. J., Smoller, J. W., Pato, C. N., Pato, M. T., Petryshen, T. L., Kolonel, L. N., Lander, E. S., Sklar, P., Henderson, B., Hirschhorn, J. N. and Altshuler, D. Assessing the impact of population stratification on genetic association studies. *Nat Genet* 2004. 36 (4): 388-393.

Friebe, A., Mergia, E., Dangel, O., Lange, A. and Koesling, D. Fatal gastrointestinal obstruction and hypertension in mice lacking nitric oxide-sensitive guanylyl cyclase. *Proc Natl Acad Sci U S A* 2007. 104 (18): 7699-7704.

Fukumura, D., Gohongi, T., Kadambi, A., Izumi, Y., Ang, J., Yun, C. O., Buerk, D. G., Huang, P. L. and Jain, R. K. Predominant role of endothelial nitric oxide synthase in vascular endothelial growth factor-induced angiogenesis and vascular permeability. *Proc Natl Acad Sci U S A* 2001. 98 (5): 2604-2609.

G. B. D. Diseases and Injuries Collaborators. Global burden of 369 diseases and injuries in 204 countries and territories, 1990-2019: a systematic analysis for the Global Burden of Disease Study 2019. *Lancet* 2020. 396 (10258): 1204-1222.

Galan-Caridad, J. M., Harel, S., Arenzana, T. L., Hou, Z. E., Doetsch, F. K., Mirny, L. A. and Reizis, B. Zfx controls the self-renewal of embryonic and hematopoietic stem cells. *Cell* 2007. 129 (2): 345-357.

Garcia, C. K., Wilund, K., Arca, M., Zuliani, G., Fellin, R., Maioli, M., Calandra, S., Bertolini, S., Cossu, F., Grishin, N., Barnes, R., Cohen, J. C. and Hobbs, H. H. Autosomal recessive hypercholesterolemia caused by mutations in a putative LDL receptor adaptor protein. *Science* 2001. 292 (5520): 1394-1398.

Gautier, E. L., Huby, T., Witztum, J. L., Ouzilleau, B., Miller, E. R., Saint-Charles, F., Aucouturier, P., Chapman, M. J. and Lesnik, P. Macrophage apoptosis exerts divergent effects on atherogenesis as a function of lesion stage. *Circulation* 2009. 119 (13): 1795-1804.

Gebska, M. A., Stevenson, B. K., Hemnes, A. R., Bivalacqua, T. J., Haile, A., Hesketh, G. G., Murray, C. I., Zaiman, A. L., Halushka, M. K., Krongkaew, N., Strong, T. D., Cooke, C. A., El-Haddad, H., Tuder, R. M., Berkowitz, D. E. and Champion, H. C. Phosphodiesterase-5A (PDE5A) is localized to the endothelial caveolae and modulates NOS3 activity. *Cardiovasc Res* 2011. 90 (2): 353-363.

Geiselhoringer, A., Werner, M., Sigl, K., Smital, P., Worner, R., Acheo, L., Stieber, J., Weinmeister, P., Feil, R., Feil, S., Wegener, J., Hofmann, F. and Schlossmann, J. IRAG is essential for relaxation of receptor-triggered smooth muscle contraction by cGMP kinase. *EMBO J* 2004. 23 (21): 4222-4231.

Gerthoffer, W. T. Mechanisms of vascular smooth muscle cell migration. *Circ Res* 2007. 100 (5): 607-621.

Getz, G. S. and Reardon, C. A. Animal models of atherosclerosis. *Arterioscler Thromb Vasc Biol* 2012. 32 (5): 1104-1115.

Ghofrani, H. A., Osterloh, I. H. and Grimminger, F. Sildenafil: from angina to erectile dysfunction to pulmonary hypertension and beyond. *Nat Rev Drug Discov* 2006. 5 (8): 689-702.

Gokhman, D., Livyatan, I., Sailaja, B. S., Melcer, S. and Meshorer, E. Multilayered chromatin analysis reveals E2f, Smad and Zfx as transcriptional regulators of histones. *Nat Struct Mol Biol* 2013. 20 (1): 119-126.

Goldstein, I., Lue, T. F., Padma-Nathan, H., Rosen, R. C., Steers, W. D. and Wicker, P. A. Oral sildenafil in the treatment of erectile dysfunction. Sildenafil Study Group. *N Engl J Med* 1998. 338 (20): 1397-1404.

Goldstein, J. L. and Brown, M. S. A century of cholesterol and coronaries: from plaques to genes to statins. *Cell* 2015. 161 (1): 161-172.

Greene, S. J., Gheorghiade, M., Borlaug, B. A., Pieske, B., Vaduganathan, M., Burnett, J. C., Jr., Roessig, L., Stasch, J. P., Solomon, S. D., Paulus, W. J. and Butler, J. The cGMP signaling pathway as a therapeutic target in heart failure with preserved ejection fraction. *J Am Heart Assoc* 2013. 2 (6): e000536.

Gresele, P., Momi, S. and Falcinelli, E. Anti-platelet therapy: phosphodiesterase inhibitors. *Br J Clin Pharmacol* 2011. 72 (4): 634-646.

Guazzi, M., Vicenzi, M., Arena, R. and Guazzi, M. D. PDE5 inhibition with sildenafil improves left ventricular diastolic function, cardiac geometry, and clinical status in patients with stable systolic heart failure: results of a 1-year, prospective, randomized, placebo-controlled study. *Circ Heart Fail* 2011. 4 (1): 8-17.

Gupta, R. M., Hadaya, J., Trehan, A., Zekavat, S. M., Roselli, C., Klarin, D., Emdin, C. A., Hilvering, C. R. E., Bianchi, V., Mueller, C., Khera, A. V., Ryan, R. J. H., Engreitz, J. M., Issner, R., Shoresh, N., Epstein, C. B., de Laat, W., Brown, J. D., Schnabel, R. B., Bernstein, B. E. and Kathiresan, S. A Genetic Variant Associated with Five Vascular Diseases Is a Distal Regulator of Endothelin-1 Gene Expression. *Cell* 2017. 170 (3): 522-533 e515.

Hanafy, K. A., Martin, E. and Murad, F. CCTeta, a novel soluble guanylyl cyclase-interacting protein. *J Biol Chem* 2004. 279 (45): 46946-46953.

Hegge, L. C., Wobst, J., Hoehne, C., Winter, H., Dang, T. A., Maegdefessel, L., Schunkert, H. and Kessler, T. Abstract 288: The Long Non-coding RNA LINC02502 as a Candidate for the Molecular Genetic Mechanism Linking Genotype and Phenotype at the PDE5A Locus. *Arteriosclerosis, Thrombosis, and Vascular Biology* 2020. 40 (Suppl_1): A288-A288.

Hoehne, C., Wobst, J., Hegge, L., Winter, H., Dang, T., Maegdefessel, L., Schunkert, H. and Kessler, T. Investigation of a long non-coding RNA at the 4Q26 coronary artery disease locus. *Atherosclerosis* 2020. 315: e37.

Hoogendoorn, B., Coleman, S. L., Guy, C. A., Smith, K., Bowen, T., Buckland, P. R. and O'Donovan, M. C. Functional analysis of human promoter polymorphisms. *Hum Mol Genet* 2003. 12 (18): 2249-2254.

Horowitz, J. D., Henry, C. A., Syrjanen, M. L., Louis, W. J., Fish, R. D., Antman, E. M. and Smith, T. W. Nitroglycerine/N-acetylcysteine in the management of unstable angina pectoris. *Eur Heart J* 1988. 9 Suppl A: 95-100.

Hubner, N. C., Nguyen, L. N., Hornig, N. C. and Stunnenberg, H. G. A quantitative proteomics tool to identify DNA-protein interactions in primary cells or blood. *J Proteome Res* 2015. 14 (2): 1315-1329.

Ignarro, L. J. and Kadowitz, P. J. The pharmacological and physiological role of cGMP in vascular smooth muscle relaxation. *Ann Rev Pharmacol Toxicol* 1985. 25: 171-191.

International Consortium for Blood Pressure Genome-Wide Association Studies, Ehret, G. B., Munroe, P. B., Rice, K. M., Bochud, M., Johnson, A. D., Chasman, D. I., Smith, A. V., Tobin, M. D., Verwoert, G. C., Hwang, S. J., Pihur, V., Vollenweider, P., O'Reilly, P. F., Amin, N., Bragg-Gresham, J. L., Teumer, A., Glazer, N. L., Launer, L., Zhao, J. H., Aulchenko, Y., Heath, S., Sober, S., Parsa, A., Luan, J., Arora, P., Dehghan, A., Zhang, F., Lucas, G., Hicks, A. A., Jackson, A. U., Peden, J. F., Tanaka, T., Wild, S. H., Rudan, I., Igl, W., Milaneschi, Y., Parker, A. N., Fava, C., Chambers, J. C., Fox, E. R., Kumari, M., Go, M. J., van der Harst, P., Kao, W. H., Sjogren, M., Vinay, D. G., Alexander, M., Tabara, Y., Shaw-Hawkins, S., Whincup, P. H., Liu, Y., Shi, G., Kuusisto, J., Tayo, B., Seielstad, M., Sim, X., Nguyen, K. D., Lehtimaki, T., Matullo, G., Wu, Y., Gaunt, T. R., Onland-Moret, N. C., Cooper, M. N., Platou, C. G., Org, E., Hardy, R., Dahgam, S., Palmen, J., Vitart, V., Braund, P. S., Kuznetsova, T., Uiterwaal, C. S., Adeyemo, A., Palmas, W., Campbell, H., Ludwig, B., Tomaszewski, M., Tzoulaki, I., Palmer, N. D., consortium, C. A., Consortium, C. K., KidneyGen, C., EchoGen, c., consortium, C.-H., Aspelund, T., Garcia, M., Chang, Y. P., O'Connell, J. R., Steinle, N. I., Grobbee, D. E., Arking, D. E., Kardia, S. L., Morrison, A. C., Hernandez, D., Najjar, S., McArdle, W. L., Hadley, D., Brown, M. J., Connell, J. M., Hingorani, A. D., Day, I. N., Lawlor, D. A., Beilby, J. P., Lawrence, R. W., Clarke, R., Hopewell, J. C., Ongen, H., Dreisbach, A. W., Li, Y., Young, J. H., Bis, J. C., Kahonen, M., Viikari, J., Adair, L. S., Lee, N. R., Chen, M. H., Olden, M., Pattaro, C., Bolton, J. A., Kottgen, A., Bergmann, S., Mooser, V., Chaturvedi, N., Frayling, T. M., Islam, M., Jafar, T. H., Erdmann, J., Kulkarni, S. R., Bornstein, S. R., Grassler, J., Groop, L., Voight, B. F., Kettunen, J., Howard, P., Taylor, A., Guarrera, S., Ricceri, F., Emilsson, V., Plump, A., Barroso, I., Khaw, K. T., Weder, A. B., Hunt, S. C., Sun, Y. V., Bergman, R. N., Collins, F. S., Bonnycastle, L. L., Scott, L. J., Stringham, H. M., Peltonen, L., Perola, M., Vartiainen, E., Brand, S. M., Staessen, J. A., Wang, T. J., Burton, P. R., Soler Artigas, M., Dong, Y., Snieder, H., Wang, X., Zhu, H., Lohman, K. K., Rudock, M. E., Heckbert, S. R., Smith, N. L., Wiggins, K. L., Doumatey, A., Shriner, D., Veldre, G., Viigimaa, M., Kinra, S., Prabhakaran, D., Tripathy, V., Langefeld, C. D., Rosengren, A., Thelle, D. S., Corsi, A. M., Singleton, A., Forrester, T., Hilton, G., McKenzie, C. A., Salako, T., Iwai, N., Kita, Y., Ogihara, T., Ohkubo, T., Okamura, T., Ueshima, H., Umemura, S., Eyheramendy, S., Meitinger, T., Wichmann, H. E., Cho, Y. S., Kim, H. L., Lee, J. Y., Scott, J., Sehmi, J. S., Zhang, W., Hedblad, B., Nilsson, P., Smith, G. D., Wong, A., Narisu, N., Stancakova, A., Raffel, L. J., Yao, J., Kathiresan, S., O'Donnell, C. J., Schwartz, S. M., Ikram, M. A., Longstreth, W. T., Jr., Mosley, T. H., Seshadri, S., Shrine, N. R., Wain, L. V., Morken, M. A., Swift, A. J., Laitinen, J., Prokopenko, I., Zitting, P., Cooper, J. A., Humphries, S. E., Danesh, J., Rasheed, A., Goel, A., Hamsten, A., Watkins, H., Bakker, S. J., van Gilst, W. H., Janipalli, C. S., Mani, K. R., Yajnik, C. S., Hofman, A., Mattace-Raso, F. U., Oostra, B. A., Demirkan, A., Isaacs, A., Rivadeneira, F., Lakatta, E. G., Orru, M., Scuteri, A., Ala-Korpela, M., Kangas, A. J., Lyytikainen, L. P., Soininen, P., Tukiainen, T., Wurtz, P., Ong, R. T., Dorr, M., Kroemer, H. K., Volker, U., Volzke, H., Galan, P., Hercberg, S., Lathrop, M., Zelenika, D., Deloukas, P., Mangino, M., Spector, T. D., Zhai, G., Meschia, J. F., Nalls, M. A., Sharma, P., Terzic, J., Kumar, M. V., Denniff, M., Zukowska-Szczechowska, E., Wagenknecht, L. E., Fowkes, F. G., Charchar, F. J., Schwarz, P. E., Hayward, C., Guo, X., Rotimi, C., Bots, M. L., Brand, E., Samani, N. J., Polasek, O., Talmud, P. J., Nyberg, F., Kuh, D., Laan, M., Hveem, K., Palmer, L. J., van der

Schouw, Y. T., Casas, J. P., Mohlke, K. L., Vineis, P., Raitakari, O., Ganesh, S. K., Wong, T. Y., Tai, E. S., Cooper, R. S., Laakso, M., Rao, D. C., Harris, T. B., Morris, R. W., Dominiczak, A. F., Kivimaki, M., Marmot, M. G., Miki, T., Saleheen, D., Chandak, G. R., Coresh, J., Navis, G., Salomaa, V., Han, B. G., Zhu, X., Kooner, J. S., Melander, O., Ridker, P. M., Bandinelli, S., Gyllensten, U. B., Wright, A. F., Wilson, J. F., Ferrucci, L., Farrall, M., Tuomilehto, J., Pramstaller, P. P., Elosua, R., Soranzo, N., Sijbrands, E. J., Altshuler, D., Loos, R. J., Shuldiner, A. R., Gieger, C., Meneton, P., Uitterlinden, A. G., Wareham, N. J., Gudnason, V., Rotter, J. I., Rettig, R., Uda, M., Strachan, D. P., Witteman, J. C., Hartikainen, A. L., Beckmann, J. S., Boerwinkle, E., Vasan, R. S., Boehnke, M., Larson, M. G., Jarvelin, M. R., Psaty, B. M., Abecasis, G. R., Chakravarti, A., Elliott, P., van Duijn, C. M., Newton-Cheh, C., Levy, D., Caulfield, M. J. and Johnson, T. Genetic variants in novel pathways influence blood pressure and cardiovascular disease risk. *Nature* 2011. 478 (7367): 103-109.

Jager, R., Schwede, F., Genieser, H. G., Koesling, D. and Russwurm, M. Activation of PDE2 and PDE5 by specific GAF ligands: delayed activation of PDE5. *Br J Pharmacol* 2010. 161 (7): 1645-1660.

Johnson, A. D., Wang, D. and Sadee, W. Polymorphisms affecting gene regulation and mRNA processing: broad implications for pharmacogenetics. *Pharmacol Ther* 2005. 106 (1): 19-38.

Johnson, A. D., Yanek, L. R., Chen, M. H., Faraday, N., Larson, M. G., Tofler, G., Lin, S. J., Kraja, A. T., Province, M. A., Yang, Q., Becker, D. M., O'Donnell, C. J. and Becker, L. C. Genome-wide meta-analyses identifies seven loci associated with platelet aggregation in response to agonists. *Nat Genet* 2010. 42 (7): 608-613.

Kass, D. A., Champion, H. C. and Beavo, J. A. Phosphodiesterase type 5: expanding roles in cardiovascular regulation. *Circ Res* 2007. 101 (11): 1084-1095.

Kaun, K. R., Riedl, C. A., Chakaborty-Chatterjee, M., Belay, A. T., Douglas, S. J., Gibbs, A. G. and Sokolowski, M. B. Natural variation in food acquisition mediated via a Drosophila cGMP-dependent protein kinase. *J Exp Biol* 2007. 210 (Pt 20): 3547-3558.

Kaupp, U. B. and Seifert, R. Cyclic nucleotide-gated ion channels. *Physiol Rev* 2002. 82 (3): 769-824.

Kessler, T., Wobst, J., Wolf, B., Eckhold, J., Vilne, B., Hollstein, R., von Ameln, S., Dang, T. A., Sager, H. B., Moritz Rumpf, P., Aherrahrou, R., Kastrati, A., Bjorkegren, J. L. M., Erdmann, J., Lusis, A. J., Civelek, M., Kaiser, F. J. and Schunkert, H. Functional Characterization of the GUCY1A3 Coronary Artery Disease Risk Locus. *Circulation* 2017. 136 (5): 476-489.

Kessler, T. and Schunkert, H. Coronary Artery Disease Genetics Enlightened by Genome-Wide Association Studies. *JACC Basic Transl Sci* 2021. 6 (7): 610-623.

Khera, A. V., Won, H. H., Peloso, G. M., Lawson, K. S., Bartz, T. M., Deng, X., van Leeuwen, E. M., Natarajan, P., Emdin, C. A., Bick, A. G., Morrison, A. C., Brody, J. A., Gupta, N., Nomura, A., Kessler, T., Duga, S., Bis, J. C., van Duijn, C. M., Cupples, L. A., Psaty, B., Rader, D. J., Danesh, J., Schunkert, H., McPherson, R., Farrall, M., Watkins, H., Lander, E., Wilson, J. G., Correa, A., Boerwinkle, E., Merlini, P. A., Ardissino, D., Saleheen, D., Gabriel, S. and Kathiresan, S. Diagnostic Yield and Clinical Utility of Sequencing Familial Hypercholesterolemia Genes in Patients With Severe Hypercholesterolemia. *J Am Coll Cardiol* 2016. 67 (22): 2578-2589.

Khera, A. V., Chaffin, M., Aragam, K. G., Haas, M. E., Roselli, C., Choi, S. H., Natarajan, P., Lander, E. S., Lubitz, S. A., Ellinor, P. T. and Kathiresan, S. Genome-wide polygenic scores

for common diseases identify individuals with risk equivalent to monogenic mutations. *Nat Genet* 2018. 50 (9): 1219-1224.

Klarin, D., Zhu, Q. M., Emdin, C. A., Chaffin, M., Horner, S., McMillan, B. J., Leed, A., Weale, M. E., Spencer, C. C. A., Aguet, F., Segre, A. V., Ardlie, K. G., Khera, A. V., Kaushik, V. K., Natarajan, P., Consortium, C. A. D. and Kathiresan, S. Genetic analysis in UK Biobank links insulin resistance and transendothelial migration pathways to coronary artery disease. *Nat Genet* 2017. 49 (9): 1392-1397.

Knight, J. C. Regulatory polymorphisms underlying complex disease traits. *J Mol Med (Berl)* 2005. 83 (2): 97-109.

Landry, J. R., Mager, D. L. and Wilhelm, B. T. Complex controls: the role of alternative promoters in mammalian genomes. *Trends Genet* 2003. 19 (11): 640-648.

Lavi, S., McConnell, J. P., Rihal, C. S., Prasad, A., Mathew, V., Lerman, L. O. and Lerman, A. Local production of lipoprotein-associated phospholipase A2 and lysophosphatidylcholine in the coronary circulation: association with early coronary atherosclerosis and endothelial dysfunction in humans. *Circulation* 2007. 115 (21): 2715-2721.

Lehners, M., Dobrowinski, H., Feil, S. and Feil, R. cGMP Signaling and Vascular Smooth Muscle Cell Plasticity. *J Cardiovasc Dev Dis* 2018. 5 (2).

Li, A. C. and Glass, C. K. The macrophage foam cell as a target for therapeutic intervention. *Nat Med* 2002. 8 (11): 1235-1242.

Li, W., Mital, S., Ojaimi, C., Csiszar, A., Kaley, G. and Hintze, T. H. Premature death and age-related cardiac dysfunction in male eNOS-knockout mice. *J Mol Cell Cardiol* 2004. 37 (3): 671-680.

Libby, P., Ridker, P. M. and Hansson, G. K. Progress and challenges in translating the biology of atherosclerosis. *Nature* 2011. 473 (7347): 317-325.

Libby, P., Buring, J. E., Badimon, L., Hansson, G. K., Deanfield, J., Bittencourt, M. S., Tokgozoglu, L. and Lewis, E. F. Atherosclerosis. *Nat Rev Dis Primers* 2019. 5 (1): 56.

Lin, C. S., Lau, A., Tu, R. and Lue, T. F. Expression of three isoforms of cGMP-binding cGMP-specific phosphodiesterase (PDE5) in human penile cavernosum. *Biochem Biophys Res Commun* 2000a. 268 (2): 628-635.

Lin, C. S., Lau, A., Tu, R. and Lue, T. F. Identification of three alternative first exons and an intronic promoter of human PDE5A gene. *Biochem Biophys Res Commun* 2000b. 268 (2): 596-602.

Lin, C. S. Tissue expression, distribution, and regulation of PDE5. *Int J Impot Res* 2004. 16 Suppl 1: S8-S10.

Lincoln, T. M., Wu, X., Sellak, H., Dey, N. and Choi, C. S. Regulation of vascular smooth muscle cell phenotype by cyclic GMP and cyclic GMP-dependent protein kinase. *Front Biosci* 2006. 11: 356-367.

Liu, J., Lewinger, J. P., Gilliland, F. D., Gauderman, W. J. and Conti, D. V. Confounding and heterogeneity in genetic association studies with admixed populations. *Am J Epidemiol* 2013. 177 (4): 351-360.

Lukowski, R., Krieg, T., Rybalkin, S. D., Beavo, J. and Hofmann, F. Turning on cGMP-dependent pathways to treat cardiac dysfunctions: boom, bust, and beyond. *Trends Pharmacol Sci* 2014. 35 (8): 404-413.

Ma, S. and Shi, G. On rare variants in principal component analysis of population stratification. *BMC Genet* 2020. 21 (1): 34.

Maass, P. G., Aydin, A., Luft, F. C., Schachterle, C., Weise, A., Stricker, S., Lindschau, C., Vaegler, M., Qadri, F., Toka, H. R., Schulz, H., Krawitz, P. M., Parkhomchuk, D., Hecht, J., Hollfinger, I., Wefeld-Neuenfeld, Y., Bartels-Klein, E., Muhl, A., Kann, M., Schuster, H., Chitayat, D., Bialer, M. G., Wienker, T. F., Ott, J., Rittscher, K., Liehr, T., Jordan, J., Plessis, G., Tank, J., Mai, K., Naraghi, R., Hodge, R., Hopp, M., Hattenbach, L. O., Busjahn, A., Rauch, A., Vandeput, F., Gong, M., Ruschendorf, F., Hubner, N., Haller, H., Mundlos, S., Bilginturan, N., Movsesian, M. A., Klussmann, E., Toka, O. and Bahring, S. PDE3A mutations cause autosomal dominant hypertension with brachydactyly. *Nat Genet* 2015. 47 (6): 647-653.

Majewski, J., Schwartzentruber, J., Lalonde, E., Montpetit, A. and Jabado, N. What can exome sequencing do for you? *J Med Genet* 2011. 48 (9): 580-589.

Mann, M. Functional and quantitative proteomics using SILAC. *Nat Rev Mol Cell Biol* 2006. 7 (12): 952-958.

Mathieson, I. and McVean, G. Differential confounding of rare and common variants in spatially structured populations. *Nat Genet* 2012. 44 (3): 243-246.

Matsuura, E., Hughes, G. R. and Khamashta, M. A. Oxidation of LDL and its clinical implication. *Autoimmun Rev* 2008. 7 (7): 558-566.

McCormick, K. and Baillie, G. S. Compartmentalisation of second messenger signalling pathways. *Curr Opin Genet Dev* 2014. 27: 20-25.

McPherson, R. and Tybjaerg-Hansen, A. Genetics of Coronary Artery Disease. *Circ Res* 2016. 118 (4): 564-578.

Mergia, E., Russwurm, M., Zoidl, G. and Koesling, D. Major occurrence of the new alpha2beta1 isoform of NO-sensitive guanylyl cyclase in brain. *Cell Signal* 2003. 15 (2): 189-195.

Mergia, E. and Stegbauer, J. Role of Phosphodiesterase 5 and Cyclic GMP in Hypertension. *Curr Hypertens Rep* 2016. 18 (5): 39.

Mollnau, H., Wendt, M., Szöcs, K., Lassègue, B., Schulz, E., Oelze, M., Li, H., Bodenschatz, M., August, M., Kleschyov, A. L., Tsilimingas, N., Walter, U., Förstermann, U., Meinertz, T., Griendling, K. and Münzel, T. Effects of Angiotensin II Infusion on the Expression and Function of NAD(P)H Oxidase and Components of Nitric Oxide/cGMP Signaling. *Circulation Research* 2002. 90 (4).

Momozawa, Y. and Mizukami, K. Unique roles of rare variants in the genetics of complex diseases in humans. *J Hum Genet* 2021. 66 (1): 11-23.

Moro, M. A., Russel, R. J., Cellek, S., Lizasoain, I., Su, Y., Darley-Usmar, V. M., Radomski, M. W. and Moncada, S. cGMP mediates the vascular and platelet actions of nitric oxide: Confirmation using an inhibitor of the soluble guanylyl cyclase. *Proc Natl Acad Sci U S A* 1995. 93: 1480-1485.

Morton, N. E. Sequential tests for the detection of linkage. *Am J Hum Genet* 1955. 7 (3): 277-318.

Mozaffarian, D., Benjamin, E. J., Go, A. S., Arnett, D. K., Blaha, M. J., Cushman, M., de Ferranti, S., Despres, J. P., Fullerton, H. J., Howard, V. J., Huffman, M. D., Judd, S. E., Kissela, B. M., Lackland, D. T., Lichtman, J. H., Lisabeth, L. D., Liu, S., Mackey, R. H., Matchar, D. B., McGuire, D. K., Mohler, E. R., 3rd, Moy, C. S., Muntner, P., Mussolino, M. E., Nasir, K., Neumar, R. W., Nichol, G., Palaniappan, L., Pandey, D. K., Reeves, M. J., Rodriguez, C. J., Sorlie, P. D., Stein, J., Towfighi, A., Turan, T. N., Virani, S. S., Willey, J. Z., Woo, D., Yeh, R. W., Turner, M. B., American Heart Association Statistics, C. and Stroke Statistics, S. Heart disease and stroke statistics--2015 update: a report from the American Heart Association. *Circulation* 2015. 131 (4): e29-322.

Mullershausen, F., Russwurm, M., Thompson, W. J., Liu, L., Koesling, D. and Friebe, A. Rapid nitric oxide-induced desensitization of the cGMP response is caused by increased activity of phosphodiesterase type 5 paralleled by phosphorylation of the enzyme. *J Cell Biol* 2001. 155 (2): 271-278.

Mullershausen, F., Russwurm, M., Koesling, D. and Friebe, A. In vivo reconstitution of the negative feedback in nitric oxide/cGMP signaling: role of phosphodiesterase type 5 phosphorylation. *Mol Biol Cell* 2004. 15 (9): 4023-4030.

Mungrue, I. N., Husain, M. and Stewart, D. J. The role of NOS in heart failure: lessons from murine genetic models. *Heart Fail Rev* 2002. 7 (4): 407-422.

Myocardial Infarction Genetics, Investigators, C. A. E. C., Stitziel, N. O., Stirrups, K. E., Masca, N. G., Erdmann, J., Ferrario, P. G., Konig, I. R., Weeke, P. E., Webb, T. R., Auer, P. L., Schick, U. M., Lu, Y., Zhang, H., Dube, M. P., Goel, A., Farrall, M., Peloso, G. M., Won, H. H., Do, R., van Iperen, E., Kanoni, S., Kruppa, J., Mahajan, A., Scott, R. A., Willenberg, C., Braund, P. S., van Capelleveen, J. C., Doney, A. S., Donnelly, L. A., Asselta, R., Merlini, P. A., Duga, S., Marziliano, N., Denny, J. C., Shaffer, C. M., El-Mokhtari, N. E., Franke, A., Gottesman, O., Heilmann, S., Hengstenberg, C., Hoffman, P., Holmen, O. L., Hveem, K., Jansson, J. H., Jockel, K. H., Kessler, T., Kriebel, J., Laugwitz, K. L., Marouli, E., Martinelli, N., McCarthy, M. I., Van Zuydam, N. R., Meisinger, C., Esko, T., Mihailov, E., Escher, S. A., Alver, M., Moebus, S., Morris, A. D., Muller-Nurasyid, M., Nikpay, M., Olivieri, O., Lemieux Perreault, L. P., AlQarawi, A., Robertson, N. R., Akinsanya, K. O., Reilly, D. F., Vogt, T. F., Yin, W., Asselbergs, F. W., Kooperberg, C., Jackson, R. D., Stahl, E., Strauch, K., Varga, T. V., Waldenberger, M., Zeng, L., Kraja, A. T., Liu, C., Ehret, G. B., Newton-Cheh, C., Chasman, D. I., Chowdhury, R., Ferrario, M., Ford, I., Jukema, J. W., Kee, F., Kuulasmaa, K., Nordestgaard, B. G., Perola, M., Saleheen, D., Sattar, N., Surendran, P., Tregouet, D., Young, R., Howson, J. M., Butterworth, A. S., Danesh, J., Ardissino, D., Bottinger, E. P., Erbel, R., Franks, P. W., Girelli, D., Hall, A. S., Hovingh, G. K., Kastrati, A., Lieb, W., Meitinger, T., Kraus, W. E., Shah, S. H., McPherson, R., Orho-Melander, M., Melander, O., Metspalu, A., Palmer, C. N., Peters, A., Rader, D., Reilly, M. P., Loos, R. J., Reiner, A. P., Roden, D. M., Tardif, J. C., Thompson, J. R., Wareham, N. J., Watkins, H., Willer, C. J., Kathiresan, S., Deloukas, P., Samani, N. J. and Schunkert, H. Coding Variation in ANGPTL4, LPL, and SVEP1 and the Risk of Coronary Disease. *N Engl J Med* 2016. 374 (12): 1134-1144.

Myocardial Infarction Genetics Consortium, Kathiresan, S., Voight, B. F., Purcell, S., Musunuru, K., Ardissino, D., Mannucci, P. M., Anand, S., Engert, J. C., Samani, N. J., Schunkert, H., Erdmann, J., Reilly, M. P., Rader, D. J., Morgan, T., Spertus, J. A., Stoll, M., Girelli, D., McKeown, P. P., Patterson, C. C., Siscovick, D. S., O'Donnell, C. J., Elosua, R., Peltonen, L., Salomaa, V., Schwartz, S. M., Melander, O., Altshuler, D., Ardissino, D., Merlini, P. A., Berzuini, C., Bernardinelli, L., Peyvandi, F., Tubaro, M., Celli, P., Ferrario, M., Fetiveau, R., Marziliano, N., Casari, G., Galli, M., Ribichini, F., Rossi, M., Bernardi, F.,

Zonzin, P., Piazza, A., Mannucci, P. M., Schwartz, S. M., Siscovick, D. S., Yee, J., Friedlander, Y., Elosua, R., Marrugat, J., Lucas, G., Subirana, I., Sala, J., Ramos, R., Kathiresan, S., Meigs, J. B., Williams, G., Nathan, D. M., MacRae, C. A., O'Donnell, C. J., Salomaa, V., Havulinna, A. S., Peltonen, L., Melander, O., Berglund, G., Voight, B. F., Kathiresan, S., Hirschhorn, J. N., Asselta, R., Duga, S., Spreafico, M., Musunuru, K., Daly, M. J., Purcell, S., Voight, B. F., Purcell, S., Nemesh, J., Korn, J. M., McCarroll, S. A., Schwartz, S. M., Yee, J., Kathiresan, S., Lucas, G., Subirana, I., Elosua, R., Surti, A., Guiducci, C., Gianniny, L., Mirel, D., Parkin, M., Burtt, N., Gabriel, S. B., Samani, N. J., Thompson, J. R., Braund, P. S., Wright, B. J., Balmforth, A. J., Ball, S. G., Hall, A., Wellcome Trust Case Control, C., Schunkert, H., Erdmann, J., Linsel-Nitschke, P., Lieb, W., Ziegler, A., Konig, I., Hengstenberg, C., Fischer, M., Stark, K., Grosshennig, A., Preuss, M., Wichmann, H. E., Schreiber, S., Schunkert, H., Samani, N. J., Erdmann, J., Ouwehand, W., Hengstenberg, C., Deloukas, P., Scholz, M., Cambien, F., Reilly, M. P., Li, M., Chen, Z., Wilensky, R., Matthai, W., Qasim, A., Hakonarson, H. H., Devaney, J., Burnett, M. S., Pichard, A. D., Kent, K. M., Satler, L., Lindsay, J. M., Waksman, R., Knouff, C. W., Waterworth, D. M., Walker, M. C., Mooser, V., Epstein, S. E., Rader, D. J., Scheffold, T., Berger, K., Stoll, M., Huge, A., Girelli, D., Martinelli, N., Olivieri, O., Corrocher, R., Morgan, T., Spertus, J. A., McKeown, P., Patterson, C. C., Schunkert, H., Erdmann, E., Linsel-Nitschke, P., Lieb, W., Ziegler, A., Konig, I. R., Hengstenberg, C., Fischer, M., Stark, K., Grosshennig, A., Preuss, M., Wichmann, H. E., Schreiber, S., Holm, H., Thorleifsson, G., Thorsteinsdottir, U., Stefansson, K., Engert, J. C., Do, R., Xie, C., Anand, S., Kathiresan, S., Ardissino, D., Mannucci, P. M., Siscovick, D., O'Donnell, C. J., Samani, N. J., Melander, O., Elosua, R., Peltonen, L., Salomaa, V., Schwartz, S. M. and Altshuler, D. Genome-wide association of early-onset myocardial infarction with single nucleotide polymorphisms and copy number variants. *Nat Genet* 2009. 41 (3): 334-341.

Myocardial Infarction Genetics Consortium Investigators, Stitziel, N. O., Won, H. H., Morrison, A. C., Peloso, G. M., Do, R., Lange, L. A., Fontanillas, P., Gupta, N., Duga, S., Goel, A., Farrall, M., Saleheen, D., Ferrario, P., Konig, I., Asselta, R., Merlini, P. A., Marziliano, N., Notarangelo, M. F., Schick, U., Auer, P., Assimes, T. L., Reilly, M., Wilensky, R., Rader, D. J., Hovingh, G. K., Meitinger, T., Kessler, T., Kastrati, A., Laugwitz, K. L., Siscovick, D., Rotter, J. I., Hazen, S. L., Tracy, R., Cresci, S., Spertus, J., Jackson, R., Schwartz, S. M., Natarajan, P., Crosby, J., Muzny, D., Ballantyne, C., Rich, S. S., O'Donnell, C. J., Abecasis, G., Sunaev, S., Nickerson, D. A., Buring, J. E., Ridker, P. M., Chasman, D. I., Austin, E., Kullo, I. J., Weeke, P. E., Shaffer, C. M., Bastarache, L. A., Denny, J. C., Roden, D. M., Palmer, C., Deloukas, P., Lin, D. Y., Tang, Z. Z., Erdmann, J., Schunkert, H., Danesh, J., Marrugat, J., Elosua, R., Ardissino, D., McPherson, R., Watkins, H., Reiner, A. P., Wilson, J. G., Altshuler, D., Gibbs, R. A., Lander, E. S., Boerwinkle, E., Gabriel, S. and Kathiresan, S. Inactivating mutations in NPC1L1 and protection from coronary heart disease. *N Engl J Med* 2014. 371 (22): 2072-2082.

Nabel, E. G. Cardiovascular disease. *N Engl J Med* 2003. 349 (1): 60-72.

Nakashima, Y., Wight, T. N. and Sueishi, K. Early atherosclerosis in humans: role of diffuse intimal thickening and extracellular matrix proteoglycans. *Cardiovasc Res* 2008. 79 (1): 14-23.

Nelson, C. P., Goel, A., Butterworth, A. S., Kanoni, S., Webb, T. R., Marouli, E., Zeng, L., Ntalla, I., Lai, F. Y., Hopewell, J. C., Giannakopoulou, O., Jiang, T., Hamby, S. E., Di Angelantonio, E., Assimes, T. L., Bottinger, E. P., Chambers, J. C., Clarke, R., Palmer, C. N. A., Cubbon, R. M., Ellinor, P., Ermel, R., Evangelou, E., Franks, P. W., Grace, C., Gu, D., Hingorani, A. D., Howson, J. M. M., Ingelsson, E., Kastrati, A., Kessler, T., Kyriakou, T., Lehtimaki, T., Lu, X., Lu, Y., Marz, W., McPherson, R., Metspalu, A., Pujades-Rodriguez, M., Ruusalepp, A., Schadt, E. E., Schmidt, A. F., Sweeting, M. J., Zalloua, P. A., AlGhalayini, K., Keavney, B. D., Kooner, J. S., Loos, R. J. F., Patel, R. S., Rutter, M. K., Tomaszewski, M., Tzoulaki, I., Zeggini, E., Erdmann, J., Dedoussis, G., Bjorkegren, J. L. M., Consortium, E.-C.,

CardioGramplusC4D, group, U. K. B. C. C. C. w., Schunkert, H., Farrall, M., Danesh, J., Samani, N. J., Watkins, H. and Deloukas, P. Association analyses based on false discovery rate implicate new loci for coronary artery disease. *Nat Genet* 2017. 49 (9): 1385-1391.

Nikpay, M., Goel, A., Won, H. H., Hall, L. M., Willenborg, C., Kanoni, S., Saleheen, D., Kyriakou, T., Nelson, C. P., Hopewell, J. C., Webb, T. R., Zeng, L., Dehghan, A., Alver, M., Armasu, S. M., Auro, K., Bjonnes, A., Chasman, D. I., Chen, S., Ford, I., Franceschini, N., Gieger, C., Grace, C., Gustafsson, S., Huang, J., Hwang, S. J., Kim, Y. K., Kleber, M. E., Lau, K. W., Lu, X., Lu, Y., Lyytikainen, L. P., Mihailov, E., Morrison, A. C., Pervjakova, N., Qu, L., Rose, L. M., Salfati, E., Saxena, R., Scholz, M., Smith, A. V., Tikkanen, E., Uitterlinden, A., Yang, X., Zhang, W., Zhao, W., de Andrade, M., de Vries, P. S., van Zuydam, N. R., Anand, S. S., Bertram, L., Beutner, F., Dedoussis, G., Frossard, P., Gauguier, D., Goodall, A. H., Gottesman, O., Haber, M., Han, B. G., Huang, J., Jalilzadeh, S., Kessler, T., Konig, I. R., Lannfelt, L., Lieb, W., Lind, L., Lindgren, C. M., Lokki, M. L., Magnusson, P. K., Mallick, N. H., Mehra, N., Meitinger, T., Memon, F. U., Morris, A. P., Nieminen, M. S., Pedersen, N. L., Peters, A., Rallidis, L. S., Rasheed, A., Samuel, M., Shah, S. H., Sinisalo, J., Stirrups, K. E., Trompet, S., Wang, L., Zaman, K. S., Ardissino, D., Boerwinkle, E., Borecki, I. B., Bottinger, E. P., Buring, J. E., Chambers, J. C., Collins, R., Cupples, L. A., Danesh, J., Demuth, I., Elosua, R., Epstein, S. E., Esko, T., Feitosa, M. F., Franco, O. H., Franzosi, M. G., Granger, C. B., Gu, D., Gudnason, V., Hall, A. S., Hamsten, A., Harris, T. B., Hazen, S. L., Hengstenberg, C., Hofman, A., Ingelsson, E., Iribarren, C., Jukema, J. W., Karhunen, P. J., Kim, B. J., Kooner, J. S., Kullo, I. J., Lehtimaki, T., Loos, R. J., Melander, O., Metspalu, A., Marz, W., Palmer, C. N., Perola, M., Quertermous, T., Rader, D. J., Ridker, P. M., Ripatti, S., Roberts, R., Salomaa, V., Sanghera, D. K., Schwartz, S. M., Seedorf, U., Stewart, A. F., Stott, D. J., Thiery, J., Zalloua, P. A., O'Donnell, C. J., Reilly, M. P., Assimes, T. L., Thompson, J. R., Erdmann, J., Clarke, R., Watkins, H., Kathiresan, S., McPherson, R., Deloukas, P., Schunkert, H., Samani, N. J., Farrall, M. and Consortium, C. A. D. A comprehensive 1,000 Genomes-based genome-wide association meta-analysis of coronary artery disease. *Nat Genet* 2015. 47 (10): 1121-1130.

Pagani, F. and Baralle, F. E. Genomic variants in exons and introns: identifying the splicing spoilers. *Nat Rev Genet* 2004. 5 (5): 389-396.

Pahkala, K., Hietalampi, H., Laitinen, T. T., Viikari, J. S., Ronnemaa, T., Niinikoski, H., Lagstrom, H., Talvia, S., Jula, A., Heinonen, O. J., Juonala, M., Simell, O. and Raitakari, O. T. Ideal cardiovascular health in adolescence: effect of lifestyle intervention and association with vascular intima-media thickness and elasticity (the Special Turku Coronary Risk Factor Intervention Project for Children [STRIP] study). *Circulation* 2013. 127 (21): 2088-2096.

Pantopoulos, K. and Hentze, M. W. Nitric oxide signaling to iron-regulatory protein: direct control of ferritin mRNA translation and transferrin receptor mRNA stability in transfected fibroblasts. *Proc Natl Acad Sci U S A* 1995. 92 (5): 1267-1271.

Pokreisz, P., Vandenwijngaert, S., Bito, V., Van den Bergh, A., Lenaerts, I., Busch, C., Marsboom, G., Gheysens, O., Vermeersch, P., Biesmans, L., Liu, X., Gillijns, H., Pellens, M., Van Lommel, A., Buys, E., Schoonjans, L., Vanhaecke, J., Verbeken, E., Sipido, K., Herijgers, P., Bloch, K. D. and Janssens, S. P. Ventricular phosphodiesterase-5 expression is increased in patients with advanced heart failure and contributes to adverse ventricular remodeling after myocardial infarction in mice. *Circulation* 2009. 119 (3): 408-416.

Pryma, C. S., Ortega, C., Dubland, J. A. and Francis, G. A. Pathways of smooth muscle foam cell formation in atherosclerosis. *Curr Opin Lipidol* 2019. 30 (2): 117-124.

Pula, G., Schuh, K., Nakayama, K., Nakayama, K. I., Walter, U. and Poole, A. W. PKCdelta regulates collagen-induced platelet aggregation through inhibition of VASP-mediated filopodia formation. *Blood* 2006. 108 (13): 4035-4044.

Raal, F. J., Pilcher, G. J., Panz, V. R., van Deventer, H. E., Brice, B. C., Blom, D. J. and Marais, A. D. Reduction in mortality in subjects with homozygous familial hypercholesterolemia associated with advances in lipid-lowering therapy. *Circulation* 2011. 124 (20): 2202-2207.

Rabbani, B., Tekin, M. and Mahdieh, N. The promise of whole-exome sequencing in medical genetics. *J Hum Genet* 2014. 59 (1): 5-15.

Rajfer, J., Aronson, W. J., Bush, P. A., Dorey, F. J. and Ignarro, L. J. Nitric oxide as a mediator of relaxation of the corpus cavernosum in response to nonadrenergic, noncholinergic neurotransmission. *N Engl J Med* 1992. 326 (2): 90-94.

Robbins, N., Thompson, A., Mann, A. and Blomkalns, A. L. Isolation and excision of murine aorta; a versatile technique in the study of cardiovascular disease. *J Vis Exp* 2014. (93): e52172.

Rodrigues, B. P., Campagnaro, B. P., Balarini, C. M., Pereira, T. M., Meyrelles, S. S. and Vasquez, E. C. Sildenafil ameliorates biomarkers of genotoxicity in an experimental model of spontaneous atherosclerosis. *Lipids Health Dis* 2013. 12: 128.

Roth, G. A., Mensah, G. A., Johnson, C. O., Addolorato, G., Ammirati, E., Baddour, L. M., Barengo, N. C., Beaton, A. Z., Benjamin, E. J., Benziger, C. P., Bonny, A., Brauer, M., Brodmann, M., Cahill, T. J., Carapetis, J., Catapano, A. L., Chugh, S. S., Cooper, L. T., Coresh, J., Criqui, M., DeCleene, N., Eagle, K. A., Emmons-Bell, S., Feigin, V. L., Fernandez-Sola, J., Fowkes, G., Gakidou, E., Grundy, S. M., He, F. J., Howard, G., Hu, F., Inker, L., Karthikeyan, G., Kassebaum, N., Koroshetz, W., Lavie, C., Lloyd-Jones, D., Lu, H. S., Mirijello, A., Temesgen, A. M., Mokdad, A., Moran, A. E., Muntner, P., Narula, J., Neal, B., Ntsekhe, M., Moraes de Oliveira, G., Otto, C., Owolabi, M., Pratt, M., Rajagopalan, S., Reitsma, M., Ribeiro, A. L. P., Rigotti, N., Rodgers, A., Sable, C., Shakil, S., Sliwa-Hahnle, K., Stark, B., Sundstrom, J., Timpel, P., Tleyjeh, I. M., Valgimigli, M., Vos, T., Whelton, P. K., Yacoub, M., Zuhlke, L., Murray, C., Fuster, V. and Group, G.-N.-J. G. B. o. C. D. W. Global Burden of Cardiovascular Diseases and Risk Factors, 1990-2019: Update From the GBD 2019 Study. *J Am Coll Cardiol* 2020. 76 (25): 2982-3021.

Ruiz, J. L., Hutcheson, J. D. and Aikawa, E. Cardiovascular calcification: current controversies and novel concepts. *Cardiovasc Pathol* 2015. 24 (4): 207-212.

Rybalkin, S. D., Rybalkina, I. G., Feil, R., Hofmann, F. and Beavo, J. A. Regulation of cGMP-specific phosphodiesterase (PDE5) phosphorylation in smooth muscle cells. *J Biol Chem* 2002. 277 (5): 3310-3317.

Rybalkin, S. D., Rybalkina, I. G., Shimizu-Albergine, M., Tang, X. B. and Beavo, J. A. PDE5 is converted to an activated state upon cGMP binding to the GAF A domain. *Embo j* 2003. 22 (3): 469-478.

Sakuma, I., Togashi, H., Yoshioka, M., Saito, H., Yanagida, M., Tamura, M., Kobayashi, T., Yasuda, H., Gross, S. S. and Levi, R. NG-methyl-L-arginine, an inhibitor of L-arginine-derived nitric oxide synthesis, stimulates renal sympathetic nerve activity in vivo. A role for nitric oxide in the central regulation of sympathetic tone? *Circ Res* 1992. 70 (3): 607-611.

Salloum, F., Yin, C., Xi, L. and Kukreja, R. C. Sildenafil induces delayed preconditioning through inducible nitric oxide synthase-dependent pathway in mouse heart. *Circ Res* 2003. 92 (6): 595-597.

Salloum, F. N., Chau, V. Q., Hoke, N. N., Abbate, A., Varma, A., Ockaili, R. A., Toldo, S. and Kukreja, R. C. Phosphodiesterase-5 inhibitor, tadalafil, protects against myocardial ischemia/reperfusion through protein-kinase g-dependent generation of hydrogen sulfide. *Circulation* 2009. 120 (11 Suppl): S31-36.

Salvi, E., Kuznetsova, T., Thijs, L., Lupoli, S., Stolarz-Skrzypek, K., D'Avila, F., Tikhonoff, V., De Astis, S., Barcella, M., Seidlerova, J., Benaglio, P., Malyutina, S., Frau, F., Velayutham, D., Benfante, R., Zagato, L., Title, A., Braga, D., Marek, D., Kawecka-Jaszcz, K., Casiglia, E., Filipovsky, J., Nikitin, Y., Rivolta, C., Manunta, P., Beckmann, J. S., Barlassina, C., Cusi, D. and Staessen, J. A. Target sequencing, cell experiments, and a population study establish endothelial nitric oxide synthase (eNOS) gene as hypertension susceptibility gene. *Hypertension* 2013. 62 (5): 844-852.

Schlossmann, J. and Desch, M. IRAG and novel PKG targeting in the cardiovascular system. *Am J Physiol Heart Circ Physiol* 2011. 301 (3): H672-682.

Schlossmann, J. and Schinner, E. cGMP becomes a drug target. *Naunyn Schmiedebergs Arch Pharmacol* 2012. 385 (3): 243-252.

Schmidt, H. H., Lohmann, S. M. and Walter, U. The nitric oxide and cGMP signal transduction system: regulation and mechanism of action. *Biochim Biophys Acta* 1993. 1178 (2): 153-175.

Schneider, C. A., Rasband, W. S. and Eliceiri, K. W. NIH Image to ImageJ: 25 years of image analysis. *Nat Methods* 2012. 9 (7): 671-675.

Schneider-Gadicke, A., Beer-Romero, P., Brown, L. G., Mardon, G., Luoh, S. W. and Page, D. C. Putative transcription activator with alternative isoforms encoded by human ZFX gene. *Nature* 1989. 342 (6250): 708-711.

Schulz, C. and Massberg, S. Platelets in atherosclerosis and thrombosis. *Handb Exp Pharmacol* 2012. (210): 111-133.

Schunkert, H., Konig, I. R., Kathiresan, S., Reilly, M. P., Assimes, T. L., Holm, H., Preuss, M., Stewart, A. F., Barbalic, M., Gieger, C., Absher, D., Aherrahrou, Z., Allayee, H., Altshuler, D., Anand, S. S., Andersen, K., Anderson, J. L., Ardissino, D., Ball, S. G., Balmforth, A. J., Barnes, T. A., Becker, D. M., Becker, L. C., Berger, K., Bis, J. C., Boekholdt, S. M., Boerwinkle, E., Braund, P. S., Brown, M. J., Burnett, M. S., Buysschaert, I., Cardiogenics, Carlquist, J. F., Chen, L., Cichon, S., Codd, V., Davies, R. W., Dedoussis, G., Dehghan, A., Demissie, S., Devaney, J. M., Diemert, P., Do, R., Doering, A., Eifert, S., Mokhtari, N. E., Ellis, S. G., Elosua, R., Engert, J. C., Epstein, S. E., de Faire, U., Fischer, M., Folsom, A. R., Freyer, J., Gigante, B., Girelli, D., Gretarsdottir, S., Gudnason, V., Gulcher, J. R., Halperin, E., Hammond, N., Hazen, S. L., Hofman, A., Horne, B. D., Illig, T., Iribarren, C., Jones, G. T., Jukema, J. W., Kaiser, M. A., Kaplan, L. M., Kastelein, J. J., Khaw, K. T., Knowles, J. W., Kolovou, G., Kong, A., Laaksonen, R., Lambrechts, D., Leander, K., Lettre, G., Li, M., Lieb, W., Loley, C., Lotery, A. J., Mannucci, P. M., Maouche, S., Martinelli, N., McKeown, P. P., Meisinger, C., Meitinger, T., Melander, O., Merlini, P. A., Mooser, V., Morgan, T., Muhleisen, T. W., Muhlestein, J. B., Munzel, T., Musunuru, K., Nahrstaedt, J., Nelson, C. P., Nothen, M. M., Olivieri, O., Patel, R. S., Patterson, C. C., Peters, A., Peyvandi, F., Qu, L., Quyyumi, A. A., Rader, D. J., Rallidis, L. S., Rice, C., Rosendaal, F. R., Rubin, D., Salomaa, V., Sampietro, M. L., Sandhu, M. S., Schadt, E., Schafer, A., Schillert, A., Schreiber, S., Schrezenmeir, J., Schwartz, S. M., Siscovick, D. S., Sivananthan, M., Sivapalaratnam, S., Smith, A., Smith, T. B., Snoep, J. D., Soranzo, N., Spertus, J. A., Stark, K., Stirrups, K., Stoll, M., Tang, W. H., Tennstedt, S., Thorgeirsson, G., Thorleifsson, G., Tomaszewski, M., Uitterlinden, A. G., van Rij, A. M., Voight, B. F., Wareham, N. J., Wells, G. A., Wichmann, H. E., Wild, P. S., Willenborg, C., Witteman, J. C., Wright, B. J., Ye, S., Zeller, T., Ziegler, A.,

Cambien, F., Goodall, A. H., Cupples, L. A., Quertermous, T., Marz, W., Hengstenberg, C., Blankenberg, S., Ouwehand, W. H., Hall, A. S., Deloukas, P., Thompson, J. R., Stefansson, K., Roberts, R., Thorsteinsdottir, U., O'Donnell, C. J., McPherson, R., Erdmann, J., Consortium, C. A. and Samani, N. J. Large-scale association analysis identifies 13 new susceptibility loci for coronary artery disease. *Nat Genet* 2011. 43 (4): 333-338.

Schunkert, H., von Scheidt, M., Kessler, T., Stiller, B., Zeng, L. and Vilne, B. Genetics of coronary artery disease in the light of genome-wide association studies. *Clin Res Cardiol* 2018. 107 (Suppl 2): 2-9.

Schunkert, H., Erdmann, J., Samani, N. J., Deloukas, P. and Zeng, L. Genetics of educational attainment and coronary risk in Mendelian randomization studies. *Eur Heart J* 2020. 41 (7): 894-895.

Schwenke, D. C. and St Clair, R. W. Influx, efflux, and accumulation of LDL in normal arterial areas and atherosclerotic lesions of white Carneau pigeons with naturally occurring and cholesterol-aggravated aortic atherosclerosis. *Arterioscler Thromb* 1993. 13 (9): 1368-1381.

Segura-Puimedon, M., Mergia, E., Al-Hasani, J., Aherrahrou, R., Stoelting, S., Kremer, F., Freyer, J., Koesling, D., Erdmann, J., Schunkert, H., de Wit, C. and Aherrahrou, Z. Proatherosclerotic Effect of the alpha1-Subunit of Soluble Guanylyl Cyclase by Promoting Smooth Muscle Phenotypic Switching. *Am J Pathol* 2016. 186 (8): 2220-2231.

Shabeeh, H., Khan, S., Jiang, B., Brett, S., Melikian, N., Casadei, B., Chowienczyk, P. J. and Shah, A. M. Blood Pressure in Healthy Humans Is Regulated by Neuronal NO Synthase. *Hypertension* 2017. 69 (5): 970-976.

Shan, X., Quaile, M. P., Monk, J. K., French, B., Cappola, T. P. and Margulies, K. B. Differential expression of PDE5 in failing and nonfailing human myocardium. *Circ Heart Fail* 2012. 5 (1): 79-86.

Soutar, A. K. and Naoumova, R. P. Mechanisms of disease: genetic causes of familial hypercholesterolemia. *Nat Clin Pract Cardiovasc Med* 2007. 4 (4): 214-225.

Stasch, J. P., Schmidt, P., Alonso-Alija, C., Apeler, H., Dembowsky, K., Haerter, M., Heil, M., Minuth, T., Perzborn, E., Pleiss, U., Schramm, M., Schroeder, W., Schroder, H., Stahl, E., Steinke, W. and Wunder, F. NO- and haem-independent activation of soluble guanylyl cyclase: molecular basis and cardiovascular implications of a new pharmacological principle. *Br J Pharmacol* 2002. 136 (5): 773-783.

Stauss, H. M., Godecke, A., Mrowka, R., Schrader, J. and Persson, P. B. Enhanced blood pressure variability in eNOS knockout mice. *Hypertension* 1999. 33 (6): 1359-1363.

Stitziel, N. O., Khera, A. V., Wang, X., Bierhals, A. J., Vourakis, A. C., Sperry, A. E., Natarajan, P., Klarin, D., Emdin, C. A., Zekavat, S. M., Nomura, A., Erdmann, J., Schunkert, H., Samani, N. J., Kraus, W. E., Shah, S. H., Yu, B., Boerwinkle, E., Rader, D. J., Gupta, N., Frossard, P. M., Rasheed, A., Danesh, J., Lander, E. S., Gabriel, S., Saleheen, D., Musunuru, K., Kathiresan, S., Promis and Myocardial Infarction Genetics Consortium, I. ANGPTL3 Deficiency and Protection Against Coronary Artery Disease. *J Am Coll Cardiol* 2017. 69 (16): 2054-2063.

Strong, J. P., Malcom, G. T., Newman, W. P., 3rd and Oalmann, M. C. Early lesions of atherosclerosis in childhood and youth: natural history and risk factors. *J Am Coll Nutr* 1992. 11 Suppl: 51S-54S.

Tabas, I., Williams, K. J. and Boren, J. Subendothelial lipoprotein retention as the initiating process in atherosclerosis: update and therapeutic implications. *Circulation* 2007. 116 (16): 1832-1844.

Takimoto, E., Champion, H. C., Li, M., Belardi, D., Ren, S., Rodriguez, E. R., Bedja, D., Gabrielson, K. L., Wang, Y. and Kass, D. A. Chronic inhibition of cyclic GMP phosphodiesterase 5A prevents and reverses cardiac hypertrophy. *Nat Med* 2005. 11 (2): 214-222.

Thieme, M., Sivritas, S. H., Mergia, E., Potthoff, S. A., Yang, G., Hering, L., Grave, K., Hoch, H., Rump, L. C. and Stegbauer, J. Phosphodiesterase 5 inhibition ameliorates angiotensin II-dependent hypertension and renal vascular dysfunction. *Am J Physiol Renal Physiol* 2017. 312 (3): F474-F481.

Thomas, D. C. and Witte, J. S. Point: population stratification: a problem for case-control studies of candidate-gene associations? *Cancer Epidemiol Biomarkers Prev* 2002. 11 (6): 505-512.

Thomas, M. K., Francis, S. H. and Corbin, J. D. Substrate- and kinase-directed regulation of phosphorylation of a cGMP-binding phosphodiesterase by cGMP. *J Biol Chem* 1990a. 265 (25): 14971-14978.

Thomas, M. K., Francis, S. H. and Corbin, J. D. Characterization of a purified bovine lung cGMP-binding cGMP phosphodiesterase. *J Biol Chem* 1990b. 265 (25): 14964-14970.

Tonelli, A. R., Haserodt, S., Aytekin, M. and Dweik, R. A. Nitric oxide deficiency in pulmonary hypertension: Pathobiology and implications for therapy. *Pulm Circ* 2013. 3 (1): 20-30.

Tsai, E. J. and Kass, D. A. Cyclic GMP signaling in cardiovascular pathophysiology and therapeutics. *Pharmacol Ther* 2009. 122 (3): 216-238.

Ursell, P. C. and Mayes, M. The majority of nitric oxide synthase in pig heart is vascular and not neural. *Cardiovasc Res* 1993. 27 (11): 1920-1924.

van Etten, R. W., de Koning, E. J., Verhaar, M. C., Gaillard, C. A. and Rabelink, T. J. Impaired NO-dependent vasodilation in patients with Type II (non-insulin-dependent) diabetes mellitus is restored by acute administration of folate. *Diabetologia* 2002. 45 (7): 1004-1010.

Vandenwijngaert, S., Pokreisz, P., Hermans, H., Gillijns, H., Pellens, M., Bax, N. A., Coppiello, G., Oosterlinck, W., Balogh, A., Papp, Z., Bouten, C. V., Bartunek, J., D'Hooge, J., Luttun, A., Verbeken, E., Herregods, M. C., Herijgers, P., Bloch, K. D. and Janssens, S. Increased cardiac myocyte PDE5 levels in human and murine pressure overload hypertrophy contribute to adverse LV remodeling. *PLoS One* 2013. 8 (3): e58841.

Vandeput, F., Krall, J., Ockaili, R., Salloum, F. N., Florio, V., Corbin, J. D., Francis, S. H., Kukreja, R. C. and Movsesian, M. A. cGMP-hydrolytic activity and its inhibition by sildenafil in normal and failing human and mouse myocardium. *J Pharmacol Exp Ther* 2009. 330 (3): 884-891.

Verhaar, M. C., Wever, R. M., Kastelein, J. J., van Dam, T., Koomans, H. A. and Rabelink, T. J. 5-methyltetrahydrofolate, the active form of folic acid, restores endothelial function in familial hypercholesterolemia. *Circulation* 1998. 97 (3): 237-241.

Verhaar, M. C., Wever, R. M., Kastelein, J. J., van Loon, D., Milstien, S., Koomans, H. A. and Rabelink, T. J. Effects of oral folic acid supplementation on endothelial function in familial

hypercholesterolemia. A randomized placebo-controlled trial. *Circulation* 1999. 100 (4): 335-338.

Vermeersch, P., Buys, E., Pokreisz, P., Marsboom, G., Ichinose, F., Sips, P., Pellens, M., Gillijns, H., Swinnen, M., Graveline, A., Collen, D., Dewerchin, M., Brouckaert, P., Bloch, K. D. and Janssens, S. Soluble guanylate cyclase-alpha1 deficiency selectively inhibits the pulmonary vasodilator response to nitric oxide and increases the pulmonary vascular remodeling response to chronic hypoxia. *Circulation* 2007. 116 (8): 936-943.

Vinkhuyzen, A. A., Wray, N. R., Yang, J., Goddard, M. E. and Visscher, P. M. Estimation and partition of heritability in human populations using whole-genome analysis methods. *Annu Rev Genet* 2013. 47: 75-95.

von Scheidt, M., Zhao, Y., Kurt, Z., Pan, C., Zeng, L., Yang, X., Schunkert, H. and Lusis, A. J. Applications and Limitations of Mouse Models for Understanding Human Atherosclerosis. *Cell Metab* 2017. 25 (2): 248-261.

Wacholder, S., Rothman, N. and Caporaso, N. Counterpoint: bias from population stratification is not a major threat to the validity of conclusions from epidemiological studies of common polymorphisms and cancer. *Cancer Epidemiol Biomarkers Prev* 2002. 11 (6): 513-520.

Wallis, R. M., Corbin, J. D., Francis, S. H. and Ellis, P. Tissue distribution of phosphodiesterase families and the effects of sildenafil on tissue cyclic nucleotides, platelet function, and the contractile responses of trabeculae carneae and aortic rings in vitro. *Am J Cardiol* 1999. 83 (5a): 3c-12c.

Walter, U. and Gambaryan, S. cGMP and cGMP-dependent protein kinase in platelets and blood cells. *Handb Exp Pharmacol* 2009. (191): 533-548.

Wang, H., Liu, Y., Huai, Q., Cai, J., Zoraghi, R., Francis, S. H., Corbin, J. D., Robinson, H., Xin, Z., Lin, G. and Ke, H. Multiple conformations of phosphodiesterase-5: implications for enzyme function and drug development. *J Biol Chem* 2006. 281 (30): 21469-21479.

Wang, H., Robinson, H. and Ke, H. Conformation changes, N-terminal involvement, and cGMP signal relay in the phosphodiesterase-5 GAF domain. *J Biol Chem* 2010. 285 (49): 38149-38156.

Webb, T. R., Erdmann, J., Stirrups, K. E., Stitziel, N. O., Masca, N. G., Jansen, H., Kanoni, S., Nelson, C. P., Ferrario, P. G., Konig, I. R., Eicher, J. D., Johnson, A. D., Hamby, S. E., Betsholtz, C., Ruusalepp, A., Franzen, O., Schadt, E. E., Bjorkegren, J. L., Weeke, P. E., Auer, P. L., Schick, U. M., Lu, Y., Zhang, H., Dube, M. P., Goel, A., Farrall, M., Peloso, G. M., Won, H. H., Do, R., van Iperen, E., Kruppa, J., Mahajan, A., Scott, R. A., Willenborg, C., Braund, P. S., van Capelleveen, J. C., Doney, A. S., Donnelly, L. A., Asselta, R., Merlini, P. A., Duga, S., Marziliano, N., Denny, J. C., Shaffer, C., El-Mokhtari, N. E., Franke, A., Heilmann, S., Hengstenberg, C., Hoffmann, P., Holmen, O. L., Hveem, K., Jansson, J. H., Jockel, K. H., Kessler, T., Kriebel, J., Laugwitz, K. L., Marouli, E., Martinelli, N., McCarthy, M. I., Van Zuydam, N. R., Meisinger, C., Esko, T., Mihailov, E., Escher, S. A., Alver, M., Moebus, S., Morris, A. D., Virtamo, J., Nikpay, M., Olivieri, O., Provost, S., AlQarawi, A., Robertson, N. R., Akinsansya, K. O., Reilly, D. F., Vogt, T. F., Yin, W., Asselbergs, F. W., Kooperberg, C., Jackson, R. D., Stahl, E., Muller-Nurasyid, M., Strauch, K., Varga, T. V., Waldenberger, M., Wellcome Trust Case Control, C., Zeng, L., Chowdhury, R., Salomaa, V., Ford, I., Jukema, J. W., Amouyel, P., Kontto, J., Investigators, M., Nordestgaard, B. G., Ferrieres, J., Saleheen, D., Sattar, N., Surendran, P., Wagner, A., Young, R., Howson, J. M., Butterworth, A. S., Danesh, J., Ardissino, D., Bottinger, E. P., Erbel, R., Franks, P. W., Girelli, D., Hall, A. S., Hovingh, G. K., Kastrati, A., Lieb, W., Meitinger, T., Kraus, W. E., Shah, S. H.,

McPherson, R., Orho-Melander, M., Melander, O., Metspalu, A., Palmer, C. N., Peters, A., Rader, D. J., Reilly, M. P., Loos, R. J., Reiner, A. P., Roden, D. M., Tardif, J. C., Thompson, J. R., Wareham, N. J., Watkins, H., Willer, C. J., Samani, N. J., Schunkert, H., Deloukas, P., Kathiresan, S., Myocardial Infarction, G. and Investigators, C. A. E. C. Systematic Evaluation of Pleiotropy Identifies 6 Further Loci Associated With Coronary Artery Disease. *J Am Coll Cardiol* 2017. 69 (7): 823-836.

Weber, M., Lauer, N., Mulsch, A. and Kojda, G. The effect of peroxynitrite on the catalytic activity of soluble guanylyl cyclase. *Free Radic Biol Med* 2001. 31 (11): 1360-1367.

Wechsler, J., Choi, Y. H., Krall, J., Ahmad, F., Manganiello, V. C. and Movsesian, M. A. Isoforms of cyclic nucleotide phosphodiesterase PDE3A in cardiac myocytes. *J Biol Chem* 2002. 277 (41): 38072-38078.

Wharton, J., Strange, J. W., Moller, G. M., Growcott, E. J., Ren, X., Franklyn, A. P., Phillips, S. C. and Wilkins, M. R. Antiproliferative effects of phosphodiesterase type 5 inhibition in human pulmonary artery cells. *Am J Respir Crit Care Med* 2005. 172 (1): 105-113.

Williams, K. J. and Tabas, I. The response-to-retention hypothesis of early atherogenesis. *Arterioscler Thromb Vasc Biol* 1995. 15 (5): 551-561.

Wobst, J., von Ameln, S., Wolf, B., Wierer, M., Dang, T. A., Sager, H. B., Tennstedt, S., Hengstenberg, C., Koesling, D., Friebe, A., Braun, S. L., Erdmann, J., Schunkert, H. and Kessler, T. Stimulators of the soluble guanylyl cyclase: promising functional insights from rare coding atherosclerosis-related GUCY1A3 variants. *Basic Res Cardiol* 2016. 111 (4): 51.

Xu, C., Park, J. K. and Zhang, J. Evidence that alternative transcriptional initiation is largely nonadaptive. *PLoS Biol* 2019. 17 (3): e3000197.

Xu, L., Carter, E. P., Ohara, M., Martin, P. Y., Rogachev, B., Morris, K., Cadnapaphornchai, M., Knotek, M. and Schrier, R. W. Neuronal nitric oxide synthase and systemic vasodilation in rats with cirrhosis. *Am J Physiol Renal Physiol* 2000. 279 (6): F1110-1115.

Yanaka, N., Kotera, J., Ohtsuka, A., Akatsuka, H., Imai, Y., Michibata, H., Fujishige, K., Kawai, E., Takebayashi, S.-I., Okumura, K. and Omori, K. Expression, structure, and chromosomal localization of the human cGMP-binding cGMP-specific phosphodiesterase PDE5A gene. *Eur J Biochem* 1998. 255: 391-399.

Yusuf, S., Hawken, S., Ounpuu, S., Dans, T., Avezum, A., Lanas, F., McQueen, M., Budaj, A., Pais, P., Varigos, J., Lisheng, L. and Investigators, I. S. Effect of potentially modifiable risk factors associated with myocardial infarction in 52 countries (the INTERHEART study): case-control study. *Lancet* 2004. 364 (9438): 937-952.

Zdravkovic, S., Wienke, A., Pedersen, N. L., Marenberg, M. E., Yashin, A. I. and De Faire, U. Heritability of death from coronary heart disease: a 36-year follow-up of 20 966 Swedish twins. *J Intern Med* 2002. 252 (3): 247-254.

Zhang, G., Xiang, B., Dong, A., Skoda, R. C., Daugherty, A., Smyth, S. S., Du, X. and Li, Z. Biphasic roles for soluble guanylyl cyclase (sGC) in platelet activation. *Blood* 2011. 118 (13): 3670-3679.

Zhang, M., Takimoto, E., Hsu, S., Lee, D. I., Nagayama, T., Danner, T., Koitabashi, N., Barth, A. S., Bedja, D., Gabrielson, K. L., Wang, Y. and Kass, D. A. Myocardial remodeling is controlled by myocyte-targeted gene regulation of phosphodiesterase type 5. *J Am Coll Cardiol* 2010. 56 (24): 2021-2030.

Zhu, B., Strada, S. and Stevens, T. Cyclic GMP-specific phosphodiesterase 5 regulates growth and apoptosis in pulmonary endothelial cells. *Am J Physiol Lung Cell Mol Physiol* 2005. 289 (2): L196-206.

Supplementary tables

Supplementary Table 1 FASTA sequences of the alternative promoter site cloned into the pGL4.10 vector

Name	Sequence
Alt. promoter WT	CCCTCTGTCAAAAAACCCTGAAAGTGACTAAATTGACACCAACTCTGG ATGTTCCTTAGGAAAAAAACAAAACAAAACAAAACAAAACAAGATTAAA AAGGGCCCAATTTAAGACCCTTATTAATACATCTGCAAGAGAGCAAAG AATAACAACAACAACAAAAGTTATACAGTCAATTTTCAATGATACATCGT CCCACTGGTGCCACCGGGGCGCCACCACCCAGCACCCGAGACCCGC CGCGCCCCCGGAAAAAGTGGGAAGGGACGTAGGGGGATGCTGAAGG AAGTACCTTGTTTTGTCTCCAAAGGGCAACATAGCAAACGTGGGAAGT TCGTTTTCGAACTCCGCCGATCCTGGACTCCAGGAGGCTCCGTAGGG GCAACAACGCGCGCAGGTGAGGTGAGGTGAGGTCGGCGACTCAGAA CCAGCTCCCTCACGGCCCCGGCCTCCGCGCCGCCGCCCGTCGCCTC CCGCTCGCCCCGCGCTGCGCCGCCCCCTGGCGGGGAGCGACCGGC AGAGCCGCGGCCGCGCGCCGGCGAGTGGGACCCGGGCGTCGAACC CGGGCGGGCTCCTCGACCATCACTGCCGGGCGTGTGT
Alt. promoter MUT	CCCTCTGTCAAAAAACCCTGAAAGTGACTAAATTGACACCAACTCTGG ATGTTCCTTAGGAAAAAAACAAAACAAAACAAAACAAAACAAGATTAAA AAGGGCCCAATTTAAGACCCTTATTAATACATCTGCAAGAGAGCAAAG AATAACAACAACAACAAAAGTTATACAGTCAATTTTCAATGATACATCGT CCCACTGGTGCCACCGGGGCGCCACCACCCAGCACCCGAGACCCGC CGCGCCCCCGGAAAAAGTGGGAAGGGACGTAGGGGGATGCTGAAGG AAGTACCTTGTTTAGTCTCCAAAGGGCAACATAGCAAACGTGGGAAGT TCGTTTTCGAACTCCGCCGATCCTGGACTCCAGGAGGCTCCGTAGGG GCAACAACGCGCGCAGGTGAGGTGAGGTGAGGTCGGCGACTCAGAA CCAGCTCCCTCACGGCCCCGGCCTCCGCGCCGCCGCCCGTCGCCTC CCGCTCGCCCCGCGCTGCGCCGCCCCCTGGCGGGGAGCGACCGGC AGAGCCGCGGCCGCGCGCCGGCGAGTGGGACCCGGGCGTCGAACC CGGGCGGGCTCCTCGACCATCACTGCCGGGCGTGTGT

Supplementary Table 2 Available background data of the CAD/MI family

Traditional risk factor	Values/Counts
Diabetes	n=0/36
Hypertension	n=14/36
LDL-cholesterol	median 143 mg/dl (interquartile range 126.3-176.3 mg/dl)
Body mass index	23.8 kg/m^2 (21.9-25.3)

Publications

Papers:

Dang, T. A., Kessler, T., Wobst, J., Wierer, M., Braenne, I., Strom, T. M., Tennstedt, S., Sager, H. B., Meitinger, T., Erdmann, J. and Schunkert, H. Identification of a Functional PDE5A Variant at the Chromosome 4q27 Coronary Artery Disease Locus in an Extended Myocardial Infarction Family. *Circulation* 2021. 144 (8): 662-665.

Kessler, T., Wobst, J., Wolf, B., Eckhold, J., Vilne, B., Hollstein, R., von Ameln, S., **Dang, T. A.**, Sager, H. B., Moritz Rumpf, P., Aherrahrou, R., Kastrati, A., Bjorkegren, J. L. M., Erdmann, J., Lusis, A. J., Civelek, M., Kaiser, F. J. and Schunkert, H. Functional Characterization of the GUCY1A3 Coronary Artery Disease Risk Locus. *Circulation* 2017. 136 (5): 476-489.

Wobst, J., von Ameln, S., Wolf, B., Wierer, M., **Dang, T. A.**, Sager, H. B., Tennstedt, S., Hengstenberg, C., Koesling, D., Friebe, A., Braun, S. L., Erdmann, J., Schunkert, H. and Kessler, T. Stimulators of the soluble guanylyl cyclase: promising functional insights from rare coding atherosclerosis-related GUCY1A3 variants. *Basic Res Cardiol* 2016. 111 (4): 51.

Poster abstracts:

Dang, T. A., Wobst, J., Kessler, T., Ameln, S. V., Lehm, M., Prestel, M., Braenne, I., Aherrahrou, R., Dichgans, M., Hengstenberg, C., Erdmannn, J. and Schunkert, H. Investigating the impact of a mutation in PDE5A on myocardial infarction. *BMC Pharmacology and Toxicology* 2015. 16 (1): A43.

Dang, T.A., Braenne, I., Aherrahrou, R., Tennstedt, S., Kessler, T., Hengstenberg, C., Erdmann, J., Schunkert, H. A PDE5A gene mutation affecting risk of myocardial infarction. *Circulation* 2014. 130 (suppl_2): A19944-A19944.

Reviews:

Dang, T. A., Schunkert, H. and Kessler, T. cGMP Signaling in Cardiovascular Diseases: Linking Genotype and Phenotype. *J Cardiovasc Pharmacol* 2020. 75 (6): 516-525.

Zeng, L., **Dang, T. A.** and Schunkert, H. Genetics links between transforming growth factor beta pathway and coronary disease. *Atherosclerosis* 2016. 253: 237-246.

Wobst, J., Kessler, T., **Dang, T. A.**, Erdmann, J. and Schunkert, H. Role of sGC-dependent NO signalling and myocardial infarction risk. *J Mol Med* (Berl) 2015. 93 (4): 383-394.

Wobst, J., Rumpf, P. M., **Dang, T. A.**, Segura-Puimedon, M., Erdmann, J. and Schunkert, H. Molecular variants of soluble guanylyl cyclase affecting cardiovascular risk. *Circ J* 2015. 79 (3): 463-469.